SPIN WAVE RESONANCE IN FERROMAGNETIC FILMS

Thesis by

Christopher H. Bajorek

In Partial Fulfillment of the Requirements

for the Degree of

Doctor of Philosophy

California Institute of Technology

Pasadena, California

1971

(Submitted June 25, 1971)

ACKNOWLEDGEMENTS

I am very grateful for the encouragement, guidance, and assistance of Professors C. H. Wilts and F. B. Humphrey, and for the many helpful discussions with colleague students during the course of this work. The backscattering measurements would have been very difficult without the assistance of Professors M-A. Nicolet and J. W. Mayer. The indispensable mechanical assistance of E. Mott and the secretarial assistance of K. Ellison are also gratefully acknowledged. Without the financial support of an N.S.F. Traineeship, two Tektronix and one Fairchild Fellowship, three teaching assistantships, and two summer research assistantships much of this work would not have been possible. Finally, but very importantly, I am very grateful to my wife, Janet, who encouraged, supported, and patiently endured my stay at Caltech.

ABSTRACT

The objective of this investigation has been a theoretical and experimental understanding of ferromagnetic resonance phenomena in ferromagnetic thin films, and a consequent understanding of several important physical properties of these films. Significant results have been obtained by ferromagnetic resonance, hysteresis, torque magnetometer, He ion backscattering, and X-ray fluorescence measurements for nickel-iron alloy films.

Taking into account all relevant magnetic fields, including the applied, demagnetizing, effective anisotropy and exchange fields, the spin wave resonance condition applicable to the thin film geometry is presented. On the basis of the simple exchange interaction model it is concluded that the normal resonance modes of an ideal film are expected to be unpinned. The possibility of nonideality near the surface of a real film was considered by means of surface anisotropy field, inhomogeneity in demagnetizing field and inhomogeneity of magnetization models. Numerical results obtained for reasonable parameters in all cases show that they negligibly perturb the resonance fields and the higher order mode shapes from those of the unpinned modes of ideal films for thicknesses greater than 1000 Å. On the other hand for films thinner than 1000 Å the resonance field deviations can be significant even though the modes are very nearly unpinned. A previously unnoticed but important feature of all three models is that the interpretation of the first resonance mode as the uniform mode of an ideal film allows an accurate

measurement of the average effective demagnetizing field over the film volume. Furthermore, it is demonstrated that it is possible to choose parameters which give indistinguishable predictions for all three models, making it difficult to uniquely ascertain the source of spin pinning in real films from resonance measurements alone.

Spin wave resonance measurements of 81% Ni-19% Fe coevaporated films 30 to 9000 Å thick, at frequencies from 1 to 8 GHz, at room temperature, and with the static magnetic field parallel and perpendicular to the film plane have been performed. A self-consistent analysis of the results for films thicker than 1000 Å, in which multiple excitations can be observed, shows for the first time that a unique value of exchange constant A can only be obtained by the use of unpinned mode assignments. This evidence and the resonance behavior of films thinner than 1000 Å strongly imply that the magnetization at the surfaces of permalloy films is very weakly pinned. However, resonance measurements alone cannot determine whether this pinning is due to a surface anisotropy, an inhomogeneous demagnetizing field or an inhomogeneous magnetization. The above analysis yields a value of $4\pi M = 10{,}100$ Oe and $A = (1.03 \pm .05) \times 10^{-6}$ erg/cm for this alloy. The ability to obtain a unique value of A suggests that spin wave resonance can be used to accurately characterize the exchange interaction in a ferromagnet.

In an effort to resolve the ambiguity of the source of pinning of the magnetization, a correlation of the ratio of magnetic moment and X-ray film thickness with the value of effective demagnetizing field $4\pi NM$ as determined from resonance, for films 45 to 300 Å has been performed.

The remarkable agreement of both quantities and a comparison with the predictions of five distinct models, strongly imply that the thickness dependence of both quantities is related to a thickness dependent average saturation magnetization, which is far below 10,100 Oe for very thin films. However, a series of complementary experiments shows that this large decrease of average saturation magnetization cannot be simply explained by either oxidation or interdiffusion processes. It can only be satisfactorily explained by an intrinsic decrease of the average saturation magnetization for very thin films, an effect which cannot be justified by any simple physical considerations.

Recognizing that this decrease of average saturation magnetization could be due to an oxidation process, a correlation of resonance measurements, He ion backscattering, X-ray fluorescence and torque magnetometer measurements, for films 40 to 3500 Å thick has been performed. On basis of these measurements it is unambiguously established that the oxide layer on the surface of purposefully oxidized 81% Ni-19% Fe evaporated films is predominantly Fe-oxide, and that in the oxidation process Fe atoms are removed from the bulk of the film to depths of thousands of angstroms. Extrapolation of results for pure Fe films indicates that the oxide is most likely α-Fe_2O_3. These conclusions are in agreement with results from old metallurgical studies of high temperature oxidation of bulk Fe and Ni-Fe alloys. However, X-ray fluorescence results for films oxidized at room temperature, show that although the preferential oxidation of Fe also takes place in these films, the extent of this process is by far too small to explain the large variation of their average saturation magnetization with film thickness.

TABLE OF CONTENTS

Chapter 1

INTRODUCTION

Many properties of ferromagnetic materials are a consequence of the large degree of spontaneous alignment of the electron moments responsible for their magnetization. As described in the next chapter, the effect which gives rise to this alignment is the exchange interaction, which is typically represented by the exchange constant A. This constant arises in many static and dynamic considerations of the behavior of a ferromagnet. In most cases, these considerations also involve other important characteristics of ferromagnets. Proper measurement of the latter, therefore, requires knowledge of the exchange constant for a given material. This knowledge is also essential for a test of the validity of theoretical predictions of the exchange interaction itself. Consequently, a main objective of much experimental work in magnetism has been the measurement of the exchange constant for a given material.

The experiments which are most directly suited to determine the exchange constant are 1) the study of the temperature dependence of the saturation magnetization, believed to be caused by the thermal excitation of spin waves (Argyle and Charap, 1964), 2) neutron inelastic scattering at small angles (neutron scattering from thermally excited spin waves) (Hatherly et al., 1964; Lowde, 1965), 3) switching of the magnetization under the influence of an inhomogeneous magnetic field applied by means of a current through the magnetic material (Methfessel et al., 1962; Inamura and Chikazumi, 1968), and 4) spin wave resonance (S.W.R.). The latter

technique will be considered in detail in this investigation. For a more complete description of the other three methods the reader is referred to the above references. The choice of these four, from several other possible methods, is based on the belief that they are least uncertain, theoretically and experimentally, with regard to material properties other than the exchange interaction. Independent of the limitations of each experiment, those that can be applied to the same material are expected in principle to yield the same value of A. That this is not the case can be readily seen from a review of published experimental results. First, it is common to find significant disagreement between values of A determined by two or more of the above methods for what is supposedly the same material, and second, a more unsatisfactory situation, it is not unusual to find serious disagreement between values of A obtained by any one of the above methods for the same material. For example, for 81% Ni-19% Fe alloys, A from neutron scattering is reported to be 1.29×10^{-6} erg/cm (Hatherly et al., 1964), two values of A reported from switching experiments are .5 (Methfessel et al., 1962) and 1.6×10^{-6} erg/cm (Inamura and Chikazumi, 1968), and several values of A obtained from resonance measurements range between .2 and 2×10^{-6} erg/cm (see Appendix 1). Although it is perhaps reasonable that the use of a bulk sample, as was the case in the neutron experiment, instead of a thin film, as used in the other two, might lead to some discrepancy between the corresponding exchange constants, it is unreasonable that the use of very similar samples in the switching and resonance experiments can give values of A that differ by as much as a factor of 10.

This large spread is particularly disturbing for the spin wave resonance experiments. These involve the measurement of multiple resonance spectra associated with the excitation of standing spin wave modes between the surfaces of a thin film. The wavelengths of these modes are expected to be simply related to the thickness of a film, and to the boundary conditions applicable at the film surfaces. It seems therefore that knowledge of the thickness, the boundary condition, and the corresponding resonance equations, which involve A, should allow a straightforward measurement of the exchange constant.

A closer review of previous resonance investigations shows that the conflicting values of A are a result of disagreement as to what are the appropriate boundary conditions that must be imposed on the magnetization at the film surfaces. Following Kittel's (1958) prediction of S.W.R. in thin films and the initial measurements of Seavey and Tannenwald (1958) significant work has been devoted to the interpretation of S.W.R. results in terms of three boundary condition models: the magnetization at the surfaces is 1) totally pinned, 2) unpinned, and 3) partially pinned. The efforts of Weber (1968), Wigen et al. (1964), and Lykken et al. (1970) are representative of these three main interpretations used by more than twenty authors over the last decade. Unfortunately all of these individual efforts were limited in scope and have not resulted in a consensus about which boundary condition allows a unique interpretation of S.W.R. measurements in samples of very similar physical characteristics. As implied above, this ambiguity is reflected in the wide variations in deduced values of the exchange constant since

this parameter is sensitive to the assumed boundary condition. Appendix 1 summarizes values of A, determined previously from S.W.R., for materials very near the composition used in this investigation (81% Ni-19% Fe), and prepared under very similar experimental conditions. As can be noted in this Appendix, some of the reported values of A differ by very large factors. Furthermore, no one has yet successfully identified the sources of the degree of pinning presumed in their investigations.

Facing this unsatisfactory situation it was felt that it should be possible to design a carefully controlled experiment which would allow a unique determination of A appropriate to a particular material, the degree of effective pinning of the magnetization at the film surfaces, and hopefully the sources of this pinning. It was also felt that this knowledge would give additional information about several other physical characteristics of permalloy films.

Significant results in all areas have been obtained by comprehensive ferromagnetic resonance, hysteresis, torque magnetometer, He ion backscattering and X-ray fluorescence measurements for permalloy films of 81% Ni-19% Fe.

Chapter 2

FERROMAGNETIC RESONANCE

2.1 Introduction

2.1.1 Elementary Considerations

The advanced theories of ferromagnetism suppose that the magnetization of materials is caused primarily by the magnetic moment of the electron which is associated with and in opposite direction to the spin. The concepts of spin and magnetic moment of a particle are quantum mechanical in origin. Thus one would expect that a complete understanding of magnetic effects of materials would require a quantum mechanical treatment. Unfortunately this is not possible today since nobody has yet successfully treated magnetism of solids on a purely quantum mechanical basis. It is, however, possible to gain considerable insight by a combination of quantum mechanical, classical, and phenomenological considerations. Although the following treatment of ferromagnetic resonance makes use of all three considerations, for sake of expediency and simplicity these concepts are emphasized in their classical form.

A ferromagnetic material is characterized by a magnetization $\bar{M}$ which is associated with an opposite angular momentum $\bar{L} = -\frac{1}{\gamma}\bar{M}$ where γ is the gyromagnetic ratio. Typically a ferromagnetic resonance experiment consists of placing such a magnetic sample in a static magnetic field sufficiently strong to saturate the material along the field direction. A disturbance of the magnetization from this equilibrium position will cause it to precess at the Larmor frequency about the

static field direction. This motion is associated with the gyroscopic properties of the system. The angle of this precession is limited by relaxation mechanisms. The disturbance is usually provided by a small R.F. field. The basic equation of motion for the system can be easily derived by considering the rate of change of angular momentum which is equal to the torque $\bar{M} \times \bar{H}$ acting on the system in the magnetic field $\bar{H}$:

$$\frac{\partial \bar{M}}{\partial t} = -\gamma \bar{M} \times \bar{H} \quad . \tag{2.1}$$

For the ideal case of an infinite or spherical and isotropic medium the Larmor frequency or equivalently, the resonance frequency, is given by $\omega = \gamma H$. The excitation of such a system usually consists of maintaining a fixed R.F. frequency and tuning the resonance by slowly varying the static magnetic field until the Larmor frequency condition is satisfied. At this frequency energy is coupled strongly into the system. The resulting loss from the R.F. source can be used to measure the resonance field.

For the practical case of a finite non-spherical sample the basic equation of motion 2.1 has to include the sample shape demagnetizing fields which give rise to additional torques on the magnetization. It must also include the effective torques due to magnetic anisotropies which are encountered in most magnetic materials. These effective torques are caused by the restoring forces associated with the displacement of the magnetization from certain preferred orientations in the sample. Under special circumstances it must also include torques caused by volume demagnetizing fields due to a possible nonuniform orientation of

the magnetization.

To first order the resonance behavior of ferromagnetic thin films can be very well described by the above considerations. However, for certain experimental conditions it is possible to excite and detect multiple resonances in thin films which cannot be completely described by the above considerations. These multiple excitations are associated with standing spin wave modes set up between the surfaces of a film. These modes correspond to a special nonuniform orientation of the magnetization which gives rise to an additional effective field which must also be accounted for in Eq. 2.1. The source of this field is the exchange interaction between the spins of a ferromagnet. This interaction is described in the following section.

The inclusion of all of the above considerations in Eq. 2.1 gives rise to a generally complicated expression for the resonance frequency of a system which reflects all of the corresponding effective fields. A judicious choice of experimental conditions like sample geometry, orientation relative to a static field direction, R.F. frequency and temperature, can be then conveniently used to simultaneously measure many properties of a magnetic material. The complete resonance condition applicable to thin films will be presented in Section 2.1.3.

2.1.2 The Exchange Interaction and Spin Waves

A very important characteristic of ferromagnetic materials is their very large magnetization. This strong magnetization is caused by a high degree of parallel alignment of the electron moments responsible for the magnetization. In the transition elements these are thought to

be primarily the electrons of the unfilled 3d shell. These are considered to be localized relative to the nuclei of the atoms. One model explains the interatomic alignment of these localized electrons via intermediary electrons, like the conduction electrons in a metal, in conjunction with the exclusion principle which tends to prevent two electrons from being in the same condition with regard to location and spin orientation. This interaction can be visualized by considering the motion of a conduction electron which senses the alignment of the localized electrons of one atom and transmits the information to the next atom with a resulting interatomic alignment of the localized electrons. It must be emphasized that this is an oversimplified model for what undoubtedly is a very complex interaction which nobody has yet been able to describe quantitatively. Nevertheless it is this interaction which is accepted as responsible for the strong magnetization of ferromagnets and it is called the exchange interaction. At present its inclusion in theoretical considerations of the macroscopic behavior of a ferromagnet is of necessity phenomenological. A widely used but perhaps oversimplified model for this interaction is described below. It has the advantage that it allows simple calculations whose results can be put to the test of experiments.

The exchange interaction in ferromagnetic materials is characterized by constructing the Heisenberg exchange Hamiltonian which has the form

$$\mathcal{H}_{exch} = - J \sum_{i,j} \bar{S}_i \cdot \bar{S}_j \quad . \tag{2.2}$$

$\bar{S}_i$ are the spins of the localized magnetic electrons and J is an exchange parameter known as the exchange integral. For a review of exchange interactions see C. Herring (1966). The j summation is over the nearest neighbors of $\bar{S}_i$ and the i summation is over the N spins of the ferromagnetic system. It is usually convenient to cast this equation in terms of the magnetic moments of the spins and an effective magnetic field called the exchange field. By using the definitions:

$$\bar{\mu}_i \equiv -g \mu_B \bar{S}_i \tag{2.3}$$

and

$$\bar{H}_{\text{exch } i} \equiv -\frac{2J}{g\mu_B} \sum_j \bar{S}_j, \tag{2.4}$$

where the j summation is over the nearest neighbors of $\bar{S}_i$, equation 2.2 takes the form

$$\mathcal{H}_{\text{exch}} = -\frac{1}{2} \sum_i \bar{\mu}_i \cdot \bar{H}_{\text{exch } i} \tag{2.5}$$

In the above equations: g = g- factor of the gyromagnetic ratio $\gamma \equiv \frac{ge}{2mc}$ and $\mu_B \equiv \frac{-e\hbar}{2mc}$ is the Bohr magneton. The factors 1 in Eq. 2.2 and $\frac{1}{2}$ in Eq. 2.5 account for the double counting of interacting pairs in the summation over the N spins of the system. This definition of the exchange field can be incorporated into the equation of motion for this system which in the absence of any additional fields and within the notation of this section has the form:

$$\frac{\hbar \partial \bar{S}_i}{\partial t} = \bar{\mu}_i \times \bar{H}_{\text{exch } i} \cdot \tag{2.6}$$

The elementary excitations of such a spin system have a wave-like form and are called spin waves or, when quantized, magnons. Fig. 2-1 shows a classical interpretation of such a spin wave. Each spin is tipped at a small angle α_i from the average spin orientation which in the presence of a magnetic field coincides with the direction of the field. The angle between each pair of spins is δ_{ij}. The shortest distance between parallel spins (except in the plane containing all parallel spins) defines the wavelength and the propagation direction of the wave. The wavevector $\bar{k}$ has magntiude $\frac{2\pi}{\lambda}$ and is directed along the propagation direction. Each spin precesses about its equilibrium position at the frequency ω_k which in general is a complicated function of k . This dispersion relation is derived in the next section. The ellipticity of the cone of precession is caused by the demagnetizing field associated with a nonvanishing volume divergence of the magnetization which arises whenever $\bar{k}$ is not along the direction of average magnetization (z axis in Fig. 2.1).

Equations 2.2 through 2.6 have been presented as a foundation to the following development of the concepts and equations related to the resonance excitation of spin waves. For a summary of quantum mechanical treatments of spin waves see Sparks (1964).

2.1.3 Spin Wave Resonance

Prior to developing the concepts and equations of spin wave resonance in thin films, it is convenient to express the exchange field of Eq. 2.4 in terms of the macroscopic parameters of a ferromagnet. This can be easily done by considering an inhomogeneous dynamic excitation

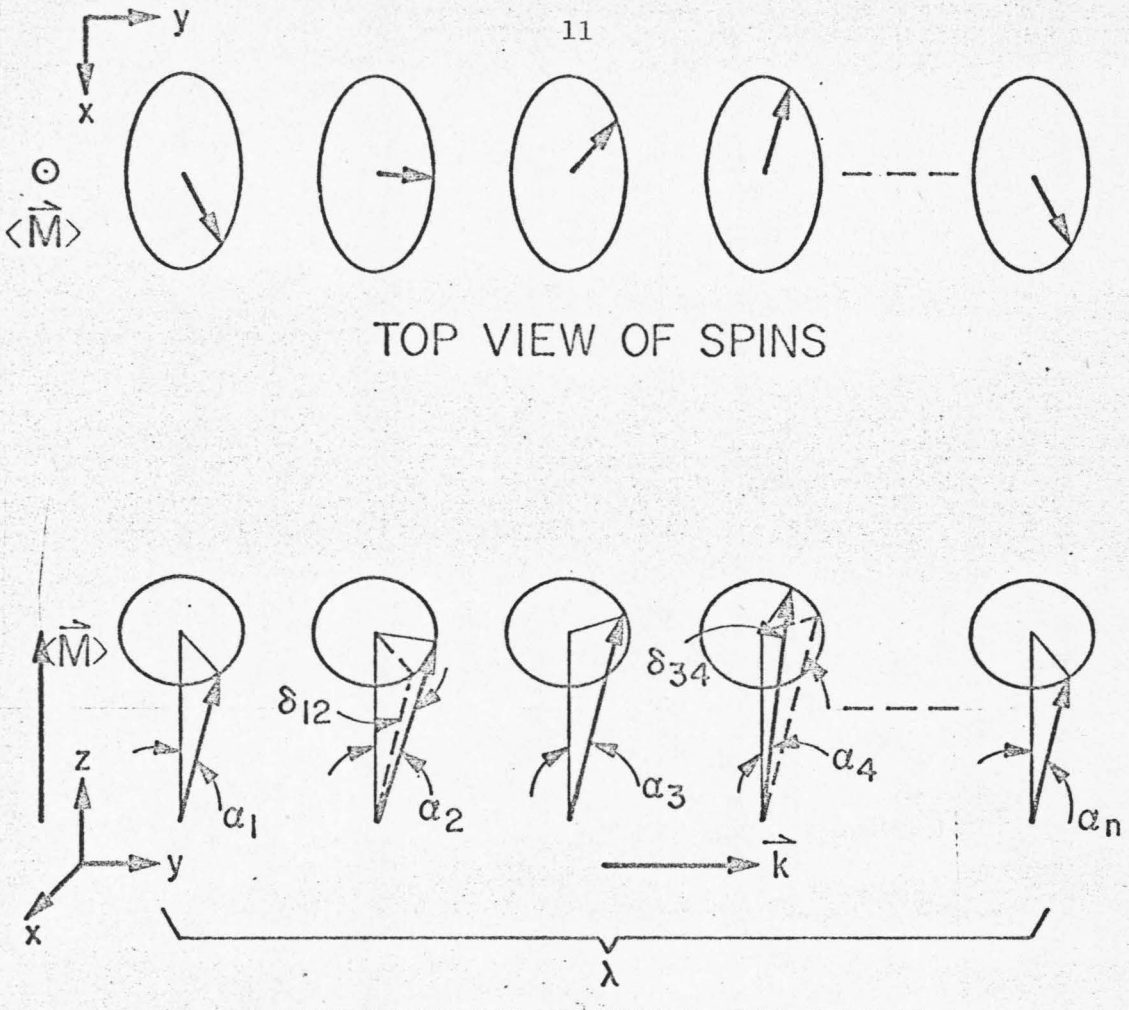

Fig. 2-1 Spin wave propagating along the y axis. All spins precess about the z axis at a characteristic frequency ω_k. All the spins in any plane perpendicular to y are parallel.

of a ferromagnetic system whose characteristic wavelength is much larger than the lattice spacing of the material, ka << 1. For this case the exchange field of Eq. 2.4 is simply given by

$$\bar{H}_{exch} = \frac{2A}{M^2} \nabla^2 \bar{M} \tag{2.7}$$

where $A \equiv \frac{\rho JS^2}{a}$, ρ is a numerical factor related to crystal structure which is 2 for b.c.c., 4 for f.c.c., and $\sqrt{8}$ for hexagonal crystal structures. The constant A is usually known as the exchange constant. Equation 2.7 can be simply derived from Eq. 2.4, by considering the first three terms of Taylor series expansions for $\Sigma_j \bar{S}_j$ relative to $\bar{S}_i$. For the practical case of a ferromagnetic sample of finite size in an applied magnetic field, in addition to the exchange term, the equation of motion (2.6), must also account for the fields outlined in Section 2.1.1, namely, the demagnetizing fields due to the sample shape and volume inhomogeneities of $\bar{M}$, and the effective fields due to the possible presence of magnetic anisotropies of the material.

The dispersion relation for the thin film geometry which involves the above considerations can be simply derived by assuming that the dynamic deviations of the magnetization from saturation are small ($\bar{M} = M\bar{e}_z + \bar{m}$), that m has the temporal and spatial dependence $e^{i(\omega t - k\xi)}$ where ξ is the variable along the direction normal to the film plane and by solving Eq. 2.1 with the inclusion of the applied, demagnetizing, anisotropy and exchange fields. The dispersion relation or equivalently the resonance equation for m is given by:

$$\frac{\omega^2}{\gamma^2} = \left[H \cos\beta + H_{k_{\parallel}} \cos 2\theta - (4\pi NM - H_{k_{\perp}}) \cos^2\phi + \frac{2A}{M} k^2 \right] \left[H \cos\beta + H_{k_{\parallel}} \cos^2\theta - (4\pi NM - H_{k_{\perp}}) \cos 2\phi + \frac{2A}{M} k^2 \right] \tag{2.8}$$

In the above equation

$\bar{H}$ = applied magnetic field

M = saturation magnetization

γ = gyromagnetic ratio $\frac{ge}{2mc}$

A = exchange constant corresponding to the exchange field of the form $\frac{2A}{M^2} \frac{\partial^2 \bar{M}}{\partial \xi^2}$ due to nonuniformity in the orientation of $\bar{M}$.

$N \equiv (N_{\perp} - N_{\parallel})$ = difference of the perpendicular and planar demagnetizing factors associated with the corresponding shape demagnetizing fields.

$H_{k_{\parallel}} = \frac{2K_{\parallel}}{M}$ = effective torque field due to a planar anisotropy energy density of the form $K_{\parallel} \sin^2\theta$, where θ is the angle between $\bar{M}$ and the planar easy axis of magnetization.

$H_{k_{\perp}} = \frac{2K_{\perp}}{M}$ = effective torque field due to a perpendicular anisotropy energy density of the form $K_{\perp} \sin^2\phi$, where ϕ is the angle between $\bar{M}$ and the film normal which is also assumed to be an easy axis of magnetization.

β = angle between $\bar{H}$ and $\bar{M}$

As can be noticed the above equation contains a wealth of information about several important material parameters. In particular it involves

the exchange term $\frac{2A}{M} k^2$ corresponding to a spin wave of wavevector $\bar{k}$ along the direction normal to the film plane. The ability to select the excitation of a spin wave of known $\bar{k}$ coupled with knowledge about the other parameters of the material would allow the determination of the exchange constant A. As mentioned in Chapter 1 this possibility was initially recognized and described by Kittel (1958). He theorized that a thin film would allow the excitation of standing spin wave modes between its surfaces whose wavevector would be simply related to the film thickness. He predicted the excitation by means of ferromagnetic resonance, namely that by applying an R.F. field at frequency ω to a film in a magnetic field H and by varying the field it would be possible to selectively tune standing spin wave modes whenever Eq. 2.8 is satisfied. This effect was first observed experimentally by Seavey and Tannenwald (1958) and is known as spin wave resonance.

The main problem in an accurate measurement of A is an accurate determination of k. This requires knowledge about the thickness of a film, and the other parameters in Eq. 2.8, but more importantly, it also requires knowledge about the boundary conditions at the film surfaces which in turn dictate the allowable excitations. Over the last decade more than twenty investigators addressed themselves to this problem. Unfortunately as mentioned in Chapter 1, and outlined in Appendix 1, their efforts have not resulted in a consensus as to what the appropriate boundary conditions are and consequently as to what is the exchange constant for a given material. It is felt that the experiment described in Chapter 3 for the first time uniquely answers both questions.

Before turning to a detailed discussion of the boundary conditions and their implication on the determination of A it is important to completely explain the assumptions that were used in deriving Eq. 2.8.

First, Eq. 2.8 is specialized to the thin film geometry by only accounting for inhomogeneities of $\bar{M}$ whose characteristic wavevector $\bar{k}$ is parallel to the film normal. This approximation is valid for the films considered in this investigation since their aspect ratio, the ratio of film thickness to lateral dimensions is very small, typically less than 10^{-4}. This small aspect ratio is expected to give rise to negligible planar inhomogeneities or equivalently small planar components of $\bar{k}$. It should be emphasized, however, that this approximation breaks down for larger aspect ratios and except for the thin film case and for samples of relatively large dimensions it is very difficult to derive an accurate analytic form for the dispersion relation since the equation of motion is very complicated and nonlinear due to both the exchange and the demagnetizing contributions from Maxwell's equations.

Second, Eq. 2.8 was derived without taking into account the eddy current contributions from Maxwell's equations and intrinsic relaxation contributions to the equation of motion. These omissions are justified in terms of both the experimental results of this investigation and the careful theoretical considerations of M. H. Seavey (1961). His theoretical treatment of both effects predicts small deviations from Eq. 2.8 which are only significant for the long wavelength spin wave modes and negligible for the higher order modes. The predicted shifts of the resonance fields are much smaller than the experimental shifts

observed in this survey and therefore justify their omission from Eq. 2.8.

Third, it must be clarified that Eq. 2.8 only rigorously applies to ideal films, films with perfect surfaces, and whose magnetic characteristics are uniform over their volume on a macroscopic scale. For such films the demagnetizing factor N = 1.0, since $N_{\perp} = 1.0$ and $N_{\parallel} = 0$. The reason why the difference in demagnetizing factors N is explicitly included in Eq. 2.8 is because as shown in Sec. 2.3 below, this equation can also be used for films with an inhomogeneous demagnetizing field or an inhomogeneous magnetization as might be the case in real films. As explained below, in the presence of such inhomogeneities the $4\pi NM$ terms of Eq. 2.8 represent the average demagnetizing field or average magnetization over the film volume.

One source of an inhomogeneous demagnetizing field can be the polycrystalline nature of evaporated permalloy samples which gives rise to a film surface roughness of the crystallite size, which in turn causes inhomogeneous demagnetizing fields through the volume of the film whose spatial average is characterized by $N_{\perp}$ and $N_{\parallel}$. E. Schlömann (1970) has calculated these fields assuming a periodic surface roughness in which the inclination of the local film surface relative to the mean surface is less than 45° and the film is uniformly magnetized. A first order estimate of N is given by $\left[1 - \frac{3\pi\langle a\rangle^2}{\lambda L}\right]$ where $\langle a\rangle^2$ is the mean square deviation of the actual film surface from the mean surface, λ the wavelength of the surface roughness, and L the film thickness. By using values of $\sqrt{\langle a\rangle^2} = 10$ Å and $\lambda = 100$ Å, which might reasonably characterize the surface of typical permalloy films, and L = 30 Å, one

calculates $N \simeq 0.7$. Thus it is expected that surface roughness can significantly reduce the effective demagnetizing factor for very thin films and this possibility must be, therefore, accounted for in Eq. 2.8.

An inhomogeneous magnetization can arise from an inhomogeneity in film composition, such as can be caused by the preferential oxidation of one of the film constituents. This possibility is also accounted for in the $4\pi NM$ terms of Eq. 2.8 except that in this case this quantity stands for the average saturation magnetization, as opposed to the average demagnetizing field, over the film volume.

With the above understandings, Eq. 2.11 will be the basis for the interpretation of the experimental results discussed in Chapters 3 and 4.

2.2 Boundary Conditions

2.2.1 Exchange Boundary Condition

The exchange field in a ferromagnetic material gives rise to the exchange boundary condition which the magnetization must satisfy in addition to the usual boundary conditions imposed on the electromagnetic field. This boundary condition can be simply derived by considering a finite chain of equally spaced spins which are acted upon by the applied magnetic field and by the effective exchange forces caused by the adjacent spins. A fundamental requirement on a normal mode of this system is that all spins precess at the same frequency, or equivalently, that the same torque acts on all spins for a given spatial variation of their transverse component. In the continuum approximation this requirement is satisfied if

$$\frac{\partial \bar{m}}{\partial n} = 0 \text{ at } \xi = \pm \frac{L}{2} \tag{2.9}$$

where n is the outward film normal. Within the approximations of Sec. 2.1.3 the solutions for m which satisfy Eq. 2.9 are trigonometric functions of $k\xi$ for which $k = \frac{p\pi}{L}$ where p = 0, the uniform mode, or p = integer. These solutions are called the unpinned spin wave modes and are the ones expected to be excited in an ideal film. However the existence of ideal films is highly unlikely. For example all films are polycrystalline and as discussed in Sec. 2.1.3 their surface roughness is expected to give rise to an inhomogeneous demagnetizing field through the film volume. The possibility of preferential oxidation of one element in an alloy film can give rise to inhomogeneities in both the composition and magnetization near one surface. Also it is not unreasonable to expect intrinsic inhomogeneities of exchange and magnetization near the surface of a film due to the abrupt termination of material at the surface. Furthermore, it is an experimental fact that it is not possible to explain all resonance results, particularly for very thin films, in terms of the ideal unpinned model. Therefore an investigation of real films must also account for the implications of the above effects on their resonance behavior. The remainder of the chapter is devoted to these considerations.

2.2.2 Surface Anisotropy

As mentioned above, it is plausible that the effective magnetocrystalline field acting on the surface spins of a ferromagnetic material can be different from the fields acting on the interior spins. The lack

of symmetry at the surface of a crystal and possible magnetic coupling to an antiferromagnetic surface oxide layer have been invoked as possible sources for such effects. As suggested by Kittel (1958), this effect at the surface can be conveniently approximated phenomenologically by a surface anisotropy energy density of the form $K_s \sin^2 \phi$, where ϕ is the angle between the surface spins and the film normal which for positive K_s is an easy axis. It should of course be emphasized that this choice of anisotropy function is arbitrary. Nevertheless if K_s is assumed equal on both surfaces, in the continuum approximation this imposes the following boundary conditions on m:

a) for H applied perpendicular to the film plane

$$A \frac{\partial \bar{m}}{\partial n} + K_s \bar{m} = 0 \quad \text{at } \xi = \pm \frac{L}{2} \tag{2.10}$$

b) for H applied parallel to the film plane

$$\left.\begin{aligned} A \frac{\partial m_n}{\partial n} - K_s m_n &= 0 \\ \frac{\partial m_p}{\partial n} &= 0 \end{aligned}\right\} \quad \text{at } \xi = \pm \frac{L}{2} \tag{2.11}$$

where,

m_n = component of $\bar{m}$ perpendicular to the film plane

m_p = component of $\bar{m}$ parallel to the film plane .

In considering the possible values of K_s it can be readily seen that only $K_s < 4\pi M^2 \frac{L}{4}$ is compatible with permalloy films since in the absence of an applied field a value of K_s larger than this would magnetize the film perpendicular to its plane, a situation never encountered in 81% Ni

permalloy films. For a non-zero K_s, Eq. 2.10 can be satisfied by trigonometric functions of $k\xi$ as solutions for m. However in the parallel resonance case Eq. 2.11 can only be satisfied by using a sum of hyperbolic and trigonometric functions of $|k|\xi$ as solutions for m, except that if K_s is not too large ($K_s \lesssim 1$ erg/cm^2) the first parallel mode only consists of a sum of two hyperbolic functions. For the latter case the first parallel resonance mode is characterized by a negative exchange term, $k^2 < 0$, or equivalently the amplitude of m is larger at the film surface than at its center. For both resonance geometries, $|k| = \frac{p\pi}{L}$ where p is obtained from well known transcendental equations (Soohoo, 1963; Wolf, 1963) which only allow non-integer values which are different for the parallel and perpendicular resonance geometries. These solutions for m are usually called the partially pinned spin wave modes. The transcendental equation for all the modes in perpendicular resonance is

$$\cot \frac{kL}{2} = \frac{Ak}{K_s} , \tag{2.12}$$

The transcendental equation for the first mode in parallel resonance mode if $K_s \lesssim 1$ erg/cm^2 is

$$\coth \frac{|k|L}{2} = -\frac{A|k|}{K_{eff}} \tag{2.13}$$

and the transcendental equation for the higher order modes or all the modes if $K_s \gtrsim 1$ erg/cm^2 in parallel resonance is

$$\cot \frac{kL}{2} = \frac{Ak}{K_{eff}} \tag{2.14}$$

where K_{eff} is a complicated function of K_s, ω, $\gamma 4\pi M$, $\frac{L}{2}$, and k. For the

customary range of the above parameters $K_{eff} << K_s$; therefore the effective pinning in parallel resonance is considerably smaller than in perpendicular resonance.

Another boundary condition which was often used in the past assumes that m was constrained by some unknown mechanism to be zero at the film surface for both or either resonance geometries. This condition is known as the perfectly pinned boundary condition. Although it can be obtained in perpendicular resonance from Eq. 2.10, by setting $K_s = \infty$, Eq. 2.11 shows that this boundary condition cannot be derived for parallel resonance from this anisotropy model. However, assuming that this boundary condition is correct, the solutions for m in both geometries are trigonometric functions of $k\xi$ for which $k = \frac{p\pi}{L}$ where p = integer only (excluding zero, the uniform mode). The discussion of the quantitative details of this surface anisotropy model is deferred until Sec. 2.3.2.

A surface anisotropy like the one discussed above does not necessarily have to be localized at the surface spins. It is plausible for it to extend into the volume of the film and thus give rise to an inhomogeneous effective field distributed across the film thickness. It can be easily shown that the effective field due to a typical magnetic anisotropy function and its effect on resonance is additive to and indistinguishable from other possible sources of inhomogeneities such as a decrease of demagnetizing field or magnetization near the film surface. A good example of this can be seen in the $(4\pi NM-H_{k\perp})$ terms of Eq. 2.8, where $H_{k\perp}$ is the effective field of a perpendicular anisotropy which is assumed to extend throughout the film volume. Therefore the implications

of an inhomogeneous effective field near the film surface can be more conveniently treated by explicitly considering the inhomogeneity of either the demagnetizing field or the magnetization as is done in the next section.

2.3 Inhomogeneity Effects

2.3.1 Introduction

In considering the implications of inhomogeneities localized near the film surface on the resonance behavior of thin films it is reasonable to expect inhomogeneities in 1) the anisotropy field which as mentioned above is indistinguishable from the demagnetizing field, 2) the demagnetizing field, 3) the magnetization, and 4) the exchange interaction. In principle it is possible to account for all four effects simultaneously, however this task can be simplified significantly by considering each effect independently of the others. Furthermore it could be further simplified if it were possible to a priori determine the absence of any of these effects in real films.

As mentioned above an inhomogeneity in the surface anisotropy field is indistinguishable from an inhomogeneity in demagnetizing field and can, therefore, be accounted for by considering the latter possibility. As discussed in Sec. 2.1.3 Schlömann (1970) has predicted that the surface roughness associated with the polycrystalline nature of permalloy films can give rise to an inhomogeneous demagnetizing field across the film thickness.

The films used in this investigation undoubtedly oxidize upon exposure to air after their evaporation. It is also possible that some

oxidation can take place at the film substrate (glass) interface. Furthermore this oxidation could be more severe for either constituent of the film alloy (Fe, Ni) causing an inhomogeneity in composition near the film surfaces. This could in turn give rise to an inhomogeneous magnetization. It has also been suggested that the magnetization near the film surface could be lower than at the interior without invoking an inhomogeneity in composition.

Finally, the inhomogeneity in exchange interaction near the surface is probably unlikely since the Curie temperature of thin films is experimentally known to be independent of film thickness down to 20 Å (Neugebauer, 1961). The Curie temperature is believed to be a direct measure of the exchange interaction and any sizeable inhomogeneity near the surface is expected to affect the average Curie temperature of very thin films. On the other hand the presence of such an inhomogeneity can be conveniently made part of the other possible inhomogeneities implied in the surface anisotropy model.

On basis of the above arguments it was decided to only explicitly consider the implications of 1) an inhomogeneous demagnetizing field and 2) an inhomogeneous magnetization. These are discussed in Secs. 2.3.2 and 2.3.3 below.

The lack of detailed knowledge of the spatial dependence of any inhomogeneity across the film thickness makes it difficult to make complete estimates of its effect on resonance. However the choice of special physical models makes it possible to answer important qualitative and quantitative questions. Several authors have considered these

effects on basis of two easily tractable models: a parabolic inhomogeneity across the film thickness as initially proposed by A. Portis (1963) and an abrupt inhomogeneity within a layer near the film surface as considered by M. Sparks (1969). Both models are used in the following considerations.

2.3.2 Inhomogeneity of Demagnetizing Field

The boundary condition applicable at the surface in the case of an inhomogeneous demagnetizing field is the boundary condition given in Eq. 2.9. However in the abrupt inhomogeneity model with a surface layer of reduced demagnetizing field, it is also necessary to impose an additional boundary condition at the interface between the surface layer and the bulk of the film. For the perpendicular resonance case this interface condition can be easily derived by torque considerations and is given by

$$\frac{1}{m_b} \frac{\partial m_b}{\partial \xi} = \frac{1}{m_s} \frac{\partial m_s}{\partial \xi} \tag{2.15}$$

where m_b and m_s stand for the bulk and surface R.F. components of the magnetization. Independent of the model, as discussed below, such an inhomogeneity modifies the spatial dependence of the normal mode of the homogeneous system in a way macroscopically equivalent to the partial pinning of m caused by an anisotropy localized at the film surface. (See Sec. 2.2.2). It is, therefore, convenient to discuss the surface anisotropy calculations in this section.

Detailed calculations of the spectral behavior and mode shape of the spin wave modes based on the following three models and their

appropriate boundary conditions have been made: 1) surface anisotropy with easy axis perpendicular to the film plane, 2) a parabolic variation of demagnetizing field across the film thickness, and 3) an abrupt surface layer of reduced demagnetizing field. The first two models were applied to both the parallel and perpendicular resonance geometries. Due to the complexity of the parallel resonance calculation the third model was only applied to the perpendicular resonance case. The results are in agreement with previous calculations but the scope of the calculations was expanded to include the large frequency and thickness variations considered experimentally. The results for the parabolic model are based on computer calculations. The mathematical details are outlined in Appendix 3. A comparison of the results obtained for the three models show that they are analogous. For the sake of brevity only the behavior of the main resonance mode of both geometries and the behavior of the higher order modes for perpendicular resonance are discussed. These are the modes observed experimentally.

A very important feature, previously unnoticed, of all three models is that for a reasonable anisotropy or inhomogeneity a special interpretation of Eq. 2.8 allows the measurement of the average effective demagnetizing field across the film thickness. This is accomplished by setting $k^2 = 0$ and interpreting the terms involving N as the average demagnetizing field. This is because both the surface anisotropy and the two inhomogeneity models shift the resonance fields of the first mode in parallel and perpendicular resonance by an amount which is nearly equal to the difference between uniform resonance with $4\pi NM$ equal to

$4\pi M$ and the average or effective demagnetizing field across the film thickness. This shift is due to a positive exchange term for perpendicular resonance and due to a negative exchange term in parallel resonance.

The effective demagnetizing field for a surface anisotropy K_s is $4\pi M \left[1 - \frac{K_s}{L\pi M^2}\right]$. The effective demagnetizing field for the parabolic inhomogeneity is $4\pi M[1 - \frac{\alpha}{3}]$ where α is the per unit decrease of the demagnetizing field at the film surface. The same shift is predicted in the case of the abrupt surface layer of reduced demagnetizing field for the first mode in perpendicular resonance. In this case the effective demagnetizing field is $4\pi M[1 - \frac{2\beta\varepsilon}{L}]$ where β is the per unit decrease of the demagnetizing field within the surface layers each of thickness ε. As can be noted from these equations it is possible to choose very reasonable inhomogeneity parameters and predict an identical effective demagnetizing field for all three models. For example values of $M = 800$ G, $K_s = .22$ erg/cm^2, $\alpha = 3.3 \times 10^{-7}/L$ and $\beta = \frac{1}{2}$ for $\varepsilon = 11$ Å, all predict a thickness dependent effective demagnetizing field of $[1 - \frac{11 \times 10^{-8}}{L}]$. The detailed results of the main mode calculations for both $\perp$ and $\parallel$ resonance are summarized in Tables 2-1 and 2-2. Note the remarkable similarity of the predictions for all three models.

It is this averaging feature of all three inhomogeneity models when the main resonance mode of both geometries is interpreted as the uniform mode that makes it reasonable to interpret $4\pi NM$ of Eq. 2.8 in terms of the average demagnetizing field of any other inhomogeneity model, for example the case of film surface roughness as calculated by Schlömann. His theoretical prediction of the thickness dependence of N is

Table 2-1

ance fields from fields of unpinned modes in ideal films. ΔHK_s, $\Delta H\alpha$ and $\Delta H\varepsilon$ correspond to deviations calculated lic inhomogeneity of demagnetizing field and abrupt surface layer of reduced demagnetizing field models res- were used: $\gamma = 2.94$ MHz/Oe, $A = 10^{-6}$ erg/cm, $4\pi M = 10^4$G, $K_s = .22$ erg/cm^2, $\alpha = 3.3 \times 10^{-7}/L$, $\beta = 1/2$ for predictions for all three models. Column 2 represents the deviation of the effective demagnetizing field ree models. The deviation of the resonance field of the first mode (Column 3) corresponds closely to the field.

	p = 4			p = 6			p = 8			p = 18		
ε	K_s	α	ε	K_s	α	ε	K_s	α	ε	K_s	α	ε
37.5	46.9	50.3	47.7	50.6	47.1	50.0	52.3	46.6	53.0	54.6	46.6	50.0
--	104	74	--	107	73	--	108	73	---	109	73	--
206	215	133	217	218	133	218	219	133	219	219	133	188
431	435	260	433	438	230	417						

Table 2-2

Difference between the demagnetizing field of an ideal film, $4\pi M$, and the effective demagnetizing field for the anisotropy and parabolic inhomogeneity in demagnetizing field models as calculated from the main mode parallel resonance fields. The following parameters were used: $\gamma = 2.94$ MHz/Oe, $A = 10^{-6}$ erg/cm, $4\pi M = 10^4$ G, $K_s = .22$ erg/cm^2, $\alpha = 3.3 \times 10^{-7}/L$, $f = 9.8$ and 4.9 GHz. The results are independent of frequency for both models. Note the similarity of the predictions for both models and their agreement with Column 2 which shows the deviation of the effective demagnetizing field from that of the ideal film. These results should be compared with the predictions shown in Table 2-1.

Film Thickness (Å)	$10^4(\frac{11}{L})$ (Oe)	$(10^4-4\pi NM)$ (Oe) K_s	$(10^4-4\pi NM)$ (Oe) α
4000	27.5	20	44
2000	55.0	----	69
1000	110	123	127
500	220	----	224
200	550	----	566
100	1100	1140	1132
50	2200	2240	2250
33	3333	----	3380
22	5000	----	----
20	5500	5555	----

$[1 - \frac{3\pi\langle a\rangle^2}{\lambda L}]$, which for the choice of parameters in Sec. 2.1.3 is given by $[1 - \frac{11 \times 10^{-8}}{L}]$. As shown later this value of effective demagnetizing field is in excellent agreement with the experimental results. However as pointed out above this interpretation is indistinguishable from the predictions of the surface anisotropy model or the inhomogeneity of magnetization discussed further in the following section.

These models also predict shifts in the higher order mode resonance fields when these fields are compared to the expected fields for the unpinned modes of an ideal film. The shifts for the perpendicular resonance case are summarized in Table 2-1. As can be noticed from this table, for films thicker than 1000 Å, in which experimental measurements of several higher order modes are possible, these shifts are small and negligibly affect the values of A and $4\pi M$ deduced from interpreting the experimental results in terms of unpinned mode assignments. For example the field shifts expected for a 1000 Å film in perpendicular resonance for surface anisotropy and abrupt inhomogeneity parameters used above are -80 ± 1 Oe for the main mode, -205 ± 1 Oe for the second mode, and -218 ± 2 Oe for the next five or ten higher order modes when compared to the expected fields for the corresponding unpinned modes of an ideal film. For the parabolic inhomogeneity model the shifts are -110 Oe for the main mode, -154 Oe for the second mode and -133 Oe for the next eight higher order modes. For thicker films these shifts are approximately inversely proportional to thickness for all three models. For all cases the shift of the higher order modes is larger than the shift of the main

resonance mode and is essentially independent of mode number for the higher order modes typically observed experimentally. This behavior is analogous to a slightly less than quadratic field separation vs unpinned mode number for the lowest order resonance modes. The effect of these small deviations can be more clearly understood from the resonance equation appropriate to the perpendicular resonance geometry, Eq. 3.3 in the next chapter. As can be seen from this equation, for the case of ideal films, the graphical representation of H vs p^2 would allow a straightforward determination of $4\pi M$ and A. The value of $4\pi M$ could be deduced from the $p = 0$ intercept, and A from the slope of the H vs p^2 line, where, for ideal films $p = 0$ or an even integer, corresponding to the unpinned modes. However, as mentioned before, the presence of either an inhomogeneity or a surface anisotropy would partially pin the spins and only allow the excitation of modes characterized by non-integer p values. The essence of the calculations of this and the next sections is the determination of p appropriate to the surface anisotropy, inhomogeneous demagnetizing and inhomogeneous magnetization models. The calculated value of p is then used to predict the resonance field of the corresponding mode. The field deviations tabulated in Tables 2-1, 2-2, and 2-3 below, are obtained from a comparison of these resonance fields with those of the corresponding unpinned modes of an ideal film. As discussed above the calculated deviations for the higher order modes typically observed experimentally, excluding the main mode for which $0<p<1$, are nearly independent of mode number. The significance of the constant deviations for the higher order modes is that they predict a

slope of the H vs p^2 line which agrees well within 1% with the corresponding slope for an ideal film. Furthermore, the calculated deviations for the first mode, for films thicker than 1000 Å, is also less than 1% of the value of $4\pi M$ for permalloy films. However, it should be kept in mind that the deviation of the first mode is smaller than those of the higher order modes, and should therefore be excluded from the determination of the slope of the H vs p^2 line. The main conclusion that can be drawn from these elaborate considerations is that the use of unpinned mode assignments for the resonance excitations of films with a reasonable surface anisotropy or inhomogeneity, is expected to affect the deduced value of A by less than 1% if the first one or two modes are omitted, and $4\pi M$ by less than 1% if films thinner than 1000 Å are excluded.

The basic reason for the rather small resonance field deviations of the higher order modes in perpendicular resonance when compared to the expected fields for the unpinned modes of an ideal film is that the actual modes are very nearly unpinned for all three models. Detailed calculations of the mode shape for the three models have been made. As mentioned above the calculations for the abrupt inhomogeneity model were restricted to the perpendicular resonance case but the other two models were used for both resonance geometries. The curves of Fig. 2-2 show the ratio of the symmetric mode amplitude at the film surface to its amplitude at the film center vs. film thickness for the main parallel resonance mode and the lower order perpendicular resonance modes for the surface anisotropy model. The following should be emphasized. First, the amplitude of the planar component of the main

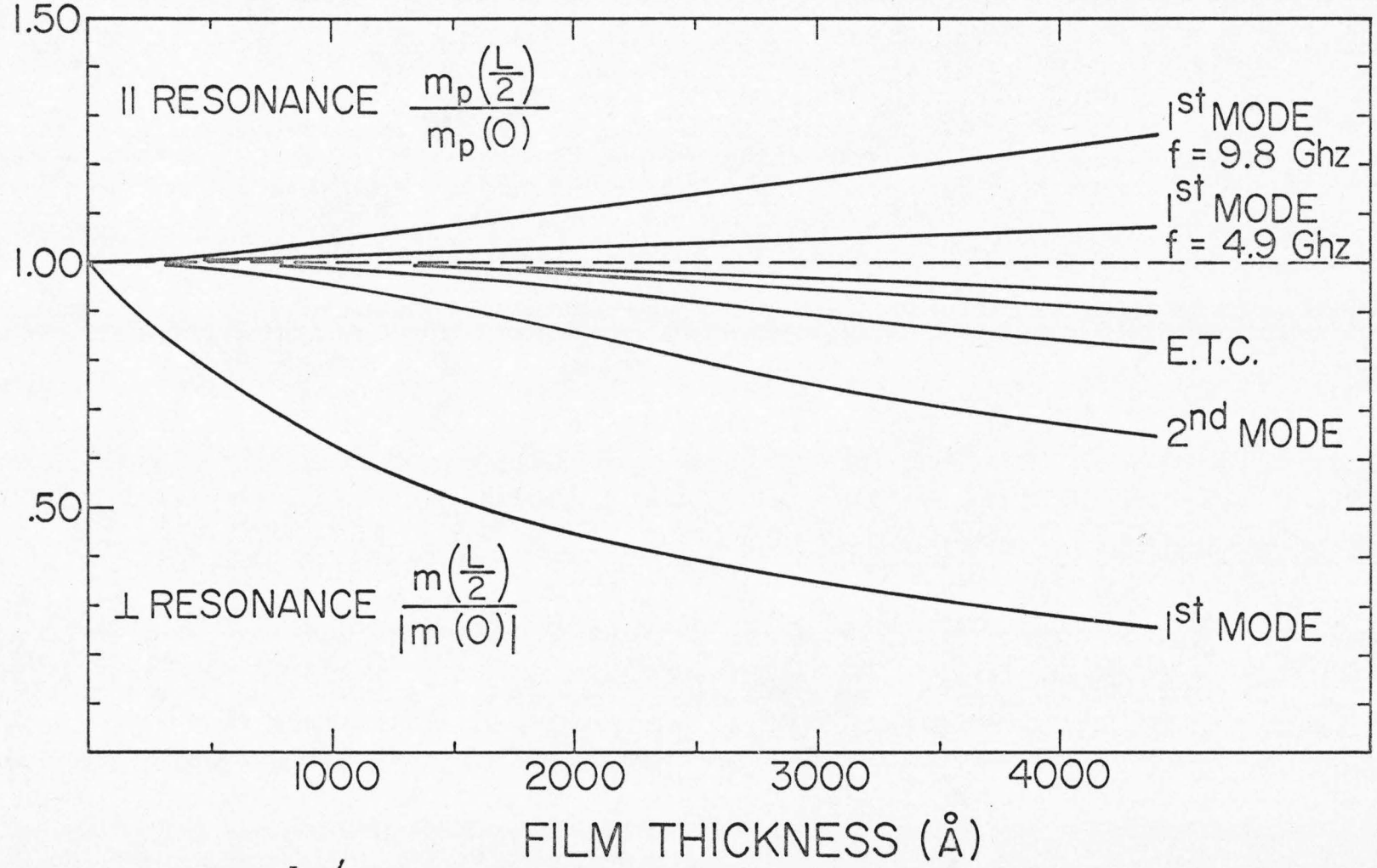

Fig. 2-2 Ratio of $m_p(\frac{L}{2})/m_p(0)$ of the first mode for parallel resonance (upper curve) and ratio of $m(\frac{L}{2})/|m(0)^p|^2$ for perpendicular resonance (lower curves) vs. film thickness. The following parameters were used: $4\pi M$ = 10 K Oe, A = 10^{-6} erg/cm, K_s = .22 erg/cm^2 and γ = 2.94 MHz/Oe.

parallel resonance mode is larger at the surface than at the film center. This is due to a negative exchange field with $k^2 < 0$. This increase in amplitude is both frequency and thickness dependent. The behavior of the normal component of m, whose absolute value is smaller than the planar component due to the elliptical precession of the magnetization caused by the large normal demagnetizing field, is very similar but evidences a slightly larger relative increase in amplitude at the surface. Second, the amplitude of the component of m for all the modes in perpendicular resonance is smaller at the surface than at the film center and corresponds to a positive exchange field with $k^2 > 0$. This decrease in amplitude is thickness dependent but independent of frequency. Third, the degree of pinning at the surface decreases rapidly with thickness and mode number. All modes for very thin films and the higher order modes for all films are very nearly unpinned. Fourth, a comparison of the thickness dependence of the relative amplitudes at the film surface for the main mode in both geometries reveals that the change for the parallel resonance case is much smaller than the corresponding change in perpendicular resonance. This is because the effective anisotropy, K_{eff} of Eqs. 2.13 and 2.14 above, is much smaller than K_s of Eq. 2.12 and consequently results in a weaker pinning of the modes in parallel resonance. The results obtained from the inhomogeneity models agree very well quantitatively with these predictions except that one must now refer to the effective or macroscopic pinning since the actual boundary condition on a microscopic scale is unpinned. This fine difference is illustrated in Fig. 2-3 for the main modes of both resonance

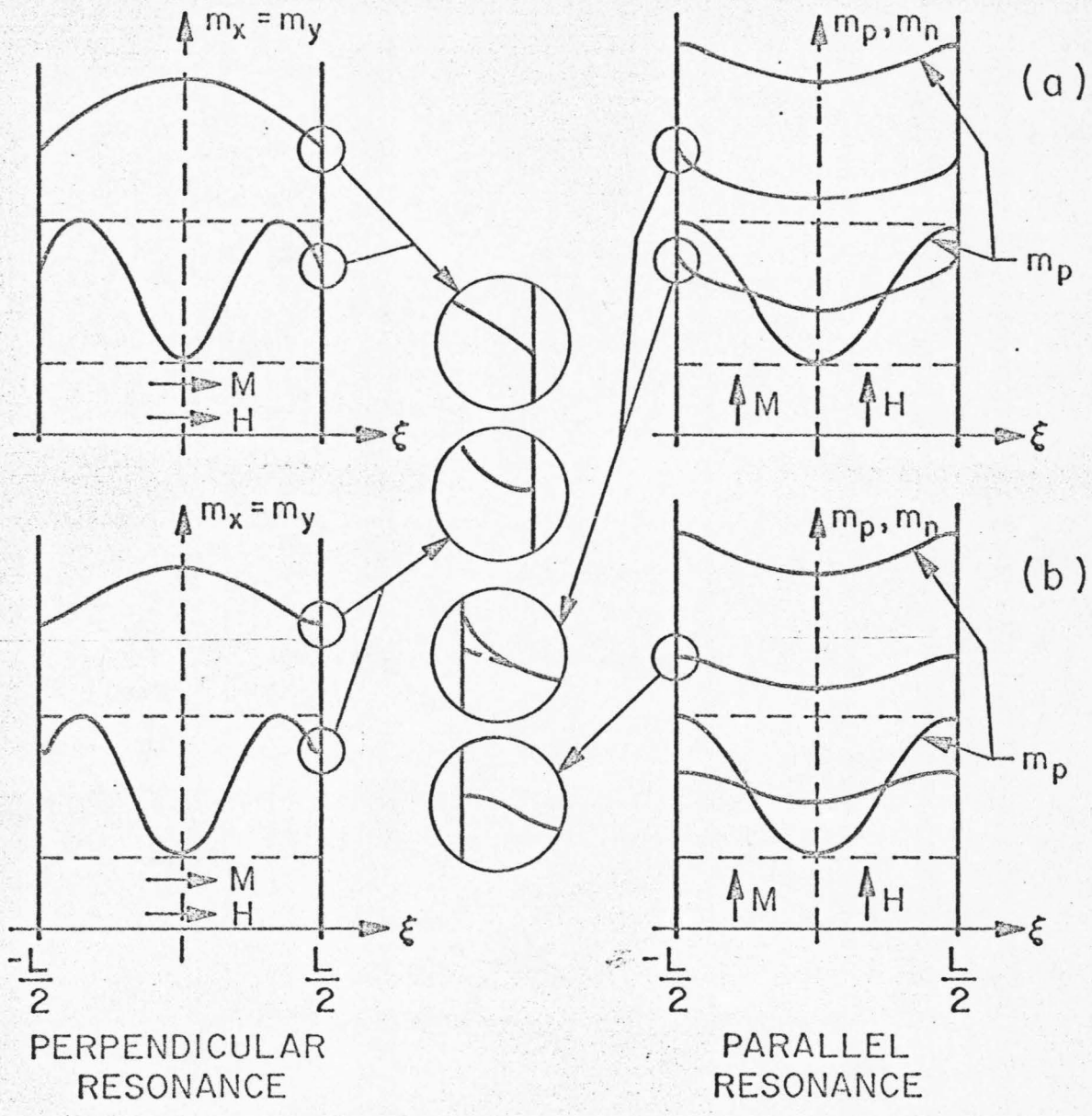

Fig. 2-3a Qualitative representation of the amplitudes of the transverse component of the magnetization for the case of a surface anisotropy K_s localized at the film surface for both the parallel and perpendicular resonance geometries. Note that only the slope of m_p at $\xi = \pm L/2$ is zero. (See Eqs. 2.10 and 2.11).

Fig. 2-3b Qualitative representation of the amplitudes of the transverse component of the magnetization for the case of an inhomogeneity in demagnetizing field or magnetization for both the parallel and perpendicular resonance geometries. Note that the slope of m at $\xi = \pm L/2$ is zero for all cases. The inserts emphasize the fine difference between both models near the surface. It should be emphasized that it is possible to choose parameters for both the anisotropy and inhomogeneity models which give indistinguishable predictions on a macroscopic scale, i.e. the macroscopic wavelengths are nearly identical.

geometries for all three models. These results are not included in Fig. 2-2 for the sake of clarity. For simplicity and on basis of the experimental evidence shown below, the above calculations were restricted to films with symmetrical properties about their center. However, these could be easily extended to account for asymmetries, and Fig. 2-2 would then approximately represent the average pinning at both surfaces.

In essence, a detailed analysis of the possible implications of a surface anisotropy or inhomogeneous demagnetizing field clearly shows that for a reasonable anisotropy or inhomogeneity the calculated resonance field of the main mode in both resonance geometries averages the effective demagnetizing field across the film thickness, and all the modes for thin films and the higher order modes for thick films are very nearly unpinned. Furthermore, the higher order mode field deviations from the corresponding unpinned mode fields for ideal films thicker than 1000 Å negligibly affect the values of A and $4\pi M$ deduced from interpreting the experimental results in terms of unpinned mode assignments. It is possible to choose parameters which give virtually indistinguishable predictions for the three models considered in this section.

2.3.3 Inhomogeneity of Magnetization

Both the parabolic and abrupt surface inhomogeneity models have been originally and specifically applied to study the resonance effects of an inhomogeneous magnetization across the film thickness by several authors (Wigen et al., 1964; Sparks, 1969). However none of the previous calculations covered the range of variables considered in this investigation. In this section detailed results for the case of an abrupt surface

layer of reduced magnetization near the surface of a film are discussed for the perpendicular resonance geometry. The parallel resonance geometry is only considered qualitatively due to the complexity of the calculation. In principle, it is also possible to make detailed calculations for the parabolic model, however, this was also avoided due to the cumbersome and complex nature of the problem when the inhomogeneity applies to the magnetization instead of just the demagnetizing field as was considered in the previous section. This difference is discussed in more detail in Sec. A3.4 of Appendix 3.

For the abrupt surface layer of reduced magnetization in the absence of a surface anisotropy the boundary condition applicable at the film surface is the exchange boundary condition of Eq. 2.9, namely, $\frac{\partial m_s}{\partial n} = 0$ at $\xi = \pm \frac{L}{2}$. However as in the case of an abrupt surface layer of reduced demagnetizing field it is also necessary to impose an additional boundary condition at the interface between the surface layer and the bulk of the film. For the perpendicular resonance case this interface condition can be easily derived by torque considerations. If the exchange coupling at the interface is assumed comparable to the exchange on both sides of the interface this condition is well approximated by:

$$\frac{1}{m_b} \frac{\partial m_b}{\partial \xi} = \frac{A_s}{A_b} \frac{1}{m_s} \frac{\partial m_s}{\partial \xi} \qquad \text{at } \xi = \pm \left(\frac{L}{2} - \varepsilon\right) \tag{2.16}$$

where m_b and m_s stand for the bulk and surface R.F. components of the magnetization and ε is the thickness of the surface layers.

In detail, the following results are obtained by assuming that $A_s = A_b$ and $M_s = \frac{1}{2} M_b$. To first order these assumptions reasonably

characterize a permalloy film with a nickel rich surface layer which could arise due to preferential oxidation of Fe in an 81% Ni-19% Fe film since the magnetization of Ni is lower than the magnetization of permalloy.

The results for the spectral behavior in perpendicular resonance are summarized in Table 2-3. These apply specifically to the case of a symmetric inhomogeneity of $\varepsilon = 22$ Å on both sides of a film whose actual thickness is L and magnetic thickness is $L_{mag} = L-22$ Å. They can be readily applied to the asymmetric case with $\varepsilon = 22$ Å on one side by halving L_{mag}. This distinction of thickness is important since experimentally it is often convenient and customary to deduce the film thickness from magnetic measurements of the average magnetic moment of a sample (see Appendix 2). The value of ε was chosen to give resonance field shifts of the same general magnitude found in the previous section.

The following details of Table 2-3 should be emphasized. First the calculated resonance fields for all the modes deviate from, and are lower than, the resonance fields for the unpinned modes of an ideal film of thickness $L = L_{mag}$. This shift is due to the partial pinning of the bulk spins at the interface $\xi = \pm \left(\frac{L}{2} - \varepsilon \right)$. For films thicker than 1000 Å these deviations are small, inversely proportional to thickness, and very similar quantitatively and qualitatively to the deviations calculated in the preceding section for the case of an inhomogeneity in demagnetizing field. As in that case, these deviations only become significant for films thinner than 1000 Å. Note that the deviations of the first and higher order modes correspond very closely to the predictions

Table 2-3

Deviation of Perpendicular Resonance Fields, $\Delta H_{M/2}$, for films with $M_s = \frac{M_b}{2}$ within a layer ε on both sides of the film, from resonance fields of unpinned modes in ideal films of $L = L_{mag}$. The following parameters were used: $4\pi M_b = 10^4$G, $4\pi M_s = 5 \times 10^3$G, $\varepsilon = 22$ Å on both sides of film, $\gamma = 2.94$ MHz/Oe, and $A_s = A_b = 10^{-6}$ erg/cm. Column 3 represents the same quantity tabulated in Column 2 of Tables 2-1 and 2-2. Note that the deviation of the first resonance mode (Column 4) corresponds very closely to this quantity making this prediction indistinguishable from the surface anisotropy and inhomogeneity of demagnetizing field models. Column 5 represents the difference between the bulk saturation magnetization and the average saturation magnetization across the film thickness. Comparison with Column 4 shows that the deviation of the first mode allows a reasonable ($\sim$ 800 G) measurement of the average saturation magnetization across the film thickness.

			Unpinned Mode Number p = 0		p = 2	p = 4	p = 6	p = 8	p = 18
Actual Film Thickness L(Å)	Magnetic Film Thickness L_{mag} (Å)	$10^4 \times \frac{11}{L_{mag}}$ (Oe)	$\frac{\Delta H}{M}$ / 2 (Oe)	$10^4 \times \frac{22}{L_{mag}+22}$ (Oe)	$\frac{\Delta H}{M}$ / 2 (Oe)	$\frac{\Delta H}{M}$ / 2 (Oe)	$\frac{\Delta H}{M}$ / 2 (Oe)	$\frac{\Delta H}{M}$ / 2 (Oe)	$\frac{\Delta H}{M}$ / 2 (Oe)
4022	4000	27.5	10.4	54.8	37.4	47.6	50.0	53.2	-51.7
2022	2000	55.0	30.2	109	----	----	----	----	----
1022	1000	110	79.6	215	205	217	217	207	-512
522	500	220	186.4	422	429	415	-----	-----	-----
222	200	550	515.3	991	926	-----	-----	-----	-----
122	100	1100	1069	1802					
72	50	2200	2186	3055					
44	22	5000	5000	5000					

of the surface anisotropy and the inhomogeneous demagnetizing field models. (Compare with Tables 2-1 and 2-2). To aid in this comparison, the quantity of $10^4 \times \frac{11}{L_{mag}}$ is tabulated in column 3. The quantity $\frac{4\pi M\varepsilon}{L_{mag} + \varepsilon}$ which represents the difference between the bulk saturation magnetization and the average magnetization across the film thickness, is also given in column 5 of this table. As can be noticed the thickness dependence of the first resonance mode deviation is in qualitative agreement with this quantity. To the extent of this agreement the interpretation of the first resonance mode as the uniform mode would in principle allow a reasonable measure of the average magnetization across the film thickness. This can be accomplished by considering the $4\pi NM$ terms of Eq. 2.11 as a measure of the average magnetization when $k^2 = 0$. Finally, these deviations are also quantiatively consistent with the degree of pinning represented in Fig. 4, namely that the first mode in thin films and the higher order modes in thick films are very nearly unpinned.

Similar predictions are expected from the deviations of the first resonance mode in parallel resonance. Although no detailed calculations were performed, this conclusion can be drawn from the parabolic inhomogeneity treatment of demagnetizing field for parallel resonance of Appendix 3 since for large film thickness and small inhomogeneity the results for an inhomogeneous demagnetizing field and magnetization are very similar.

The most important conclusion that can be drawn from the above results is that an inhomogeneous magnetization can also partially pin the spin wave modes of an ideal film. As was the case in the previous

section this affects negligibly the values of A and $4\pi M_s$ deduced from interpreting the experimental results in terms of unpinned mode assignments for films thicker than 1000 Å. On the other hand it can give rise to significant deviations of the first mode resonance field in thin films which can be used to reasonably measure the average saturation magnetization across the film thickness. However, to first order, these deviations are indistinguishable from the predictions based on an inhomogeneity in demagnetizing field or a surface anisotropy.

2.4 Summary

By taking into account the applied, demagnetizing, effective anisotropy and exchange fields, the spin wave resonance condition applicable to the thin film geometry is presented in Eq. 2.8. On basis of the exchange boundary condition, Eq. 2.9, it can be concluded that the normal resonance modes of an ideal film are expected to be unpinned. The possibility of nonideality near the surface of a film was considered by means of a surface anisotropy, inhomogeneity in demagnetizing field, and inhomogeneity of magnetization. The numerical results obtained for reasonable parameters in all cases clearly show that they negligibly perturb the resonance fields and the higher order mode shapes of the unpinned modes of ideal films for thickness greater than 1000 Å. On the other hand for films thinner than 1000 Å the resonance field deviations can be significant even though the modes are very nearly unpinned. For both the surface anisotropy and demagnetizing field inhomogeneity cases the interpretation of the first mode as the uniform mode of an ideal film allows an accurate measurement of the average effective demagnetizing

field across the film thickness. However it is possible to choose parameters which give indistinguishable results for both models. Furthermore it is possible to choose parameters for the inhomogeneous magnetization model which also give indistinguishable predictions from the above models. The discussion of the widely used perfectly pinned model in Sec. 2.2.2 shows that its use is difficult to justify on realistic physical grounds. The similarity of the pinning predictions for the surface anisotropy model and the inhomogeneity models makes it difficult to uniquely determine the source of the pinning from resonance measurements alone. This determination will require additional complementary experiments which allow a direct and independent measure of the various physical characteristics. The above conclusions will be the basis for the interpretation of the experimental results in the next chapters.

Chapter 3

SPIN WAVE RESONANCE MEASUREMENTS

3.1 Introduction

This chapter emphasizes the experimental resonance results for normal permalloy films covering a 30 to 9000 Å thickness range. The term normal refers to films which, following their evaporation, are exposed to an ambient environment without taking any measures to prevent or enhance surface oxidation. The following description of sample preparation and detection of resonance applies to all the films considered in this investigation.

3.2 Choice of Sample Composition, Preparation of Samples, and Detection Of Resonance

The film composition of 81% Ni-19% Fe was chosen because the properties of the alloy are close to ideal in terms of its resonance behavior as well as many other practical applications. Some of the important characteristics of polycrystalline permalloy of this composition are: zero magnetostriction, low coercive field ($H_c \simeq 1$ to 2 Oe), small planar anisotropy ($H_{k_{\parallel}} \simeq 5$ Oe), small perpendicular anisotropy ($H_{k_{\perp}} \simeq 100$ Oe), and small dispersion of the orientation of the magnetization. Very importantly these parameters are nearly independent of film thickness. These properties are essential if Eq. 2.8 is to be used reliably to investigate the exchange behavior, magnetization, and demagnetizing field of films over a 30 to 9000 Å thickness range. In addition this material has

relatively very small resonance linewidths making it easier to detect and accurately measure the resonance excitations. No other materials in the transition elements or their alloys are known to simultaneously possess the above properties.

The 1 cm diam permalloy films were evaporated at a rate of 500 Å/min from inductively heated melts of 83% Ni-17% Fe in alumina crucibles onto .8 mm thick Corning 0211 glass substrates at 200°C and at room temperature in a vacuum better than 1×10^{-6} Torr in the presence of a 30 Oe magnetic field parallel to the substrate. The vacuum system uses a conventional oil diffusion pump with liquid nitrogen trapping. With the aid of a liquid nitrogen trap in the evaporating chamber the system was capable of achieving a base pressure of 1×10^{-7} Torr. The substrate temperature was established by a black body cavity arrangement of the substrate holder and shutter. The applied field allowed control of the orientation of the planar anisotropy easy axis, the planar axis of preferred orientation for the magnetization. A resistively heated source allowed the option of overcoating the films with other materials immediately after their evaporation. The usual procedure followed in making overcoated films was as follows: 1) bring inductively heated permalloy source up to evaporation temperature, 2) heat resistive source just below its evaporation threshold, 3) expose substrates to permalloy source, 4) after concluding permalloy evaporation, expose films to resistively heated source, and 5) increase the temperature of the resistive source to obtain an adequate evaporation rate. The transition between steps 3 and 5, and the achievement of an adequate evaporation rate could be typically

completed in less than five seconds. Both sources had independently controlled shutters. Another special shutter arrangement specifically constructed for this investigation allowed for the simultaneous preparation of sixteen films, four each of four different thicknesses, assuring maximum composition and preparation environment uniformity for each set. The thickness range of 30 to 9000 Å was covered by overlapping the thickness range of several sets of coevaporated samples. The film thickness was determined using a hysteresis loop tracer, torquemeter and X-ray fluorescence spectrometer, all of which were calibrated with samples whose thickness was measured with a Tolansky (1948) multiple reflection interferometer. The thickness deduced from hysteresis loop tracer and torque magnetometer measurements is defined as the magnetic thickness. The thickness deduced from X-ray fluorescence measurements is defined as the ideal thickness. The magnetic thickness can only be equal to the ideal thickness if the average saturation magnetization is independent of film thickness. This difference is explained in more detail in Appendix 2. Unless otherwise specified, the film thickness used in Chapter 3 is the magnetic thickness determined by either the hysteresis loop tracer or torque magnetometer. The hysteresis looper has a field range of 100 Oe and the torque magnetometer has a field range of 700 Oe. Both fields are sufficient to fully saturate all the permalloy films used in this investigation. The composition of all samples was found to be 81 ± 1% Ni-Fe using X-ray fluorescence techniques.

All the resonance measurements were performed by placing the samples

against the ground plane of a three septum, 50Ω, strip line section driven by oscillators in the 1 to 8 GHz frequency range. The resonance excitation was determined by phase sensitive detection of the crystal output at the output end of the microwave system and displayed on an X-Y recorder. The static magnetic field perpendicular to the film plane was applied by an electromagnet with a 16 kOe range and measured with an N.M.R. spectrometer. The static magnetic field parallel to the film plane was applied by a pair of helmholtz coils with a 700 Oe range. The coils were also calibrated with an N.M.R. spectrometer. The strip line had provisions to orient the film plane and normal within 0.1° of the corresponding applied field direction.

The description of the oxidation treatments for the oxidized samples is deferred until Chap. 5.

3.3 Evidence for Partially Pinned Spin Wave Modes In Permalloy Films

Figure 3-1 shows a representative resonance spectrum obtained with the magnetic field applied parallel and perpendicular to the film plane for a film 2580 Å thick at 7.5 GHz. The perpendicular resonance case is characterized by the excitation of a strong mode, the main resonance, and a series of progressively weaker subsidiary excitations of alternating intensities. The strong and weak signals are presumably associated with symmetric and antisymmetric spin wave modes about the center of the film. This presumption would not be valid in the case of a uniform R.F. field and an ideal film since for this situation one would only expect to couple to the main resonance mode, the uniform mode. This is because the modes of an ideal film are trigonometric functions of $k\xi$ and the

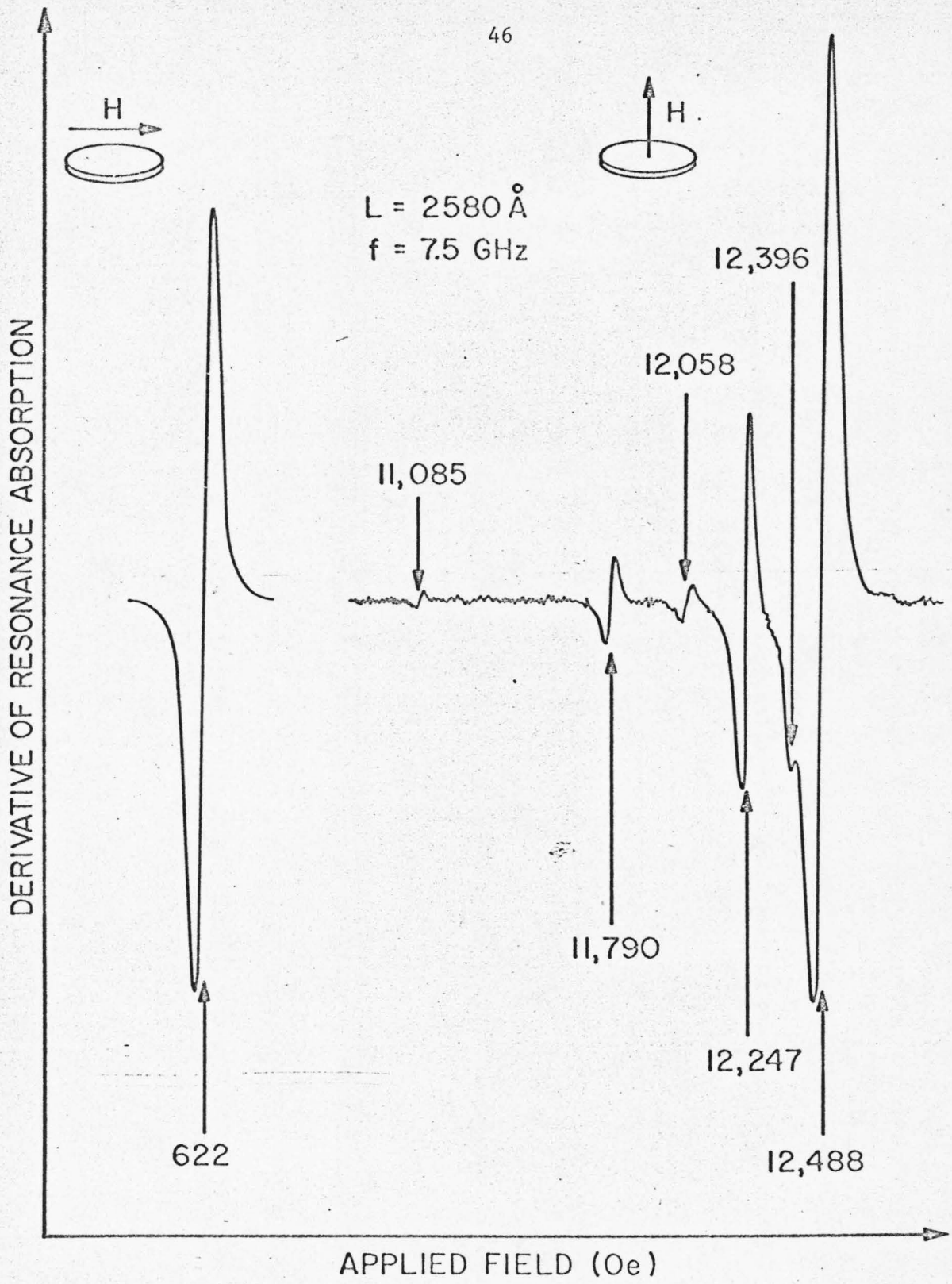

Fig. 3-1. Derivative of resonance absorption vs. applied magnetic field parallel and perpendicular to the film plane for a film 2580 Å thick at 7.5 GHz.

power absorption which is proportional to $\bar{m} \cdot \bar{h}_{R.F.}$ integrated across the sample would be zero for all the modes except for the uniform mode. However it must be kept in mind that, as discussed in Chap. 2, the presence of an inhomogeneity in demagnetizing field or magnetization, or a surface anisotropy would partially pin the spins near the surface and consequently allow the excitation of the higher order modes. Furthermore this excitation is also made favorable since these films are conductors which will give rise to an inhomogeneous R.F. field due to skin depth effects. The excitation of the alternating weaker modes is indicative of a slight asymmetry in pinning, a possible small asymmetry of the R.F. field caused by unknown strip line film interactions or a possible small asymmetry in the film properties about its center. The presence of any significant asymmetries would cause these modes to be excited as strongly as the symmetric modes. The absolute and relative field position of all the modes at a fixed frequency depends on film thickness.

The parallel resonance case is characterized by the excitation of only one observable mode whose field position is also thickness dependent. The absence of any detected higher order modes in parallel resonance is probably due to the fact that the effective pinning in parallel resonance for all the possibilities discussed in Chap. 2 is considerably weaker than the corresponding pinning in perpendicular resonance and is consequently beyond the sensitivity of the strip line system. This conclusion is supported by the results of other investigators who in some cases, with the use of resonant cavities, with greater sensitivities, have been able to detect two or three very weak higher order modes in parallel

resonance. (Nissenoff and Terhune, 1965; Bailey, 1970). A self consistent identification of these modes with varying film thickness, frequency, and resonance geometry allows a unique determination of the exchange constant and the degree of surface spin pinning.

The experimental results can be conveniently analyzed by rewriting Eq. 2.8 in the following form:

(a) H applied parallel to the film plane and perpendicular to the easy axis; $\beta = 0$, $\theta = \frac{\pi}{2}$, $\phi = \frac{\pi}{2}$

$$f^2 - \left(\frac{\gamma}{2\pi}\right)^2 H^2 = \left(\frac{\gamma}{2\pi}\right)^2 (H - H_{k_{\parallel}}) 4\pi NM \ . \tag{3.1}$$

The exchange term was omitted from Eq. 3.1 since the parallel resonance case only shows one excitation and as explained in Chap. 2 the exchange contribution can be accounted for by using the mean value of $4\pi NM$ and interpreting the resonance as an unpinned uniform mode.

(b) H applied perpendicular to the film plane; $\beta = 0$, $\theta = \frac{\pi}{2}$, $\phi = 0$

$$f = \frac{\gamma}{2\pi} H - \frac{\gamma}{2\pi}\left[4\pi NM - \frac{2A}{M}\left(\frac{\pi}{L}\right)^2 p^2\right] \tag{3.2}$$

or equivalently

$$H = \frac{2\pi f}{\gamma} + 4\pi NM - \frac{2A}{M}\left(\frac{\pi}{L}\right)^2 p^2 \ . \tag{3.3}$$

In the above equations the terms $H_{k_{\parallel}}$ and $H_{k_{\perp}}$ were excluded from the factors involving $4\pi NM$ since they are negligible for 81% Ni-19% Fe permalloy films. The exchange term, with $k = \frac{p\pi}{L}$, was not omitted since

it must be used to examine all the modes detected in perpendicular resonance. The thickness dependence of the slopes and zero intercepts of the graphical representation of $\left[f^2 - \left(\frac{\gamma}{2\pi}\right)^2 H^2\right]$ vs. H (Eq. 3.1), f vs. H (Eq. 3.2) and H vs. p^2 at a fixed frequency (Eq. 3.3) can be used to determined $4\pi M$ and the degree of surface spin pinning.

In Fig. 3-2 $\left[f^2 - \left(\frac{\gamma}{2\pi}\right)^2 H^2\right]$ as a function of applied field is displayed for the single parallel resonance mode of a set of coevaporated films 28 to 350 Å thick. The following two points should be emphasized. First, the $\left[f^2 - \left(\frac{\gamma}{2\pi}\right)^2 H^2\right] = 0$ intercept is about 5 Oe, independent of film thickness. This agrees well with the value of $H_{k_{\parallel}}$ determined by the hysteresis loop tracer. Second, the slopes of the lines decrease monotonically with thickness implying through Eq. 3.1 either a thickness dependent mean demagnetizing field or a thickness dependent mean magnetization. As pointed out in Chap. 2 a surface anisotropy, inhomogeneous demagnetizing field or inhomogeneous magnetization would give rise to a negative exchange field for the main mode of the parallel resonance geometry. This negative exchange field shifts the main mode resonance field by an amount which effectively averages the demagnetizing field or magnetization across the film thickness. The quantitative analysis of the thickness dependence of this shift and a discussion of its origin are deferred until Fig. 3-7. Independent of these details the above results clearly show that the surface spins in the parallel geometry are not perfectly pinned since this situation would not allow an $\left[f^2 - \left(\frac{\gamma}{2\pi}\right)^2 H^2\right] = 0$ intercept of +5 Oe and a monotonic decrease of slopes with thickness. For example the 2 kOe exchange field corresponding to perfect pinning

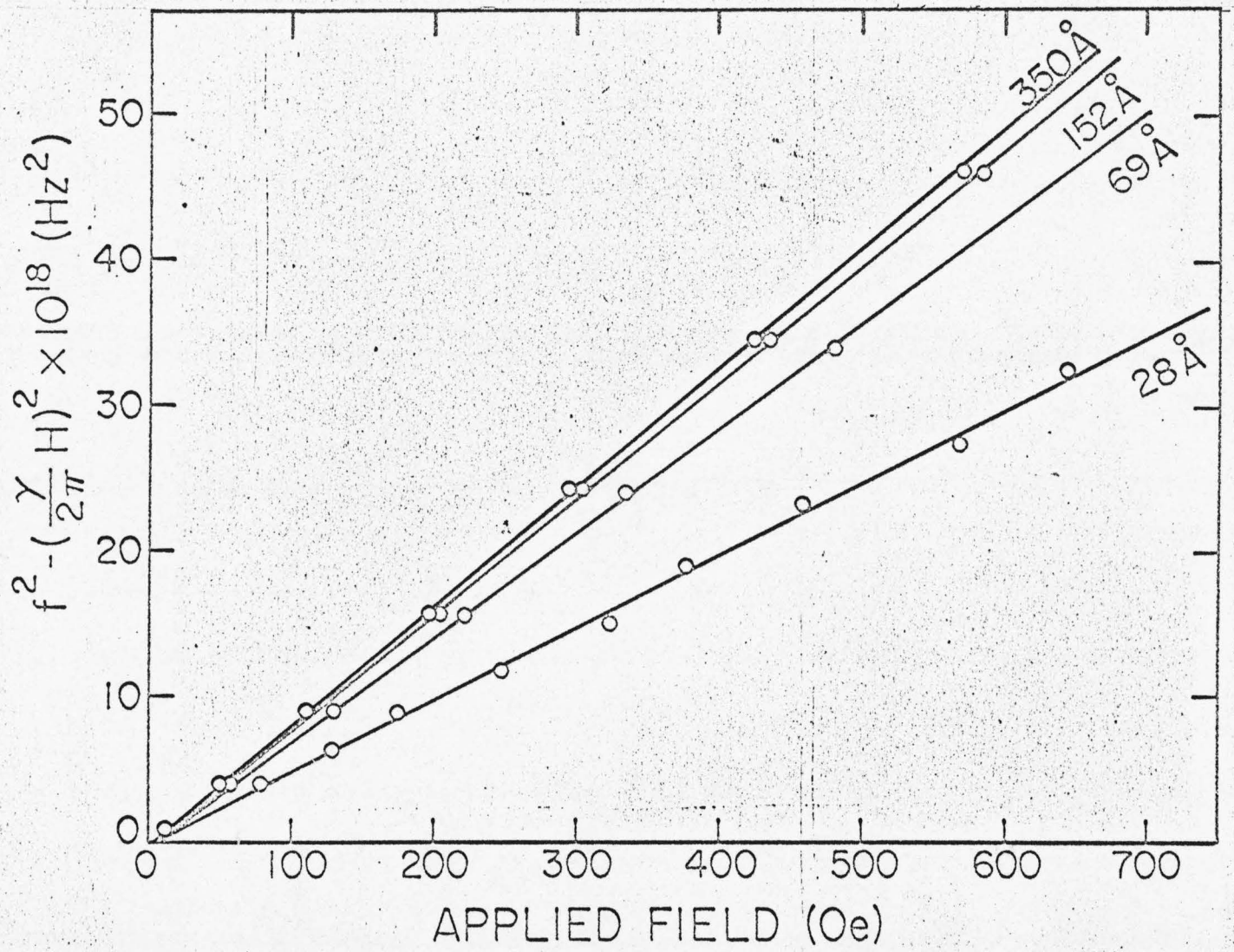

Fig. 3-2 Plot of $[f^2 - (\frac{\gamma}{2\pi})^2 H^2]$ vs. applied field parallel to the film plane for a set of coevaporated films 28 to 350 Å thick.

of the first mode of the 350 Å film would give rise to an $\left[f^2 - \left(\frac{\gamma}{2\pi}\right)^2 H^2\right]$ = 0 intercept of -1700 Oe instead of +5 Oe as can be easily calculated from Eq. 3.1 by using the magnetic parameters for 81% Ni-Fe films. Furthermore, the exchange field corresponding to perfect pinning of the first mode of the 69 Å film would cause over a tenfold increase in the corresponding slope instead of the observed 20% decrease. Data for films thicker than 350 Å are used subsequently but are not included in this figure for clarity since the lines for the thicker films fall very close to the line of the 350 Å film.

In Fig. 3-3, f as a function of applied field perpendicular to the film plane is displayed for the main resonance mode of a set of coevaporated films 28 to 350 Å thick and a set 845 to 3500 Å thick. The slopes for the thick set are equal and from Eq. 3.2 yield $\frac{\gamma}{2\pi}$ = 2.94 MHz/Oe corresponding to g = 2.10. This value is in agreement with previously reported values of g. The low frequency data for the thinner set deviates slightly from the corresponding lines of equal slope. This small deviation can be explained by lack of full saturation of the thin films at the lower fields. As discussed in Chap. 2 the zero frequency intercept can be interpreted as the effective field $4\pi NM$. This intercept decreases with thickness and agrees within 2% with the value obtained as described earlier from parallel resonance for all films 44 to 3500 Å thick. In this thickness range, $4\pi NM$ decreases by more than 20%. This decrease and agreement with the parallel resonance results are consistent with a thickness dependent mean demagnetizing field or mean magnetization. As pointed out in Chap. 2 a surface anisotropy, inhomogeneous demagnetizing

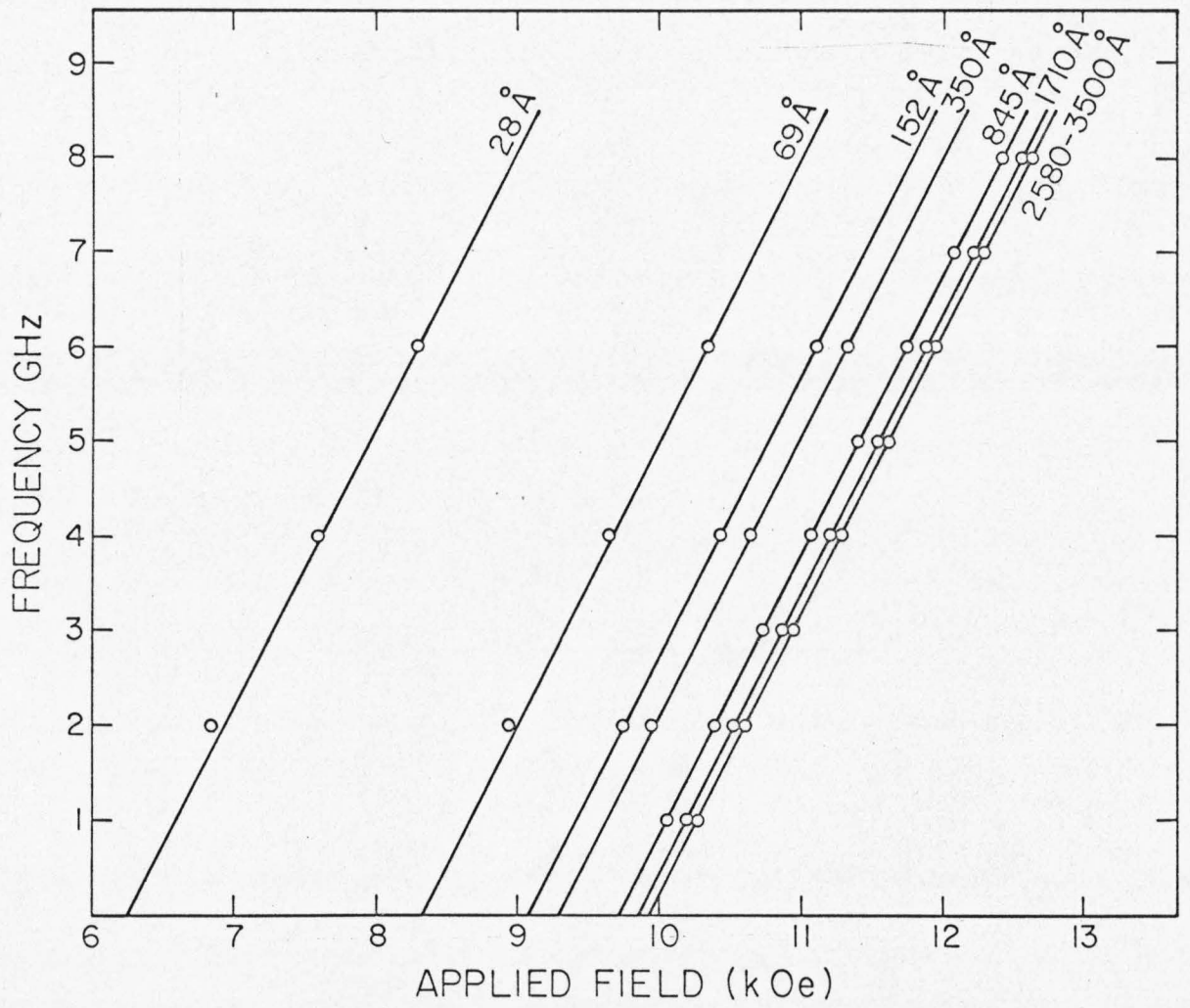

Fig. 3-3 Plot of f vs. applied field perpendicular to the film plane for a set of coevaporated films 28 to 350 Å thick and a set 845 to 3500 Å thick.

field or inhomogeneous magnetization would give rise to a positive exchange field for the main mode of the perpendicular resonance geometry. This field shifts the main mode resonance field by an amount which also effectively averages the demagnetizing field or magnetization across the film thickness. The quantitative analysis of the thickness dependence of this shift and a discussion of its origin are deferred to Fig. 3-6.

In Figs. 3-4 and 3-5, H as a function of p^2 is displayed for all the modes detected in perpendicular resonance at 7.5 GHz for the thick set of films in Fig. 3-3 and another set 1420 to 6990 Å thick. For clarity, the results for $p^2 \leq 16$ are shown on an expanded scale in Figs. 3-4b and 3-5b. The open and closed circles shown for each film correspond to the assignment of odd (pinned modes) or even (unpinned modes) p integers to the more intense resonances. For films thicker than 1500 Å straight lines are fitted to the higher order modes since, as discussed in Chap. 2, the slopes of the lines determined by these, are expected to be least affected by eddy current effects, inhomogeneities or a surface anisotropy. For the thinnest films the lines were constructed using a consistent assignment regarding the p = 0 intercept. Had a line through the actual two points been used, the results discussed in the following paragraph would be little different for the even assignment but considerably worse for the odd assignment. The following should be emphasized. Both choices allow a reasonable fit to the H vs. p^2 dependence. However, for most films investigated the first one or two modes deviate from the lines determined by the higher order modes. For the odd assignment this deviation is independent of frequency but is thickness dependent, as

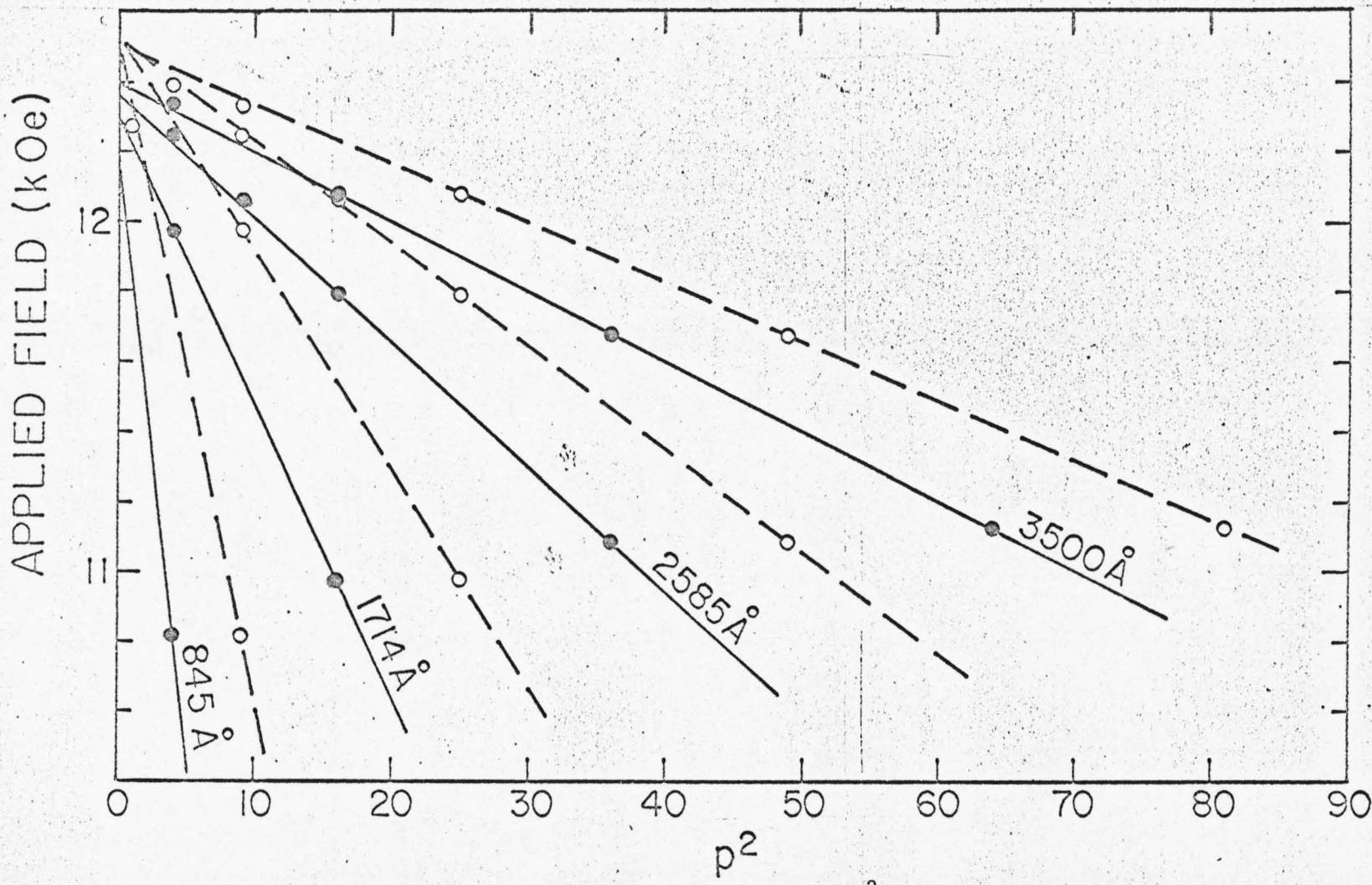

Fig. 3-4a Applied field perpendicular to the film plane vs. p^2 for a set of coevaporated films 845 to 3500 Å thick at f = 7.5 GHz. O, correspond to odd (pinned case) p assignments. ●, correspond to even (unpinned case) p assignments to the strong modes.

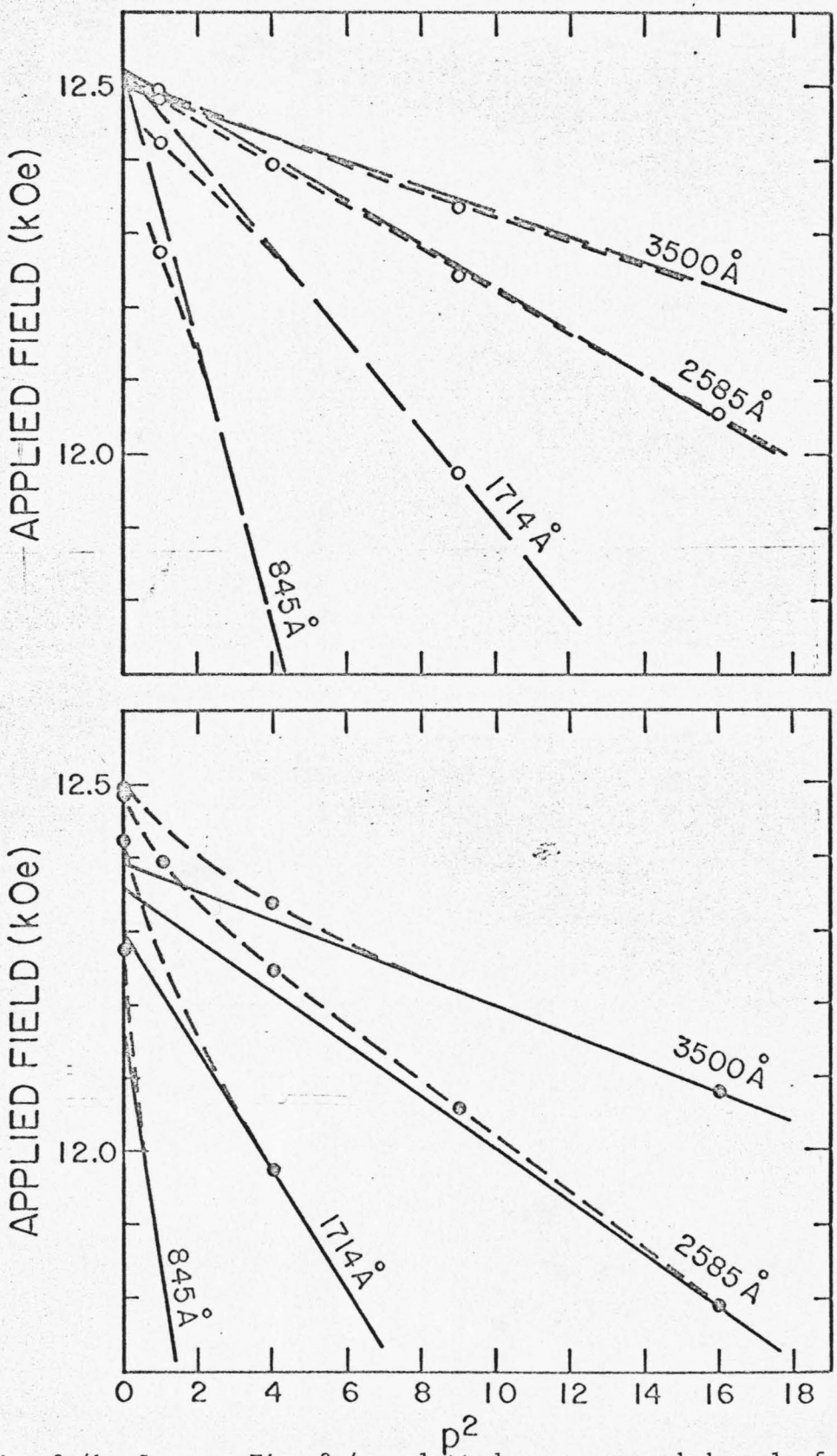

Fig. 3-4b Same as Fig. 3-4a, plotted on an expanded scale for $p^2 \leq 16$.

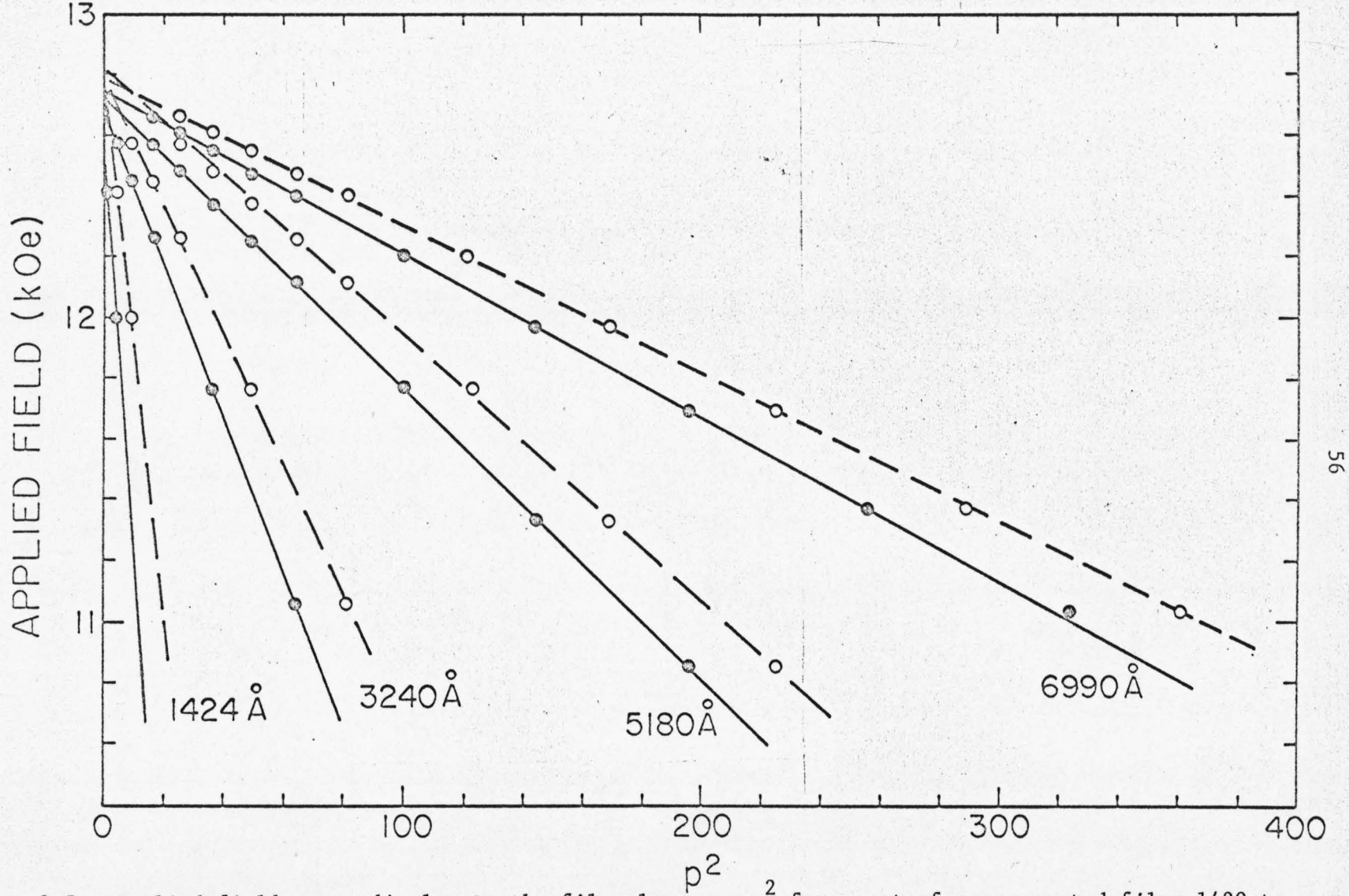

Fig. 3-5a Applied field perpendicular to the film plane vs. p^2 for a set of coevaporated films 1420 to 6990 Å thick at f = 7.5 GHz. O, correspond to odd (pinned case) p assignments. ●, correspond to even (unpinned case) p assignments to the stronger modes.

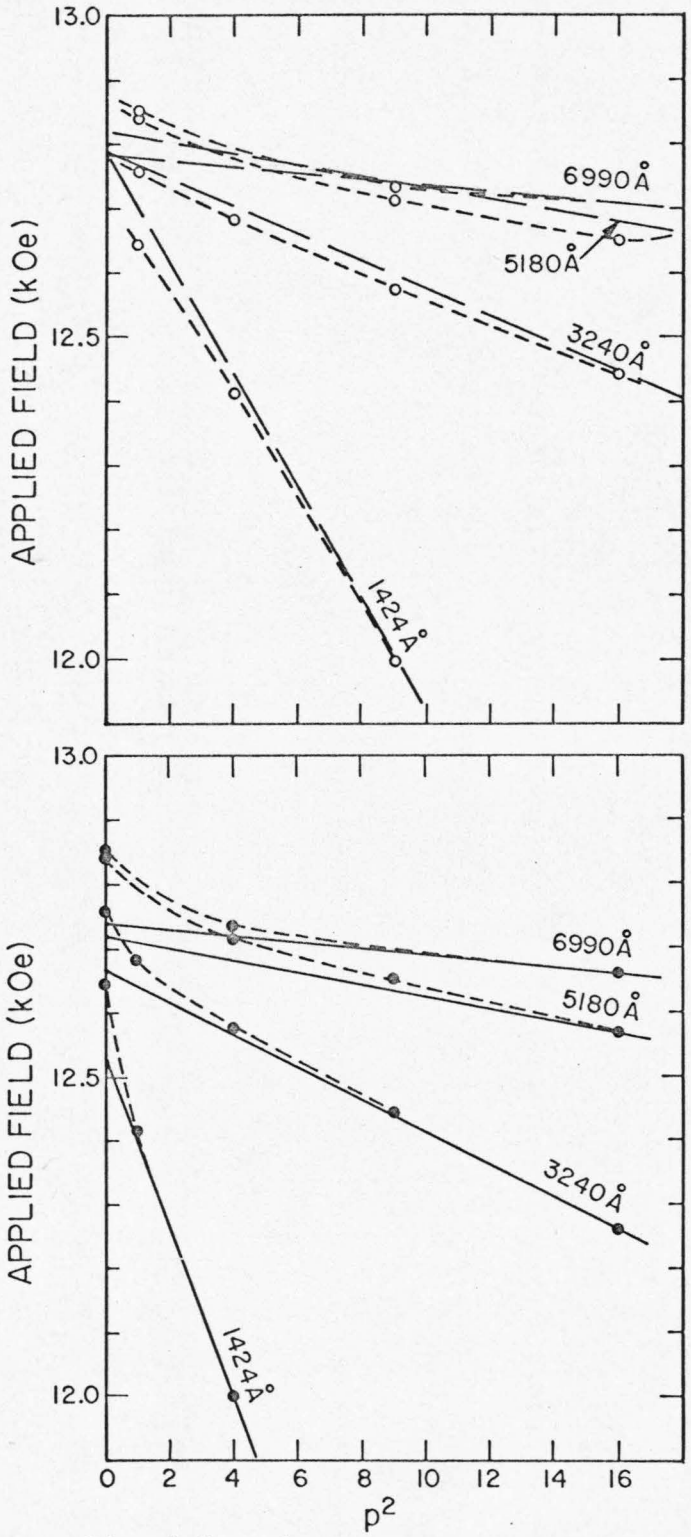

Fig. 3-5b Same as Fig. 3-5a, plotted on an expanded scale for $p^2 \leq 16$.

large as 75 Oe, positive for the p = 1 mode of the thicker film, and becoming negative for thinner films. For the even mode assignment the deviation is independent of thickness and frequency, always positive and about 110 Oe for the p = 0 mode. This deviation was measured in the frequency range of 1 to 8 GHz and found to be totally independent of frequency for all films. Both exchange conductivity shifts and volume inhomogeneities of the magnetization have been used to explain this deviation in the past. We question the exchange conductivity explanation since it should always lower the resonance field of the first mode relative to the others and should be strongly frequency dependent. On the other hand it may be significant that the observed deviation is at least in qualitative agreement with surface anisotropy and inhomogeneity models which predict the observed less than quadratic field separation for the low order modes and a quadratic field separation with unchanged slope for the higher order modes if these are labeled as unpinned modes. However this deviation is quantitatively too large for films thicker than 3500 Å since as shown in Fig. 3-5b it cannot be eliminated even by assigning odd numbers (perfect pinning) to the modes of the two thickest films. This assignment should reverse the sign of these deviations for all films. Nevertheless these unexplained small deviations insignificantly affect the interpretation of $4\pi NM$ since they are only a small fraction of this quantity.

The most important information of Figs. 3-4 and 3-5 is contained in the product of $(L)^2$ and the slope of the corresponding line (which by Eq. 3.3 is directly proportional to $\frac{A}{M}$). Data for three sets of films

including those of Figs. 3-4 and 3-5 are summarized in Table 3-1. The products corresponding to the perfect pinning assignment show 53%, 37%, and 22% spreads. These spreads reduce to only 3%, 6%, and 7% respectively for the unpinned assignment. The small residual spreads could be largely explained by errors in thickness measurements (±2%) and are consistent with a unique exchange constant A. This result strongly supports the absence of significant spin pinning for the higher order modes. The large spreads for the pinned case explain the large variations of exchange constants reported by many previous researchers who often interpreted their results in terms of the perfectly pinned model. Furthermore, if the perfectly pinned model were correct, it would imply a very large thickness dependence of the exchange constant, a possibility which is contradicted by measurements of the Curie temperature of thin films which is found to be independent of thickness down to 20 Å.

The data shown in Figs. 3-1 through 3-5 is representative of the results obtained for all sets of films investigated in this survey. In Fig. 3-6 the effective field $4\pi NM$ obtained from both perpendicular and parallel resonance is displayed as a function of film thickness from 28 to 8260 Å. The perpendicular resonance data was not corrected for the 110 Oe shift of the main mode since this shift only affects $4\pi M$ by about 1%. The excellent agreement of both measurements is consistent with the interpretation of the first mode resonance field for both geometries as a measure of the average demagnetizing field or magnetization across the film thickness. The solid curve which fits the experimental results very well corresponds to the theoretical prediction of the thickness dependence

Table 3-1

Product of $(L)^2$ and the corresponding slope for pinned and unpinned mode assignments for 3 sets of films including those of Figs. 5 and 6.

	PINNED CASE		UNPINNED CASE	
Film Thickness (Å)	Slope L^2 x 10^{-8} G cm^2		Slope L^2 x 10^{-8} G cm^2	
845	1.38	53% Spread	2.42	3% Spread
1714	1.83		2.43	
2585	1.90		2.37	
3500	2.08		2.43	
1424	1.77	37% Spread	2.72	6% Spread
3240	2.25		2.64	
5180	2.31		2.57	
6990	2.42		2.60	
2080	1.90	22% Spread	2.55	7% Spread
4150	2.28		2.62	
6300	2.42		2.65	
8260	2.33		2.47	

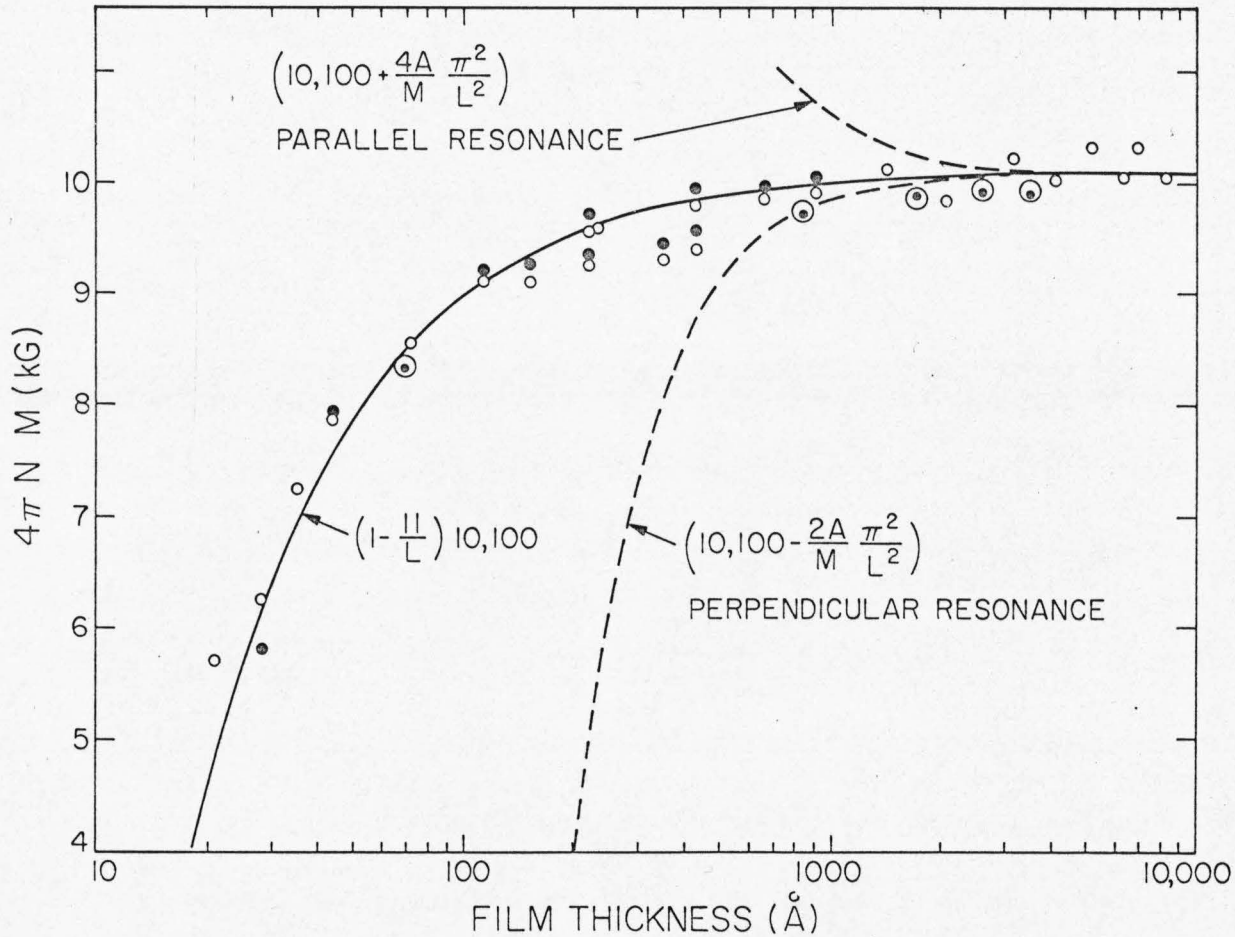

Fig. 3-6 Plot of 4πNM vs. film thickness obtained from perpendicular and parallel resonance measurements for films 28 to 8,260 Å thick. O, results from perpendicular resonance. ●, results from parallel resonance. The solid curve corresponds to 10,100 (1 - 11/L) the theoretical prediction of the thickness dependent demagnetizing field for the surface anistropy, inhomogeneous demagnetizing field and inhomogeneous magnetization models. The dashed curves represent the results expected from a perfectly pinned model for parallel and perpendicular resonance.

of $N = \left[1 - \frac{11 \times 10^{-8}}{L}\right]$. The extrapolation to infinite thickness gives $4\pi M$ = 10,100 Oe which is in excellent agreement with the value 10,200 for the bulk alloy (Bozorth, p. 109). Using $4\pi M$ = 10,100, the average exchange constant deduced from all measurements is $\left(1.03 \pm .05\right) \times 10^{-6}$ erg/cm. This value is in good agreement with some of the previously reported values of A for 81% Ni-Fe films. The dashed curves in Fig. 3-6 represent the results expected from a perfectly pinned model without any inhomogeneity corrections and clearly show that this is not the case for the films of this investigation. Since the solid line in this figure is consistent with the theoretical prediction of the mode pinning shown in Fig. 2-2, the latter figure may be plausibly assumed to depict the actual pinning for these films. Regardless of the actual mechanism responsible for the pinning, the main modes in both geometries for the thin films and the higher order modes for the thick films in perpendicular resonance are very nearly unpinned.

Finally a qualitative survey of the relative mode intensities in perpendicular resonance shows the frequency dependence pointed out by R. Weber et al. (1970), and decreasing relative higher mode intensities with decreasing film thickness. Neither result is in agreement with published calculations of mode intensities (Kittel, 1958; Pincus, 1960; Seavey, 1961; Sparks, 1969) but the latter is in qualitative agreement with the expectations for the partially pinned model. An accurate quantitative study of mode intensities which includes skin depth effects, field film interactions, and the thickness range of this investigation would require frequencies in excess of 8 GHz and resonant cavity

techniques. This would allow the excitation of a larger number of modes which are well separated from the usually broad main resonance mode and a better signal to noise ratio than can be obtained with a strip line. In any case the absence of quantitative supporting evidence should not affect the main conclusions based on the spectral behavior of the modes which was found to be independent of film position within the strip line. The location only significantly affects the absolute intensities of the modes with small effects on their relative intensities.

As mentioned above, the thickness dependence of N of Fig. 3-6 is in very good agreement with the expression, $N = \left[1 - \frac{11 \times 10^{-8}}{L}\right]$. However as pointed out in Chap. 2 a suitable choice of parameters for the surface anisotropy, inhomogeneous demagnetizing field and inhomogeneous magnetization models gives theoretical predictions all of which are virtually indistinguishable from this expression. Furthermore it is also possible that the pinning which causes this deviation could be caused by a combination of all three effects. It is clear, therefore, that resonance measurements alone cannot uniquely determine which of these mechanisms is responsible for the degree of pinning implied in Fig. 3-6. The answer to this question can only be obtained by direct control or measurement of these film characteristics by methods other than resonance.

As implied in Chap. 2 the inhomogeneity in demagnetizing field is made plausible by surface roughness considerations and in principle this contribution could be evaluated by a direct control or measurement of the surface characteristics of these films. Unfortunately the required range of roughness parameters is beyond the resolution capabilities of

present experimental techniques.

On the other hand, the possible contribution of a surface anisotropy, inhomogeneity of demagnetizing field or saturation magnetization can be evaluated by experimental methods other than resonance. For example a surface anisotropy or an inhomogeneity of demagnetizing field should not affect the magnetic moment of the film whereas it would be affected by an inhomogeneity in magnetization. The magnetic moment of a film can be measured with a hysteresis loop tracer or a torque magnetometer. The ideal film thickness as opposed to the magnetic thickness (see Appendix 2) can be measured by X-ray fluorescence. Careful interpretation of the ratio of the magnetic moment and the X-ray thickness can then answer which of the above effects is responsible for the thickness dependence of $4\pi NM$. The results of these measurements for the thinner films of Fig. 3-6 and additional films are presented in the next chapter and show that the deviations of Fig. 3-6 are explained by a thickness dependent average saturation magnetization.

3.4 Summary and Conclusions

Spin wave resonance measurements of 81% Ni-19% Fe coevaporated films 30 to 9000 Å thick, at frequencies from 1 to 8 GHz, at room temperature, and with the static magnetic field parallel and perpendicular to the film plane, have been performed. A self consistent analysis of the results for films thicker than 1000 Å, in which multiple excitations can be observed, shows that a unique value of A can only be obtained by the use of unpinned mode assignments. This evidence and the resonance behavior of films thinner than 1000 Å strongly implies that the

magnetization at the surfaces of permalloy films is very nearly unpinned. Specifically, the resonance field deviations from the corresponding fields of unpinned modes in ideal films, are consistent with the degree of pinning of Fig. 2-2. As expected from the predictions of Chap. 2, resonance alone cannot determine whether this pinning is due to a surface anisotropy, an inhomogeneous demagnetizing field or an inhomogeneous magnetization. The above analysis yields a value of $4\pi M$ = 10,100 Oe and $A = (1.03 \pm .05) \times 10^{-6}$ erg/cm for this alloy.

It must be emphasized, however, that although the 110 Oe deviations of the low order modes insignificantly affect the above values of A and $4\pi M$, these deviations are only qualitatively explained by the models considered in Chap. 2. Furthermore the residual deviations cannot be explained by eddy current effects since they are independent of frequency. Therefore, the above conclusions are uncertain to the extent of the significance of these unexplained deviations. This uncertainty applies equally to the perfectly pinned case which is however strongly negated by the above results.

The ability to obtain a unique value of A suggests that spin wave resonance can be used to accurately characterize the exchange interaction in a ferromagnet. Appendix 4 summarizes the important considerations for an extension of this method to other materials.

Chapter 4

COMPARISON OF MAGNETIC MOMENT AND RESONANCE MEASUREMENTS

4.1 Introduction

As discussed in Chapters 2 and 3, the thickness dependence of $4\pi NM$ as determined from resonance measurements can be interpreted in at least three indistinguishable ways. Specifically, the deviation of $4\pi NM$ from 10,100 can be due to a surface anisotropy, an inhomogeneous demagnetizing field or an inhomogeneous magnetization. On the other hand each of these processes should affect the magnetic moment of a film in a distinguishable way. In an effort to resolve this dilemma, it was therefore decided to measure the magnetic moment of very thin films with a very sensitive torque magnetometer. As explained below careful interpretation of the ratio of the magnetic moment and the film thickness measured by X-ray fluorescence can supply evidence as to which of these effects is responsible for the thickness dependence of $4\pi NM$. The results of such measurements for the thinner films of Fig. 3-6 and additional films show that the deviations of Fig. 3-6 are in fact primarily associated with a thickness dependent average saturation magnetization.

Prior to presenting and discussing these results it is helpful to recall the definition of magnetic moment, explain its usefulness when compared with the X-ray film thickness, and discuss in more detail several physical processes and how each can affect both the magnetic moment and $4\pi NM$ of permalloy films.

4.2 Preliminary Considerations

4.2.1 Definition of Magnetic Moment and Choice of Film Thickness

The magnetic moment is the integral of the saturation magnetization over the film volume. If the magnetization is assumed to only vary across the thickness of the film,

$$\mu \equiv A\int_{-\frac{L}{2}}^{\frac{L}{2}} M d\xi = AL\,\frac{1}{L}\int_{-\frac{L}{2}}^{\frac{L}{2}} M d\xi = AL\langle M\rangle \qquad (4.1)$$

where A is the area of the film and L its thickness. In principle, knowing the area and thickness of a film, the ratio μ/AL where μ is determined by a torque magnetometer, can then be used to measure the average saturation magnetization of a film.

As discussed in Appendix 2 there are three convenient ways of measuring the film thickness: the actual film thickness measured by interferometry, the ideal film thickness deduced from X-ray fluorescence measurements and the magnetic film thickness deduced from magnetic measurements. Although the latter thickness is useful for many considerations, it is meaningless when used in the ratio μ/AL, because it is in fact deduced from Eq. 4.1 by assuming that $\langle M\rangle$ is independent of film thickness and equal to the magnetization of the bulk material. Therefore, the thicknesses which can be meaningfully used to measure the average saturation magnetization are the actual film thickness and the ideal film thickness. However, as pointed out in Appendix 2 the actual film thickness can only be measured to an accuracy of $\pm$ 20 Å. This uncertainty would consequently result in a significant error in the ratio μ/AL for

thin films. On the other hand the ideal film thickness of films in the 20 to 200 Å range can be measured to an accuracy of ± 5%. Its use in the ratio μ/AL where μ can be measured to a ± 2% accuracy (Humphrey and Johnston, 1963) would therefore result in the smallest error in the value of the average magnetization of very thin films. It is therefore for the above reasons that the following predictions and experimental results are correlated with the ideal film thickness as measured by X-ray fluorescence.

With this understanding, the two quantities of interest in the next two sections are:

$$\frac{\frac{\mu}{L_x}}{\lim_{L_x \to \infty} \left(\frac{\mu}{L_x} \right)} \tag{4.2}$$

where L_x is the X-ray film thickness,

and

$$\frac{4\pi NM}{10,100} \cdot \tag{4.3}$$

The ratio 4.2 is by definition the relative average saturation magnetization of a film. The ratio 4.3 is a measure of the deviation of the effective demagnetizing field as measured by ferromagnetic resonance from that of an ideal film with bulk magnetic properties. The degree of correlation of the thickness dependence of both ratios and their agreement with the predictions of the next section can then supply evidence as to which effect is responsible for the thickness dependence of $4\pi NM$.

4.2.2 Possible Sources for a Thickness Dependent Relative Magnetic Moment and $4\pi NM$

As mentioned in the introduction the objective of this chapter is to establish the cause of the thickness dependence of $4\pi NM$ measured by ferromagnetic resonance. Three possible causes for the observed behavior have already been pointed out in Chap. 2. However the considerations of Chap. 2 have not emphasized how a surface anisotropy, an inhomogeneous demagnetizing field or an inhomogeneous magnetization would affect the magnetic moment of a film. Furthermore, little has been said about the possible origins of these three properties. Correct interpretation of the experimental results discussed in Sec. 4.3, therefore, requires a more comprehensive discussion of the implications of physical processes which can affect the behavior of real films. Specifically, this section describes in more detail the predictions of several processes which could affect the relative ratios of μ/L_x and $4\pi NM$.

Since the oxides of Ni and Fe can be either antiferromagnetic or ferrimagnetic it is expected that oxidation will affect both the magnetic moment and the saturation magnetization of permalloy films. The properties of the films used in this investigation are of necessity measured in air. Furthermore the films are prepared in a vacuum ranging between 10^{-7} and 10^{-6} Torr. It is well known that such environments contain some oxygen. Both conditions make it, therefore, plausible if not certain that these films undergo some oxidation.

The way in which oxidation will affect the magnetic moment and saturation magnetization depends of course on the details of the oxidation

process. For example, the preferential oxidation of either Fe or Ni will have a different effect than that expected from equal degrees of oxidation of both constituents. Similarly the effect of an oxide localized near the film surfaces is expected to be different from that of an oxide distributed throughout the film volume. These possibilities point out the difficulty of making a complete estimate of the consequences of oxidation. However, it is hoped that the use of the following two simple models can lead to some meaningful predictions whose validity can then be put to the test of experiment.

First, for the case of equal degree of oxidation of Ni and Fe and the consequent formation of an abrupt antiferromagnetic "dead" oxide layer, the relative ratio of μ/L_x is expected to depend on thickness according to Eq. 4.4 of Table 4-1. On the other hand, the ratio of $4\pi NM/10,100$ is expected to be 1.0 and independent of film thickness (Eq. 4.5 of Table 4-1). In these predictions it is assumed that the saturation magnetization of the oxygen free part of the film is the same as that of the bulk alloy, the oxide thickness is independent of film thickness, there is a negligible surface roughness and negligible pinning of the bulk spins at the film oxide interface.

Second, if one assumes the preferential oxidation of Fe, with no Ni lost to the oxide formed on the surface, the relative ratio of μ/L_x is expected to obey Eq. 4.6 of Table 4-1. The loss of Fe from the bulk of the film will change both the saturation magnetization and decrease the thickness of magnetic material. If this were the case, the results of Sec. 2.3.3 of Chap. 2 show that, in the absence of pinning of the bulk

Table 4-1

f Magnetic Moment and X-ray Film Thickness, and $4\pi NM$ for five possible processes which can affect the Properties of Thin Permalloy Films

	$\dfrac{\frac{\mu}{L_x}}{\lim_{L_x \to \infty} (\frac{\mu}{L_x})}$	$\dfrac{4\pi NM}{10{,}100}$
e	$= 1 - \dfrac{\varepsilon}{L_x}$ (4.4)	$= 1.0$ (4.5)
	$= 1 - \dfrac{\Delta\mu}{\mu_1}$ (4.6)	$\simeq 1 - (.63 \text{ to } .78)\dfrac{\Delta\mu}{\mu_1}$ (4.7)
	$= 1 - \dfrac{(\beta + \alpha - 1)\varepsilon}{L_x}$ (4.8)	$= \dfrac{L_x}{L_x + (1-\alpha)\varepsilon}\left[1 - \dfrac{(\beta + \alpha - 1)\varepsilon}{L_x}\right]$ (4.9)
	$= 1.0$ (4.10)	$= (1 - \dfrac{2\varepsilon\beta}{L_x})^*$ (4.11)
	$= 1 - \dfrac{2\varepsilon\beta}{L_x}$ (4.12)	$\simeq 1 - \dfrac{2\varepsilon\beta}{L_x}$ (4.13)

s of Fe and Ni lost to the oxide which is assumed to be independent of L_x.
magnetic moment of an unoxidized film.
of permalloy in the diffused layer and β is the per unit decrease of the average layer.
n demagnetizing field within the surface layers each of thickness ε.
n magnetization within the surface layers each of thickness ε.
of a surface anisotropy equal at both surfaces replace $2\beta\varepsilon$ in Eq. 4.11 by $\dfrac{K_s}{\pi M^2}$.

spins at the film oxide interface, $4\pi NM$ is a reasonable measure of the average saturation magnetization of a film. The preferential oxidation of Fe is therefore expected to affect $4\pi NM/10,100$ according to Eq. 4.7 of Table 4-1. The decrease ranges between the limiting values of .63 to .78 $\frac{\Delta\mu}{\mu}$, depending on the percentage depletion of Fe in the film. This relation can be readily derived from Eq. 5.5 in Chap. 5.

Another process whose influence on the ratios of Eqs. 4.2 and 4.3 can be expressed rather simply is the effect of interdiffusion of the film and oxygen or glass constituents at the film surfaces. For this case the respective ratios are expected to obey the relations in Eqs. 4.8 and 4.9 of Table 4-1.

More importantly perhaps, the contributions of an inhomogeneous demagnetizing field as might arise in the presence of surface roughness, or a surface anisotropy, are not expected to affect the relative ratio of μ/L_x, since if the film is saturated its effective demagnetizing field does not contribute to the magnetic moment. On the other hand as predicted in Sec. 2.3.2 of Chap. 2 both an inhomogeneous demagnetizing field and a surface anisotropy can give rise to a thickness dependent effective demagnetizing field. See. Eqs. 4.10 and 4.11 of Table 4-1.

The final consideration is an inhomogeneous magnetization which is intrinsically lower near the surfaces of a film. Using the notation of Sec. 2.3.3, in Chap. 2, the ratios are predicted to obey the relations of Eqs. 4.12 and 4.13 of Table 4-1. Equation 4.13 is based on the predictions of Sec. 2.3.3 of Chap. 2 which show that, in the absence of surface spin pinning, $4\pi NM$ can be a reasonable measure of the average saturation

magnetization of a film. A very important feature of this model is that it nearly equally affects both of these ratios. It should be pointed out, however, that both ratios are also expected to be nearly equal for any other process which would primarily affect the average saturation magnetization of a film while negligibly changing the thickness of magnetic material.

In conclusion, Table 4-1 summarizes the predictions for the expected thickness dependence and correlation of the relative values of μ/L_x and $4\pi NM/10{,}100$ for five possible situations which might take place in real films. Four of these have been justified in terms of concrete physical characteristics. Namely, equal degree of oxidation of Ni and Fe, preferential oxidation of Fe, interdiffusion of the glass and film constituents and an inhomogeneous demagnetizing field as would be caused by surface roughness. The latter model also applies to the case of a surface anisotropy. The fifth model, represented in Eqs. 4.12 and 4.13, allows for an intrinsic inhomogeneity in magnetization without the presence of oxidation or interdiffusion. Comparison of each pair of equations in Table 4-1 shows that the relative ratios of μ/L_x and $4\pi NM$ are distinctly related for all cases. The implications of all these predictions are further discussed in the next section along with the pertinent experimental results.

4.3 Comparison of Magnetic Moment and Resonance Measurements

Figure 4-1 displays the relative ratio of μ/L_x vs. L_x, the X-ray film thickness, for the films of Fig. 3-6 and additional films. The magnetic moments were measured with a 700 Oe torque magnetometer. The

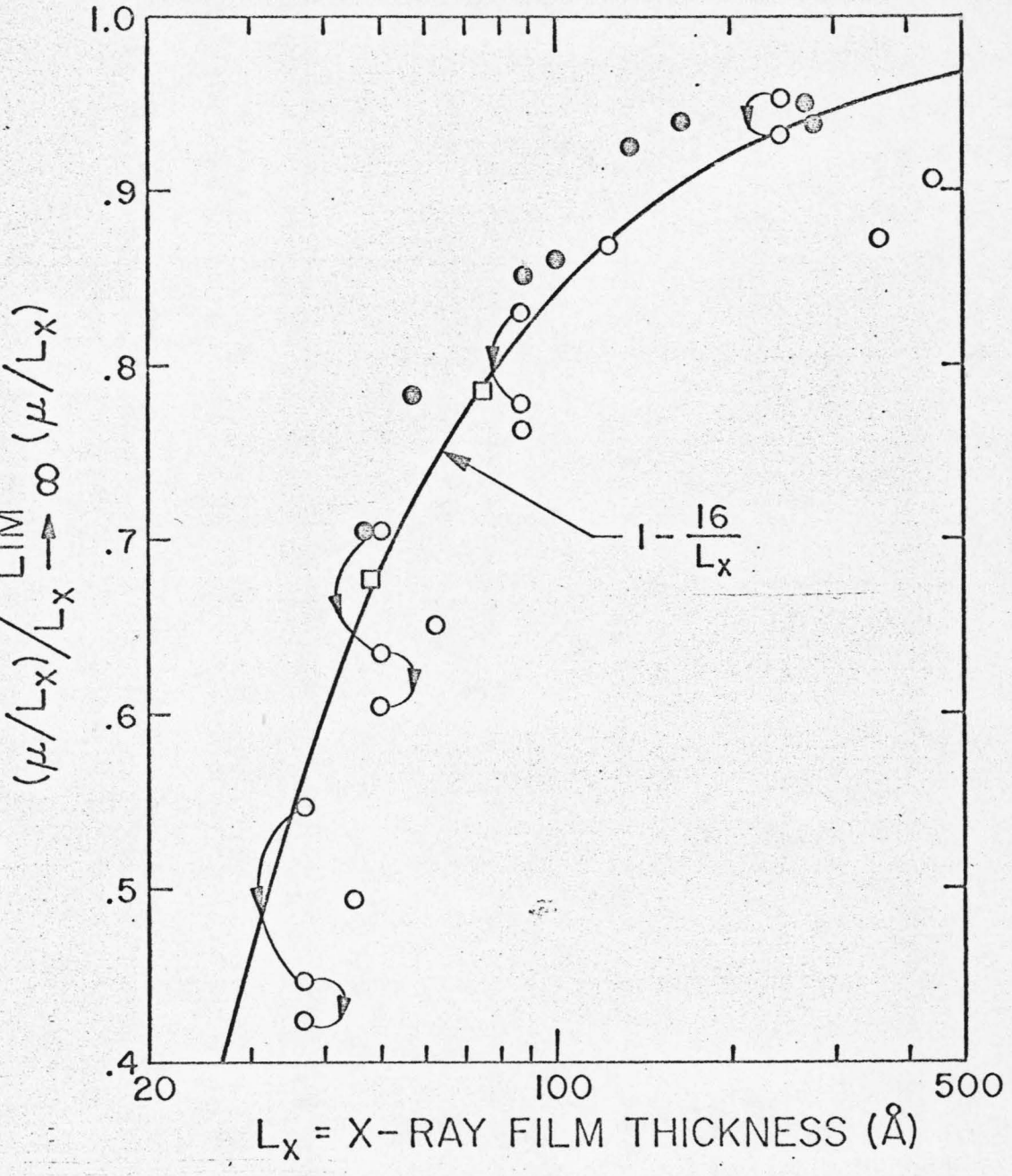

Fig. 4-1 Relative ratio of magnetic moment and X-ray film thickness vs. X-ray film thickness. The triple set of points corresponds to magnetic moment measurements taken 5 days (upper points), 60 days, and 90 days (lower points) after the evaporation of the corresponding films. Similarly, the double set of points corresponds to measurements taken 5 days and 60 days after the evaporation of the corresponding films. The other open points correspond to measurements taken 1 year after the evaporation of the films. The ● and □ points correspond to films overcoated with Aℓ and Pb respectively. The solid curve corresponds to $(1 - 16/L_X)$. This figure should be compared with Figs. 3-6 and 4-2.

triple set of points corresponds to measurements of magnetic moment taken 5 days (upper points), 60 days (middle points), and 90 days (lower points) after the evaporation of the corresponding films. The double set of points corresponds to measurements taken 5 days and 60 days after the evaporation of the corresponding films. The remaining open points correspond to measurements of the magnetic moment taken 1 year after the evaporation of the corresponding films. The solid points correspond to films overcoated with 1000 Å of Al, and the open squares correspond to films overcoated with 2000 Å of Pb. Both sets of films were overcoated within 5 seconds following their evaporation in a vacuum better than 10^{-6} Torr. The solid curve corresponds to $(1 - \frac{16}{L_x})$. The significance of this data is discussed later.

Figure 4-2 displays the ratio of $4\pi NM/10,100$, as determined from perpendicular resonance measurements, vs. X-ray film thickness for the corresponding films of Fig. 4-1. The solid curve also corresponds to $(1 - \frac{16}{L_x})$ and is useful for a comparison with the results of Fig. 3-6 and 4-1, and with the predictions of Sec. 4.2.2. The values of $4\pi NM$ determined from parallel resonance are omitted from this figure for clarity. They agree very closely with those determined from perpendicular resonance.

A comparison of the results of Fig. 4-2 with those of Fig. 3-6 shows that the film thickness deduced from magnetic measurements is lower than the film thickness measured by X-ray fluorescence. This can be readily seen by comparing the ordinate position of the 28 Å film of Fig. 3-6 with that of the corresponding 45 Å of Fig. 4-2. A film by film comparison of all the films common to both figures shows that this difference is

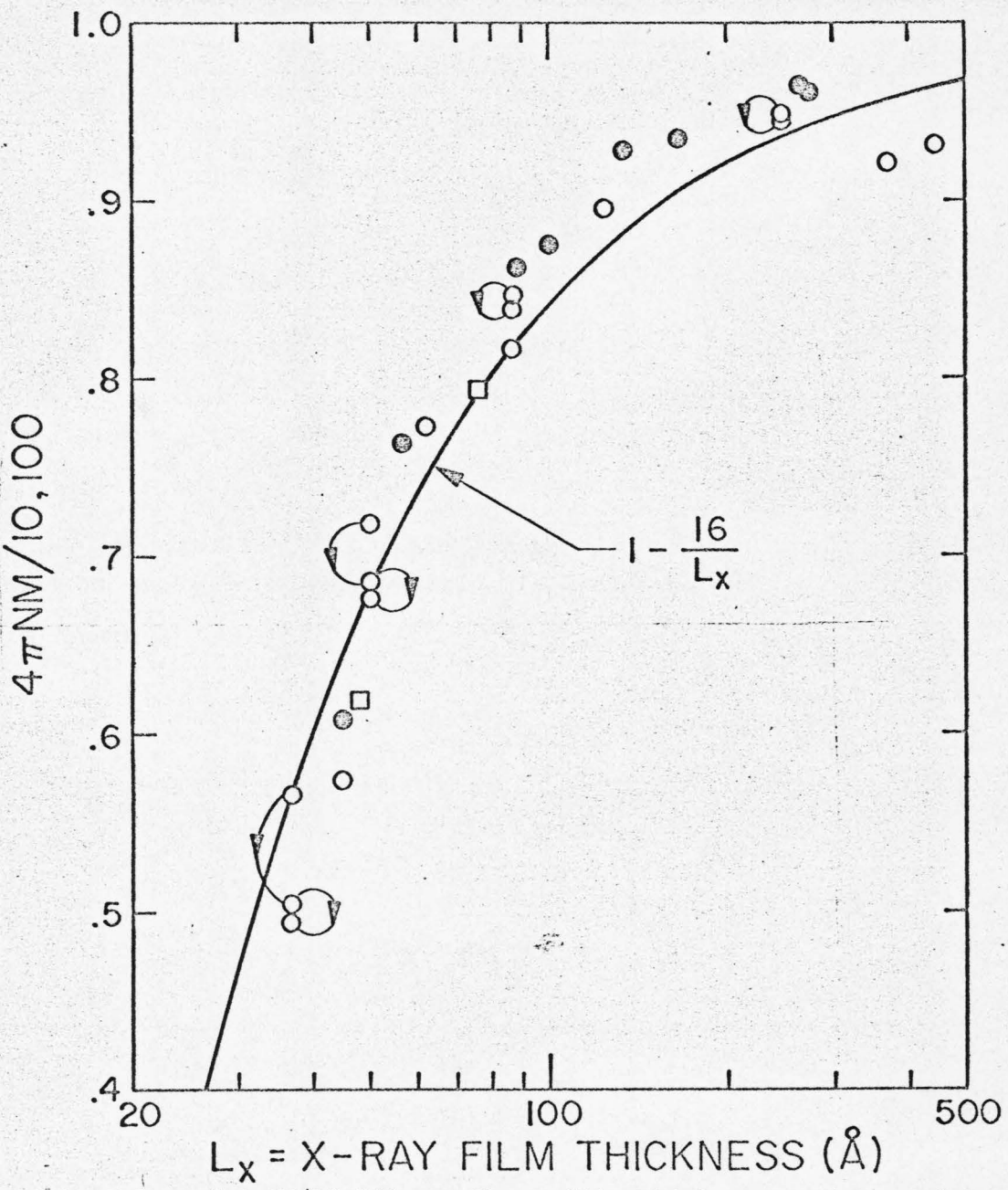

Fig. 4-2 Value of $4\pi NM/10,100$ vs. X-ray film thickness. The triple set of points corresponds to resonance measurements taken 5 days (upper points), 60 days, and 90 days (lower points) after the evaporation of the corresponding films. Similarly, the double set of points corresponds to measurements taken 5 days and 60 days after the evaporation of the corresponding films. The other open points correspond to measurements taken 1 year after the evaporation of the films. The ● and ■ points correspond to films overcoated with Aℓ and Pb respectively. The solid curve corresponds to $(1 - 16/L_X)$. This figure should be compared with Figs. 3-6 and 4-1.

independent of film thickness and about 15 to 20 Å. As discussed in Appendix 2 this difference suggests that the average saturation magnetization of thin films is far from that of thick films. The same conclusion can be readily drawn from the results of Fig. 4-1.

A comparison of the results of Figs. 4-1 and 4-2 shows that the thickness dependence of the relative ratio of $4\pi NM$ is in remarkably good agreement with that of the relative ratio of μ/L_x for all films. The significance of this agreement can be best understood from a model by model comparison with the predictions discussed in Sec. 4.2.2.

As shown in Eq. 4.4, the presence of 16 Å "dead" layer caused by equal degree of oxidation of Ni and Fe would be in agreement with the results of Fig. 4.1. However, as predicted in Eq. 4.5 such an oxide is not expected to change the average saturation magnetization of a film. As discussed in Sec. 4.2.2, if the oxide is assumed to have no effect on the pinning of the bulk spins at the film-oxide interface, it is expected that $4\pi NM$ would be 10,100 Oe and independent of thickness. This is inconsistent with the results of Fig. 4-2 which show that $4\pi NM$ depends on thickness and is 50% below this value at 30 Å. This discrepancy can be interpreted in two ways. First, it may imply the absence of this oxidation process in permalloy films, or second, $4\pi NM$ deviates from 10,100 because an oxide partially pins the bulk spins at the film-oxide interface. For example a surface anisotropy energy in the range of .15 to .25 erg/cm^2 would satisfactorily explain the results of Fig. 4-2. The possibility for the coincidence that K_s lies in this range is unlikely. It is controverted by the results obtained for the films overcoated with Al and

Pb. These results are essentially identical to those of the uncoated films. The degree of oxidation of the uncoated films is expected to be different from that of the overcoated films. On the other hand the behavior of the overcoated films supports the first interpretation, and therefore, it is concluded that an oxidation process of this magnitude is highly improbable in permalloy films.

As shown in Eqs. 4.6 and 4.7, the preferential oxidation of Fe predicts the changes observed in Figs. 4-1 and 4-2, except that the change in $4\pi NM$ is expected to be about 30% smaller than the corresponding change in μ/L_x. The existence of this oxidation process is directly supported by the multiple sets of points of these figures, which correspond to measurements taken 5 days, 60 days, and 90 days after the evaporation of these films. The corresponding changes are a result of oxidation which presumably continues to take place at a slower rate after the initial oxidation which occurs when the films are first exposed to air. This effect becomes unmeasurable after about 6 months and consequently only one set of data points is shown for the films measured 1 year after their evaporation. Furthermore the results of Chap. 5 which unequivocally establish the preferential oxidation of Fe for films oxidized at elevated temperatures, make it plausible that the same process can take place at room temperature. It is, therefore, tempting to jump to the conclusion that the anomalies of thin permalloy films can be completely explained by the preferential oxidation of Fe. However, this conclusion is directly contradicted by the etching and X-ray fluorescence results of Sec. 5.4.2, which show directly that the degree of preferential oxidation of Fe for

films oxidized at room temperature can only explain a small fraction of this effect. In view of the latter results it can be only concluded, that although some preferential oxidation of Fe takes place at room temperature, it is far too small to explain the large variations depicted in Figs. 4-1 and 4-2.

Similarly Eqs. 4.8 and 4.9 predict that the presence of interdiffusion at the film substrate interface can give rise to changes like the ones observed in Figs. 4-1 and 4-2. It should be pointed out, however, that if the interdiffusing substrate element simply dilutes the magnetic alloy ($\alpha + \beta = 1$) it is not expected to affect μ/L_x, whereas it is always expected to decrease the average saturation magnetization. Many elements decrease <M> more rapidly than straight dilution. These complications make it difficult to make a complete prediction for this model, however, as in the previous two cases this possibility is invalidated by direct experimentation. The results for several sets of films prepared at 200°C were found to be virtually indistinguishable from those for several sets of films prepared at 20°C. This would be very unlikely in the presence of significant interdiffusion since the degree of interdiffusion is expected to be very sensitive to such a large variation of the substrate temperature.

The possibility for the thickness dependence of $4\pi NM$ being primarily caused by an inhomogeneous demagnetizing field, as might be expected from surface roughness or a surface anisotropy, is denied by the results of Fig. 4-1 in conjunction with the prediction of Eq. 4.10. The magnetic moment of a film, if it is saturated, does not depend on its demagnetizing field.

Finally, the only model which is in complete agreement with the results of Figs. 4-1 amd 4-2 is the one that assumes an intrinsic decrease of the magnetization near the film surface. As can be seen from Eqs. 4.12 and 4.13 the predicted thickness dependence of μ/L_x and $4\pi NM$ is identical for both quantities and in agreement with the results of these figures. It should be pointed out that the same effect would be caused indistinguishably by a thickness dependent, uniformly lower magnetization across the film thickness.

All the above measurements were performed at room temperature. The spontaneous saturation magnetization of all ferromagnets is a maximum at 0°K, it decreases with increasing room temperature, and it vanishes at the Curie temperature which is about 870°K for the bulk 81% Ni-19% Fe alloy. One widely accepted model for the temperature dependence of the magnetization is based on the thermal excitation of spin waves. Several theoretical treatments of this problem predict that the Curie temperature of very thin films, composed of a few atomic layers, can be significantly lower than that of bulk material, (Jacobs and Bean, 1963). Similarly they predict that although the saturation magnetization of such films is equal to that of bulk material at 0°K it can decrease at a faster rate than that of bulk material at elevated temperatures. If this were the cause for the lower magnetization at room temperature of the thinner films used in this investigation, it would be expected that μ and $4\pi NM$ for the thinner films, would show a larger relative increase than those of thick films, with decreasing temperature. For example, films thicker than 1000 Å would be expected to show nearly bulk properties, a 5% increase of

both μ and $4\pi NM$ between 300 and 78°K. On the other hand films 100 Å thick would be expected to show a 20% increase over this temperature range, since their room temperature μ and $4\pi NM$ are 15% below the bulk values. However, this is clearly not the case for the films used in this investigation. The temperature dependences of μ and $4\pi NM$ between 300 and 78°K were found to be equal and independent of film thickness and in very good agreement with the expectations for bulk material. Although these results are consistent with the conclusion that $4\pi NM$ is directly associated with the saturation magnetization of these films, they negate the possibility that the room temperature magnetization of very thin films is lower than the magnetization of the thick films due to the mechanism discussed in this paragraph.

In view of the above considerations, it may be concluded that the thickness dependence of $4\pi NM$ is caused by a thickness dependent average saturation magnetization, which is far below that of bulk material for very thin films. A series of complementary experiments shows that this large decrease of average saturation magnetization cannot be simply explained by either oxidation or interdiffusion processes. It can only be satisfactorily explained by an intrinsic decrease of saturation magnetization for very thin films, an effect which cannot be justified by any simple physical consideration. This conclusion is not a completely new idea. Several other investigators (Neugebauer, 1959 and 1961; Gradmann and Müller, 1968) have observed a decrease in magnetic moment in thin magnetic films but in no case were these measurements correlated with resonance measurements, making it difficult to ascertain whether the

observed decreases were due to oxidation, interdiffusion, an intrinsic decrease in saturation magnetization, or unreliable experimental methods.

It must, of course, be remembered that these films were prepared in a vacuum ranging between 10^{-7} and 10^{-6} Torr. The oxygen and other impurity contents in this environment could very well be responsible for the observed results. This possibility will only be answered by a duplication of the measurements carried out in this investigation on films evaporated in controlled atmospheres starting from a 10^{-11} Torr range. It is furthermore imperative that all these new measurements be taken both in vacuum and in air.

The above conclusions must be reconciled with the intensities of the higher order modes detected in perpendicular resonance. As can be recalled from Fig. 3-1, the higher order modes are characterized by a series of strong excitations and a series of relatively weak excitations. The latter correspond to antisymmetric spin wave modes about the center of the film. The relative weakness of these excitations is consistent with rather small asymmetries about the film center, or equivalently with similar inhomogeneities on both sides of the film. This suggests that whichever process is responsible for the thickness dependence of μ/L_x and $4\pi NM$, it must be similar on both sides of the film. This is certainly unlikely for the case of interdiffusion, but not inconceivable for an oxidation process, or a symmetric intrinsic decrease of the magnetization near both film surfaces.

4.4 Summary and Conclusions

A correlation of the ratio of magnetic moment and X-ray film thickness, with the value of $4\pi NM$ as determined from resonance, for films 45 to 300 Å thick has been performed. The remarkable agreement of both quantities and a comparison with the predictions of five distinct models, strongly imply that the thickness dependence of both quantities is related to a thickness dependent average saturation magnetization, which is far below 10,100 Oe for very thin films. However, a series of complementary experiments shows that this large decrease of average saturation magnetization cannot be simply explained by either oxidation or interdiffusion processes. It can only be satisfactorily explained by an intrinsic decrease of the average saturation magnetization for very thin films, an effect which cannot be justified by any simple physical considerations. The rather small asymmetry implied by the weak excitation of the antisymmetric spin wave modes makes it plausible that the magnetization is lower to similar extent near both surfaces of the films.

Independent of the above difficulties, the results of this chapter strongly suggest a negligible contribution of inhomogeneous demagnetizing field or a surface anisotropy. The former conclusion and the belief in the validity of Schlömann's surface roughness model make one wonder about the character of the topology of these films.

Chapter 5

FERROMAGNETIC RESONANCE AND COMPLEMENTARY MEASUREMENTS OF OXIDIZED PERMALLOY FILMS

5.1 Introduction

The findings discussed in this chapter are a result of attempting to solve the dilemma encountered in the interpretation of the spin wave resonance measurements discussed in Chap. 3; namely, that the source of the thickness dependence of $4\pi NM$ cannot be uniquely determined from resonance measurements alone. Knowledge that Ni-Fe films oxidize when exposed to oxygen at elevated temperatures, makes it reasonable to assume that some oxidation can also take place at room temperature when the films are exposed to air after their evaporation. As discussed in the previous chapter, it is expected that oxidation will affect the magnetic moment of a film, and for the special case of preferential oxidation of Fe, it is also expected to change the saturation magnetization of the bulk part of the film. Recognizing this, it was felt that it should be possible to implement several experiments which could test the presence of such a process, and hopefully explain the effects observed in Chapters 3 and 4.

On the basis of resonance, He ion backscattering, X-ray fluorescence and complementary torque magnetometer measurements it is unambiguously established that the oxide layer on the surface of oxidized 81% Ni-19% Fe evaporated films is, indeed, predominantly Fe-oxide. Extrapolation of results for pure Fe films indicates that the oxide is most likely α-Fe_2O_3. The resonance measurements establish that the oxide negligibly affects the pinning of the bulk spins at the film oxide interface.

However, the extent of oxidation at room temperature is far too small to explain the observed thickness dependence of $4\pi NM$ and μ for thin permalloy films.

The degree of oxidation of the samples used in this part of the investigation was controlled by varying the time that the films were held at elevated temperature in air.

5.2 Results and Discussion of Resonance Measurements

Oxidation decreases the total magnetic moment of a sample as measured either with a hysteresis loop tracer or torque magnetometer. It also decreases the value of $4\pi NM$ as determined from resonance. If the oxide is due to the preferential oxidation of Fe, it is possible to calculate how it would affect both the magnetic moment and the average saturation magnetization of a film and how these would be related. A comparison of the experimentally observed changes in μ and $4\pi NM$ with the above predictions can then be used to determine the existence of this process, the extent to which $4\pi NM$ represents the average saturation magnetization of a film and the degree of pinning of the bulk spins at the film oxide interface.

The dependence of the saturation magnetization on the composition of nickel rich Ni-Fe alloys can be represented by the equation

$$M_D = (a + bD) = (480 + 1700D)G, \qquad (5.1)$$

where D is the fractional content of Fe in the alloy. This expression agrees within 1% with data given by Bozorth, p. 109, in the range

$0 \leq D \leq .35$. For the case of a thin film in which D may vary through the thickness of the film, the average saturation magnetization is, of course, given by

$$\langle M_D \rangle = (480 + 1700 \langle D \rangle)\ G, \tag{5.2}$$

where $\langle D \rangle$ is the average fractional content of Fe in the bulk of the film. In this case the average is taken across the thickness of magnetic material, excluding the oxide which is presumed to be non-magnetic or antiferromagnetic. For example the average saturation magnetization for an unoxidized 81% Ni-19% Fe film would be

$$\langle M_{.19} \rangle = 480 + 1700\ (.19) = 803\ G. \tag{5.3}$$

As defined in Chap. 4 the magnetic moment of a film is

$$\mu_D = AL \langle M_D \rangle \tag{5.4}$$

where L is the thickness of magnetic material. To first order L is proportional to the total number of ferromagnetic atoms independent of whether these are Ni or Fe atoms. (The lattice constant changes linearly with D by about 0.6% in the range $0 < D < .2$) (Bozorth, p. 105). As pointed out in Appendix 2 this thickness cannot be measured directly. However, this is of no consequence since L does not enter directly into the following considerations.

Starting with the above relations and assuming the preferential oxidation of Fe it can be easily shown that, for films with a preoxidation composition D_1, the fractional decrease of average saturation

magnetization due to the oxidation of Fe is related to the fractional decrease of magnetic moment by the expression

$$\frac{\frac{\Delta M}{M}}{\frac{\Delta \mu}{\mu}} = \left[\frac{b}{(a+b)}(1 - D_1) + \frac{(a + bD_1)}{(a+b)} \frac{\Delta M}{M} \right] \tag{5.5}$$

$$= \left(\frac{b}{(a+b)} \right)(1 - D_1) \left[1 - \frac{(a + bD_1)}{(a+b)} \frac{\Delta \mu}{\mu} \right]^{-1}$$

$$= \left(\frac{b}{a+b} \right)\left(\frac{1 - D_1}{1 - \Delta D} \right)$$

where

$$\frac{\Delta M}{M} = \frac{\langle M_{D_1} \rangle - \langle M_{D_2} \rangle}{\langle M_{D_1} \rangle}, \quad \frac{\Delta \mu}{\mu} = \frac{\mu_{D_1} - \mu_{D_2}}{\mu_{D_1}}, \quad \Delta D = (D_1 - D_2)$$

For the present case of interest, $D_1 = .19$ and Eq. 5.5 becomes

$$\frac{\frac{\Delta M}{M}}{\frac{\Delta \mu}{\mu}} = (.63 + .37 \frac{\Delta M}{M}) = .78 \left(\frac{.81}{1 - \Delta D} \right) .$$

This ratio is expected to be in the range .63 to .78, since if none of the nickel is oxidized, as can be seen from Eq. 5.3, $(\Delta M/M)_{max.} = .40$. Comparison of Eqs. 5.2 and 5.4 readily shows why this ratio is less than 1.0. The value of $\langle M_D \rangle$ is only affected by the change of $\langle D \rangle$, however μ_D is affected by both the change of $\langle M_D \rangle$ and the change of L, resulting from the loss of Fe from the magnetic part of the film.

Table 5-1 summarizes the correlation of magnetic moment and $4\pi NM$ for films 40 to 1700 Å thick. Columns 1 and 2 show the time, temperature, and environment of oxidation. Column 3 shows the X-ray film thickness.

Table 5-1

Comparison of change of magnetic moment with change of saturation magnetization measured by ferromagnetic resonance.

1	2	3	4	5	6	7	8
t_{ox}	T_{ox} (C°)	L_x (Å)	$\frac{\Delta\mu}{\mu}$	$\frac{\Delta M}{M}$**	$\frac{\Delta M}{M}\frac{\mu}{\Delta\mu}$	$4\pi NM$ Initial	L_{oxide} (Å)
2 hrs	200, 10^{-6} Torr*	49	.32	.24	.75	6,950	9?
60 days	25 air	37	.17	.11	.65	7,250	4?
		49	.11	.05	.45	5,710	2?
24 hrs	250 air	300	.23	.21	.91	9,760	50
		300	.27	.23	.85	9,760	60
24 hrs	200 air	360	.25	.20	.80	9,830	70
		390	.15	.13	.87	9,890	45
3 min		1100	.14	.12	.86	10,020	120
6 min		1130	.22	.19	.86	10,020	190
10 min	350 air	1110	.26	.22	.85	10,020	220
1 min		1700	.09	.09	1.00	10,270	115
3 min		1660	.16	.14	.87	10,270	200
5 min		1710	.19	.16	.84	10,270	250

* Gas in vacuum system of unknown composition.

** Deduced from change in $4\pi NM$ measured as described in Chap. 3 and assuming N to be unchanged by oxidation.

Columns 4 and 5 show the fractional changes of the magnetic moment and $4\pi NM$ upon oxidation. The ratio of these fractional changes is shown on Column 6. The preoxidation value of $4\pi NM$ is shown in Column 7. Finally Column 8 represents an estimate of the oxide thickness based on the assumption that it is αFe_2O_3. This thickness is 2.15 times the estimated thickness of Fe lost from the bulk of the film, the latter estimate being based on $\Delta\mu/\mu$. Specifically:

$$L_{oxide} = 2.15\ (L_1 - L_2) = 2.15\ \frac{L_1}{a+b}\ \langle M_D \rangle_1\ \frac{\Delta\mu}{\mu}\ . \qquad (5.6)$$

As can be seen from Column 6 of this table the ratio of $(\Delta M/M)/(\Delta\mu/\mu)$ is independent of film thickness except for very thin films oxidized at room temperature, and the average value of .84 is only about 20% higher than that predicted by Eq. 5.5. This discrepancy may be due to the omission of magnetostrictive effects on $4\pi NM$ which are not negligible for films whose bulk composition exceeds 81% Ni. It is known that evaporated films are usually under a significant planar, isotropic tensile stress. The presence of a similar stress in the oxidized films would give rise to a perpendicular anisotropy field via a magnetoelastic interaction. The extent of this field could be several hundred Gauss (Johnson and Wilts, 1971). Its inclusion in Eq. 2.11 would reduce the value of $\Delta 4\pi NM$ and consequently reduce the ratio in Column 6. Although this effect is qualitatively in the right direction, an accurate estimate of the perpendicular anisotropy field requires unavailable knowledge of the stress and composition within the bulk of the oxidized films. In view of this omission, the value .84 is in acceptable agreement with the prediction of Eq. 5.5. This agreement is,

therefore, consistent with the preferential oxidation of Fe and with the assumption that $4\pi NM$ is a close measure of the average saturation magnetization of the films.

In view of the above results it was felt that the same process, if extrapolated to films oxidized at room temperature would explain the initial deviation of $4\pi NM$ from 10,100 Oe for the thinnest films of this table and those considered in Chapters 3 and 4. However, the X-ray fluorescence results discussed in Sec. 5.4.2 below, clearly show that although the preferential oxidation of Fe also takes place at room temperature, it is by far too small to explain the results of Chapters 3 and 4.

The presence of the preferential oxidation of Fe and the formation of α-Fe_2O_3 are directly supported by the backscattering and X-ray fluorescence measurements described in the next two sections.

5.3 Results and Discussion of Backscattering Measurements

The complexity of the equipment and instrumentation of the backscattering spectrometer are beyond the scope of this dissertation. It should suffice to state that its heart is a 4 story, 3 MeV Van De Graaff accelerator. A better description of such a system and its applications can be found in the book by Mayer et al. The interaction which leads to backscattering is adequately described by Leighton.

In the backscattering experiment, monoenergetic He ions forming a well collimated beam of approximately 2 x 2 mm^2 impinge on the film surface. The He ions scattered back by collisions with film and substrate nuclei are detected with a Si surface barrier detector, resolved in energy,

and their numbers are recorded with a 400 channel analyzer. Figure 5-1 shows the results obtained on a pure Ni film (top), a permalloy film (center), and a pure Fe film (bottom), all on glass substrates, and each before and after partial oxidation. The high energy edge of each spectrum is replotted on an expanded scale on the right. This edge is generated by He ions scattered back from regions near the front surface of the film. Ions scattered back from deeper within the film have lower energies because of losses suffered in traversing the dense film medium of the target. The slope of the edge reflects the resolution of the system. The signals generated by the glass substrates are not shown in this figure for clarity. Their contributions appear at lower energies because of the smaller masses of the atoms composing them. For the same reason, the edge of the pure Fe film lies at slightly lower energy (approximately 20 KeV) than that of the pure Ni film. These two edges do not change their positions upon oxidation, since the oxides contain metal atoms as well, but in a modified structural configuration. This change in structure results in a change in the height of the spectra below the edge. The nonuniformity of these two spectra with depth also shows that the process of oxidation is incomplete in both cases. On the other hand, note that oxidation does change the position of the edge for the permalloy film. Before oxidation, the edge coincides with that of Ni, as expected from the presence of Ni atoms throughout and near the surface of the permalloy films. After oxidation, however, the edge recesses to that of Fe, indicating that Fe is by far the main constituent of the uppermost layer (oxide) of the film. To be consistent with the spectra shown, the oxide

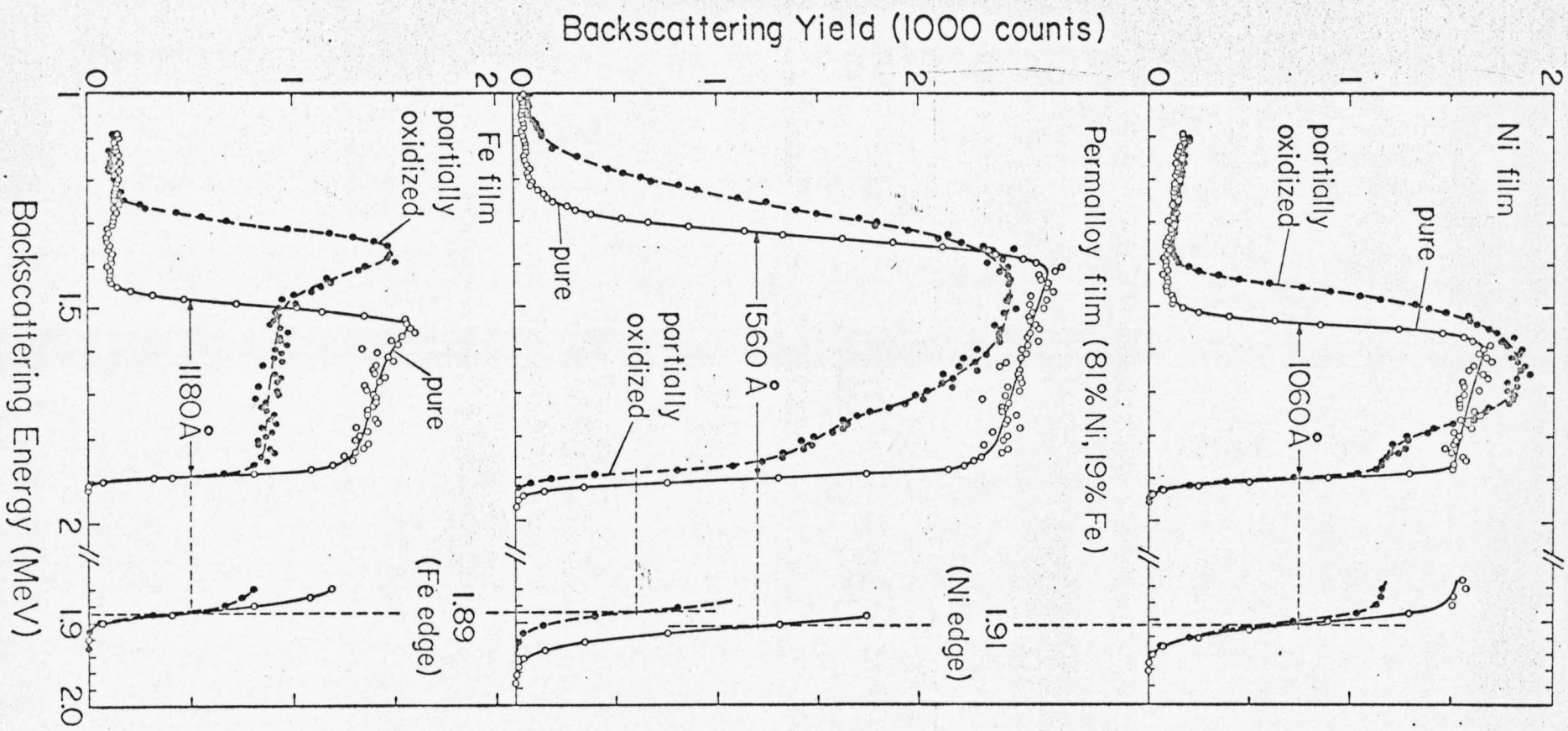

Fig. 5-1 Backscattering spectra of 2.5 MeV $^4He^+$ ions impinging on thin films of pure Ni (top), 81% Ni-19% Fe (center), and pure Fe (bottom) on glass substrates, each prior to and after partial oxidation. The backscattering angle is 164°, the integrated ion current is 18μC for Ni and Fe, and 15μC for permalloy. The Ni film was oxidized in air at 400°C for 15 min., the permalloy film at 500°C for 15 min. and the Fe film at 400°C for 1 min. Upon oxidation, the high energy edges do not shift for the Ni and Fe spectra since the oxides also contain the metal atoms. In permalloy, however, the high energy edge does shift back to the position of the Fe edge, indicating the formation of nearly pure Fe-oxide near the film surface.

must contain less than one or two percent Ni over at least the first 200 Å below the film surface. In this case too, the oxidation has not been carried out to completion. Additional experiments have shown that for very light oxidations the high energy edge of the permalloy spectrum is seen at positions between those of Ni and Fe, and that it does not shift beyond the Fe edge for heavier oxidations than shown in this figure.

Although in principle the oxide composition near the surface of Ni, Fe, and permalloy films can be determined from backscattering spectra, the resolution of the present system only allows the positive exclusion of Ni-oxide for permalloy films and FeO for Fe films. However, it does not permit one to distinguish between FeO, Fe_2O_3, and Fe_3O_4 for permalloy films, and Fe_2O_3 and Fe_3O_4 for Fe films. On the other hand, the magnetic moments of completely oxidized pure Fe films are less than 1/100 of the corresponding magnetic moments prior to oxidation as measured by a torque magnetometer at 700 Oe. The oxides of these films are red. This result suggests the formation of antiferromagnetic α-Fe_2O_3 as opposed to black, ferrimagnetic Fe_3O_4, or ferrimagnetic γ- Fe_2O_3. It is also consistent with the phase diagram of the Fe-O_2 system which excludes the latter oxides at moderate temperatures in an oxygen rich atmosphere (Hansen). This conclusion is further supported by old metallurgical studies of the high temperature oxidation of bulk Fe and Ni-Fe alloys which show that the surface oxides of both metals are predominantly Fe_2O_3 to depths of several microns (Davies et al., 1951; Foley et al., 1955; Hauffe). Therefore, it is concluded that the surface oxide of Ni-Fe alloy films is most likely α-Fe_2O_3.

The preferential oxidation of Fe and the formation of Fe-oxide are unequivocally supported by the X-ray fluorescence measurements described in the next section.

5.4 Results and Discussion of X-Ray Fluorescence Measurements

For films thinner than 3000 Å, X-ray fluorescence measurements can be accurately and directly used to measure the composition of permalloy films. Furthermore, this technique can also be used to measure the composition of the bulk of the oxidized films after etching their oxides in HCl.

5.4.1 X-Ray Fluorescence Measurements of Purposefully Oxidized Films

A 600 Å film oxidized at 400°C for 5 min. and etched for 1 min. in 37% HCl shows a 45% loss of Fe and only a 5% loss of Ni; a 2500 Å film oxidized at 500°C for 3 min. and etched for 1 min. in HCl shows a 56% loss of Fe with only a 6% loss of Ni. On the other hand, a 3200 Å film not oxidized except that occurring at room temperature and etched for 25 min. in HCl shows a 50% loss of Fe with a corresponding 48% loss of Ni. Recognizing that the oxide is dissolved much more rapidly than the metal, these results are consistent with: 1) the preferential oxidation of Fe, and 2) a rather uniform loss of Fe through the volume of the film as opposed to depletion localized near the film surface, implying a high diffusivity of Fe in Ni at these temperatures. This high diffusivity is perhaps not too surprising if one recognizes the polycrystalline nature of these films and a corresponding high density of grain boundary defects. These defects

could significantly enhance the diffusivity in these materials.

On the basis of the success of this technique for probing the composition of the purposefully oxidized films it was decided to extend it to films oxidized at room temperature.

5.4.2 X-Ray Fluorescence Measurements of Films Oxidized at Room Temperature

Having demonstrated the preferential oxidation of Fe, and successfully explained the changes of $4\pi NM$ with the depletion of Fe from the bulk of the purposefully oxidized films, it was recognized that to first order the same process could explain the thickness dependence of $4\pi NM$ and μ for films oxidized at room temperature. See the predictions of Table 4-1 and the experimental results of Figs. 4-1 and 4-2 of the previous chapter. Specifically, if the decrease of these quantities is due to the loss of Fe from the bulk of the film, this loss should change the composition of the bulk. Knowledge of $4\pi NM$ and Eq. 5.2 can be used to predict the expected composition of the bulk. This prediction can be compared with the actual composition as measured by X-ray fluorescence, after etching the films in HCl. The correlation of the predicted and experimentally measured composition can then be used to directly test the extent to which this oxidation process can explain the thickness dependence of $4\pi NM$.

Table 5-2 summarizes the results of such a comparison for 5 films in the 50 to 100 Å range. Column 1 shows the average fractional content of Fe measured by X-ray fluorescence prior to etching in HCl. This would be the actual composition of the film in the absence of oxidation.

Table 5-2

Comparison of expected composition with measured composition of the bulk of the film, after etching the films in 12% HCl.

1	2	3	4	5	6	7	8	9
<D>** Initial	$4\pi\langle M_D\rangle$initial (Oe)	$4\pi NM$ Initial (Oe)	$4\pi\Delta\langle M\rangle$ (Oe)	$\Delta\langle D\rangle$	<D>* Expected	<D>** Measured after etching	L** Initial (Å)	L** After etching (Å)
.194	10,170	8,550	1,620	.076	.118	.183	87	42
.190	10,080	7,800	2,280	.107	.083	.153	62	32
.191	10,100	7,250	2,850	.134	.057	.162	50	23
.185	9,980	6,920	3,060	.143	.042	.184	48	20
.179	9,850	6,300	3,550	.166	.013	.155	45	10

* Calculated from knowledge of $4\pi NM$ and Eq. 5.2.

** Measured by X-ray fluorescence.

Column 2 shows the saturation magnetization of bulk material for the composition of Column 1. Column 3 shows the values of $4\pi NM$ as determined from resonance. If this quantity is assumed to be a measure of the average saturation magnetization, and its decrease is due to depletion of Fe from the bulk of the film, Eq. 5.2 can be used to predict the expected average composition of the bulk of the film. This prediction is tabulated in Column 6. Column 7 shows the corresponding average composition, measured by X-ray fluorescence after partially etching the films in 12% HCl. The extent of etching is represented in the changes of the X-ray film thickness, tabulated in Columns 8 and 9.

A comparison of Columns 6 and 7 readily shows that although the relative amount of Fe in the bulk of the oxidized films is lower than 19% it is by far too large to completely explain the observed value of $4\pi NM$. This is particularly true for the 45 Å film whose bulk is expected to be almost pure nickel. This is inconsistent with the measured content of Fe in Column 7, and with the hysteresis behavior of these films, which is found to be identical to that of thick permalloy films instead of that of pure Ni films. The hysteresis characteristics of pure Ni films are radically different from those of 81% Ni-19% Fe films. It is therefore concluded that although there is evidence that Fe preferentially oxidizes at room temperature, the extent of this process is not sufficient to fully explain the deviation of $4\pi NM$, for thin films, from that of $4\pi NM$ for thick films. This conclusion also applies to the thickness dependence of the magnetic moment discussed in Chap. 4. For a more complete discussion of the implications of this finding, the reader is referred to Sec. 4.1 of

the previous chapter.

5.5 Summary and Conclusions

On basis of resonance, He ion backscattering, X-ray fluorescence and complementary torque magnetometer measurements it is unambiguously established that the oxide layer on the surface of oxidized 81% Ni-19% Fe evaporated films is predominantly Fe-oxide and that in the oxidation process iron atoms are removed from the bulk of the film to depths of thousands of Angstroms. Extrapolation of results for pure iron films indicates that the oxide is most likely α-Fe_2O_3. The conclusion is in agreement with results from old metallurgical studies of the high temperature oxidation of bulk Fe and Ni-Fe alloys.

The primary motivation for the above measurements was an attempt to explain the thickness dependence of $4\pi NM$ and μ observed in Chapters 3 and 4. However, the X-ray fluorescence results of Sec. 5.4.2, show that although the preferential oxidation of Fe takes place in films oxidized at room temperature, the extent of this process is by far too small to explain the results of the previous chapters.

APPENDIX 1

SUMMARY OF SOME PREVIOUS MEASUREMENTS OF A.

1) R. Weber and P. E. Tannenwald, J. Phys. Chem. Solids 24, 1357 (1963), Phys. Rev. 140, A498 (1965).

80-20 Permalloy Films $A = .93 \times 10^{-6}$ erg/cm

2) C. F. Kooi, et al., J. Appl. Phys. 35, 791 (1964)

Permalloy film of unknown composition $A = 1.13 \times 10^{-6}$ erg/cm

3) P. Wolf, Z. Angew. Phys. 14, 212 (1962)

81-19 Permalloy Films $A = .75$ to $.95 \times 10^{-6}$ erg/cm

4) G. I. Lykken and D. R. Schmitz, J. Appl. Phys. 41, 1024 (1970)

80-20 Permalloy Films $A = .98 \pm .02 \times 10^{-6}$ erg/cm

5) G. I. Lykken et al., J. Appl. Phys. 37, 3353 (1968)

80-20 Permalloy films 100 Å to 2500 Å thick.

$$\left(\frac{A}{M}\right)_{\perp \text{resonance}} = .02 \text{ to } 1.56 \times 10^{-9} \text{ G-cm}^2$$

$$\left(\frac{A}{M}\right)_{\parallel \text{resonance}} = 1.14 \text{ to } 1.90 \times 10^{-9} \text{ G-cm}^2$$

$\left(\frac{A}{M}\right)_{\perp}$ and $\left(\frac{A}{M}\right)_{\parallel}$ in many cases disagree by more than 50% for the same films.

6) G. I. Lykken, Phys. Rev. Letters 19, 1431 (1967)

80-20 Permalloy Films made under identical conditions

2000 Å, $\frac{A}{M} = 1.08 \times 10^{-9}$ G-cm^2 ($A = .93 \times 10^{-6}$ erg/cm)

1100 Å, $\frac{A}{M} = .88 \times 10^{-9}$ G-cm^2 ($A = .76 \times 10^{-6}$ erg/cm)

7) M. Okochi, J. Phys. Soc. of Japan 28, 897 (1970)

81-19 Permalloy Films $A = .74 \times 10^{-6}$ erg/cm

8) M. Nissenoff and R. W. Terhune, J. Appl. Phys. 36, 732 (1965)

80-20 Permalloy Films

$$\left(\frac{A}{M}\right)_{\perp \text{resonance}} = 1.29 \left(\frac{A}{M}\right)_{\parallel \text{resonance}} \quad \text{from Fig. 2, 1480 Å}$$

$$\left(\frac{A}{M}\right)_{\perp \text{resonance}} = 1.50 \left(\frac{A}{M}\right)_{\parallel \text{resonance}} \quad \text{from Fig. 6, 765 Å}$$

However the ratios of $\frac{A}{M}$ for both cases can be made to agree accurately by using even p numbers for both geometries as was done in this investigation.

A summary of the values of $\left(\frac{A}{M}\right)_{\parallel}$ for 6 films 465 to 2700 Å thick is

$$\left(\frac{A}{M}\right)_{\parallel} = 1.00 \text{ to } 1.57 \times 10^{-9} \text{ G-cm}^2 \quad \text{from Table I.}$$

9)* G. C. Bailey, J. Appl. Phys. 41, 1012 (1970)

75-25 Permalloy Films but unclear whether this is the melt or film composition which could be close to 68-32 permalloy if the above is melt composition.

$\frac{A}{M} = 1.34 \times 10^{-9}$ G-cm^2 for Film X-1 2100 Å

$\frac{A}{M} = 1.29 \times 10^{-9}$ G-cm^2 for Film T-3 1320 Å

$\frac{A}{M} = 1.31 \times 10^{-9}$ G-cm^2 for Film U-3 800 Å

The ratios of the two geometries are in very good agreement.

* This is the only publication in which the same mode numbering scheme was used as in this investigation, and clearly shows that the ratios of $\frac{A}{M}$ can even be made consistent and independent of thickness and geometry for non-coevaporated films. Bailey's results strongly support the main conclusions of Chapter 3. Unfortunately he used films of a composition different that 81% Ni - 19% Fe making it difficult to directly compare his results with those of Chapter 3. Nevertheless from his data the average value of A is 1.18×10^{-6} erg/cm^2 which is only 14.5% higher than 1.03×10^{-6}, and should be larger as expected from the comparison of the Curie temperatures of these materials (Bozorth, p. 446).

APPENDIX 2

DEFINITIONS AND MEASUREMENTS OF FILM THICKNESS

The optical or total film thickness is the average thickness determined by the Tolansky multiple reflection interference technique. Under optimum conditions, the accuracy of this measurement is ± 20 Å, and is therefore ideally suited for thickness measurements above 1000 Å. In fact it is the only direct method of accurately measuring the thickness of a film in this range.

The ideal film thickness is the thickness of a hypothetical film containing only Ni and Fe atoms of the actual film and assuming bulk density of the alloy. This thickness cannot be measured in practice since oxidation or interdiffusion at the film surfaces, especially oxidation at the outer surface, take place to some extent in real films. However, these effects become smaller with increasing film thickness and become negligible for films thicker than 1000 Å. Therefore, in this range the optical film thickness is assumed equal to the ideal film thickness.

The X-Ray film thickness is the thickness deduced from X-ray fluorescence measurements. This method measures the number of atoms per unit area of a given species, independent of whether these are in an oxide or in an alloy. By calibrating the X-ray system with optically measured standards in the 1000 to 3000 Å thickness range, the X-ray thickness becomes equal to the ideal film thickness. The accuracy of this measurement for films thinner than 1000 Å is ± 5%. It is therefore very useful to accurately measure the ideal film thickness of very thin films (20 to 2000 Å) regardless of the extent of oxidation or

interdiffusion.

The magnetic film thickness is the thickness deduced from the magnetic moment of a film. The magnetic moment can be measured equivalently with a hysteresis loop tracer or a torque magnetometer to an accuracy of ± 2%. The magnetic moment of a film is the integral of the saturation magnetization over the volume of the film. If the magnetization is assumed to only vary across the thickness of the film

$$\mu \equiv A \int_{-L/2}^{L/2} M d\xi = AL \frac{1}{L} \int_{-L/2}^{L/2} M d\xi = AL \langle M \rangle$$

where A is the area of the film, which is the same for all films and L can be one of three thicknesses: 1) the total film thickness, including the possible presence of non-magnetic or antiferromagnetic layers on the film surfaces, as would be measured by interferometry, 2) the thickness of magnetic material, excluding any "dead" layers, or 3) in the case of an ideal film, the ideal film thickness.

If it is assumed that the magnetization is uniform across, and independent of the film thickness, and if the hysteresis loop tracer and torque magnetometer are calibrated with optically measured standards, in the 1000 to 3000 Å range, the magnetic moment can then be conveniently used to determine a thickness which is defined as the magnetic film thickness. Under these assumptions, the magnetic film thickness is identical to both the thickness of magnetic material and the ideal film thickness.

However, the presence of oxidation or interdiffusion, as can take place in real films, would change the thickness of magnetic material, and could also change the saturation magnetization of the film by amounts which are not negligible in the 20 to 200 Å range. Therefore in this limit the thickness determined from magnetic measurements can be significantly different from the ideal or actual film thickness. Although this difference is not important for many applications, it is crucially important for the considerations of Chapters 4 and 5.

In summary, the actual or ideal film thickness of films thicker than 1000 Å, can be accurately and equivalently determined from optical, X-ray or magnetic measurements. However, the possible presence of oxidation or interdiffusion in very thin films can cause the thicknesses deduced using the three experimental methods to be significantly different from each other. In this limit the only thickness which can be measured directly and reliably is the X-ray fluorescence thickness which as discussed above is equivalent to the ideal film thickness.

APPENDIX 3

DETAILS OF PARABOLIC INHOMOGENEITY CALCULATIONS

A3.1 Introduction

This appendix summarizes the equations and some numerical results which describe the resonance behavior of films in which the possible presence of an inhomogeneity in demagnetizing field or magnetization across the film thickness is described by a parabolic function of the variable along the direction normal to the film plane. The motivations for this outline are the absence of an adequate description of this model in the existing literature and clarification of the numerical results used in Chapter 2. The equations in Sections A3.2 and A3.3 apply to the inhomogeneous demagnetizing field case for the perpendicular and parallel resonance geometries respectively. These equations were specifically used to calculate the resonance fields for the parabolic inhomogeneity of demagnetizing field described in Section 2.3.2 of Chapter 2. Section A3.4 outlines the implications of this model when it is applied to an inhomogeneity in magnetization.

The resonance equations for all cases are developed from the usual equation of motion (Eq. 2.1 in Chapter 2):

$$\frac{\partial \overline{M}}{\partial t} = - \gamma(\overline{M} \times \overline{H}) \qquad \text{(A3.1)}$$

where, $$\overline{H} = \overline{H}_{applied} + \overline{H}_{demagnetizing} + \overline{H}_{exchange} \qquad \text{(A3.2)}$$

$$\overline{H}_{applied} = H_o \overline{e}_z \qquad \text{(A3.3)}$$

$$\nabla \cdot \bar{H}_{\text{demagnetizing}} = -4\pi \nabla \cdot \bar{M} \tag{A3.4}$$

$$\bar{H}_{\text{exchange}} = \frac{2A}{M} \nabla^2 \bar{M} \tag{A3.5}$$

$$\bar{M} = (m_x \bar{e}_x + m_y \bar{e}_y)\, e^{i\omega t} + M\bar{e}_z \tag{A3.6}$$

The eddy current and intrinsic relaxation contributions are omitted from the above equations on the grounds described in Sec. 2.1.3. The contribution from the effective magnetic anisotropy fields is omitted for simplicity. The z axis of the cartesian coordinates is chosen to coincide with the applied field direction. This means that for perpendicular resonance the z coordinate is perpendicular to the film, while x and y are in the plane of the film. For parallel resonance the z and x coordinates are in the plane of the film, and y is perpendicular to the film plane. With this convention the demagnetizing field (Eq. A3.4 above) for perpendicular resonance is:

$$\bar{H}_{\text{demagnetizing}} = -4\pi(N_{\parallel} m_x \bar{e}_x + N_{\parallel} m_y \bar{e}_y + N_{\perp} M\bar{e}_z) \tag{A3.7}$$

and for parallel resonance:

$$\bar{H}_{\text{demagnetizing}} = -4\pi(N_{\parallel} m_x \bar{e}_x + N_{\perp} m_y \bar{e}_y + N_{\parallel} m_z \bar{e}_z) \tag{A3.8}$$

where $N_{\perp}$ and $N_{\parallel}$ are the demagnetizing factors perpendicular and parallel to the film plane. For the case of an inhomogeneous demagnetizing field it is assumed that $N = N_{\perp} - N_{\parallel}$, m_x and m_y are functions of the variable along the direction perpendicular to the film plane. For the

case of an inhomogeneous magnetization N = 1, while in addition to m_x and m_y, M and possibly A are function of this variable. In both cases all functions are assumed to be independent of the planar coordinates.

The boundary condition applicable in the case of an inhomogeneous demagnetizing field is:

$$\frac{\partial m_{x,y}}{\partial n} = 0 \text{ at the film surfaces.} \qquad \text{(A3.9)}$$

The boundary condition applicable in the case of an inhomogeneous magnetization is:

$$\frac{1}{m_{x,y}} \frac{\partial m_{x,y}}{\partial n} = \frac{1}{M} \frac{\partial M}{\partial n} \text{ at the film surfaces.} \qquad \text{(A3.10)}$$

As explained in Section 2.2 both of these equations can be simply derived by torque arguments and the requirement that all spins of the system precess at the same frequency. In both cases n is the outward film normal.

A3.2 Inhomogeneity in Demagnetizing Field for the Perpendicular Resonance Geometry

As described above, in this case M is taken to be homogeneous across the film thickness while N is a function of the variable perpendicular to the film plane, and for this geometry is defined as:

$$N \equiv 1 - \frac{4\alpha}{L^2} z^2 \quad , \qquad \text{(A3.11)}$$

where L is the film thickness and α is the per unit decrease of demagnetizing factor at the film surfaces. Starting with Eqs. (A3.1) through (A3.7) and neglecting terms of $0(m_{x,y}^2)$ since $m_{x,y} << M$, the differential equation for $m_i^+ \equiv (m_{xi} + i\, m_{yi})$ has the form:

$$\frac{\partial^2 m_i^+}{\partial z^2} = (-\lambda_i' + \delta^2 z^2) m_i^+ \tag{A3.12}$$

where

$$\lambda_i' = \frac{M}{2A}\left(\frac{\omega}{\gamma} + 4\pi M - H_i\right) \tag{A3.13}$$

and

$$\delta^2 = \frac{8\pi M^2 \alpha}{AL} \quad . \tag{A3.14}$$

For numerical computation it is convenient to rewrite Eq. (A3.12) in the form

$$\frac{\partial^2 m_i^+}{\partial \zeta^2} = (\lambda_i + \zeta^2) m_i^+ \tag{A3.15}$$

by setting, $\lambda_i = \frac{\lambda_i'}{\delta}$ and $\zeta = \sqrt{\delta}\, z$.

The subscript i denotes the i^{th} solution of the series of solutions of Eqs. (A3.12) and (A3.15) which satisfy the boundary condition of Eq. (A3.9) and which correspond to the applied field H_i. It is instructive to note that Eqs. (A3.12) and (A3.15) have the familiar form of the

wave equation for the quantum mechanical harmonic oscillator. To first order, the solutions of these equations are very similar to the harmonic oscillator wave functions. The actual solutions satisfy the requirement that their slope be zero at $z = \pm L/2$.

The resonance fields of the corresponding unpinned modes of an ideal film ($\alpha = 0$), is given in Eq. (3.3) of Chapter 3:

$$H_p = \frac{\omega}{\gamma} + 4\pi M - \frac{2A}{M}\frac{\pi^2 p^2}{L^2} \qquad \text{(A3.16)}$$

where p = 0, or even integer, correspond to the symmetric unpinned modes. This equation can then be conveniently used to calculate the expected difference between the resonance fields of an ideal film and those of a film with a parabolic inhomogeneity in demagnetizing field. From Eqs. (A3.13) and (A3.16) this difference is given by:

$$H_p - H_i = \frac{2A}{M}\left(\delta\lambda_i - \frac{\pi^2 p^2}{L^2}\right), \qquad \text{(A3.17)}$$

where i = 1,2,3,4 etc. corresponds to p = 0,2,4,6, etc.
It is this difference that is shown for the parabolic inhomogeneity case in Table 2-1 of Chapter 2. Careful analysis of the numerical results obtained from solving Eq. (A3.15) shows that H_1, the resonance field of the main mode of a film with a reasonable parabolic inhomogeneity in demagnetizing field, closely obeys the following relation:

$$H_1 = \frac{\omega}{\gamma} + \langle 4\pi NM \rangle = \frac{\omega}{\gamma} + 4\pi M\left(1 - \frac{\alpha}{3}\right) \qquad \text{(A3.18)}$$

where $\langle 4\pi NM \rangle = 4\pi M(1 - \frac{\alpha}{3})$ is the average demagnetizing field across the film thickness. It is this result, when compared with the main mode resonance field of an ideal film, H_o from Eq. (A3.16), that led to the conclusion of Chapter 2, that the interpretation of the main resonance mode of a film with an inhomogeneous demagnetizing field as the uniform mode, would allow a very good measure of its average demagnetizing field.

The procedure followed in the numerical computation of H_i is as follows:

a) choose $\frac{\omega}{\gamma}$, $4\pi M$, and A.

b) choice of α and L defines δ

c) L also defines $\zeta_{max} = \sqrt{\delta}\,\frac{L}{2}$

d) Eq. (A3.15) is then solved numerically with the constraint that $\partial m^+_i/\partial\zeta = 0$ (Eq. (A3.9)) at $\zeta_{max} = \pm\sqrt{\delta}\,\frac{L}{2}$. The value of ζ_{max} can be easily determined to an accuracy of .1%. This gives rise to a series of solutions of m^+ denoted by m^+_i with a corresponding sequence of λ_i.

e) By defining $L = m\ 10^3$ Å, the following relations are constructed:

$$m^2\alpha = \frac{2A}{10^6 M^2}(\zeta_{max})^4 \qquad \text{(A3.19)}$$

and

$$m^2(H_o - H_i) = \frac{8A}{10^6 M}\lambda_i(\zeta_{max})^2 . \qquad \text{(A3.20)}$$

f) By repeating steps b through d for several discrete combinations of α and L, the difference $H_o - H_i$ for other combinations of α and L can be conveniently obtained from the graphical representation of Eq. (A3.19) vs. Eq. (A3.20).

The results of step f are summarized in Figs. (A3-1a) and (A3-1b) for the special case of 81% Ni-19% Fe permalloy films. The data in Table 2-1 of Chapter 2 were deduced from these figures. Column 2 of this table represents $4\pi M \frac{\alpha}{3}$ where $4\pi M = 10^4$ Oe and $\alpha = 3.3 \times 10^{-7}/L$, and column 3 represents $H_o - H_1 \equiv \Delta H_\alpha$ for $p = 0$ as deduced from Fig. (A3-1b). A comparison of these results establishes the validity of Eq. (A3.18).

A3.3 Inhomogeneity in Demagnetizing Field for the Parallel Resonance Geometry

In this case the N demagnetizing factor of Eq. (A3.8) is a function of y and is defined as:

$$N \equiv 1 - \frac{4\alpha}{L^2} y^2 \ . \qquad \text{(A3.21)}$$

As in the previous case, starting with Eqs. (A3.1) through (A3.6) and Eq. (A3.8) also neglecting terms of $0(m_{x,y}^2)$ since $m_{x,y} << M$, the coupled differential equations for m_x and m_y have the form:

$$\left.\begin{aligned} \frac{\partial^2 m_x}{\partial y^2} &= h_o' m_x - \omega_o' m_y \\ \frac{\partial^2 m_y}{\partial y^2} &= (h_o' + m_o') m_y - \omega_o' m_x - \delta^2 y^2 \end{aligned}\right\} \qquad \text{(A3.22)}$$

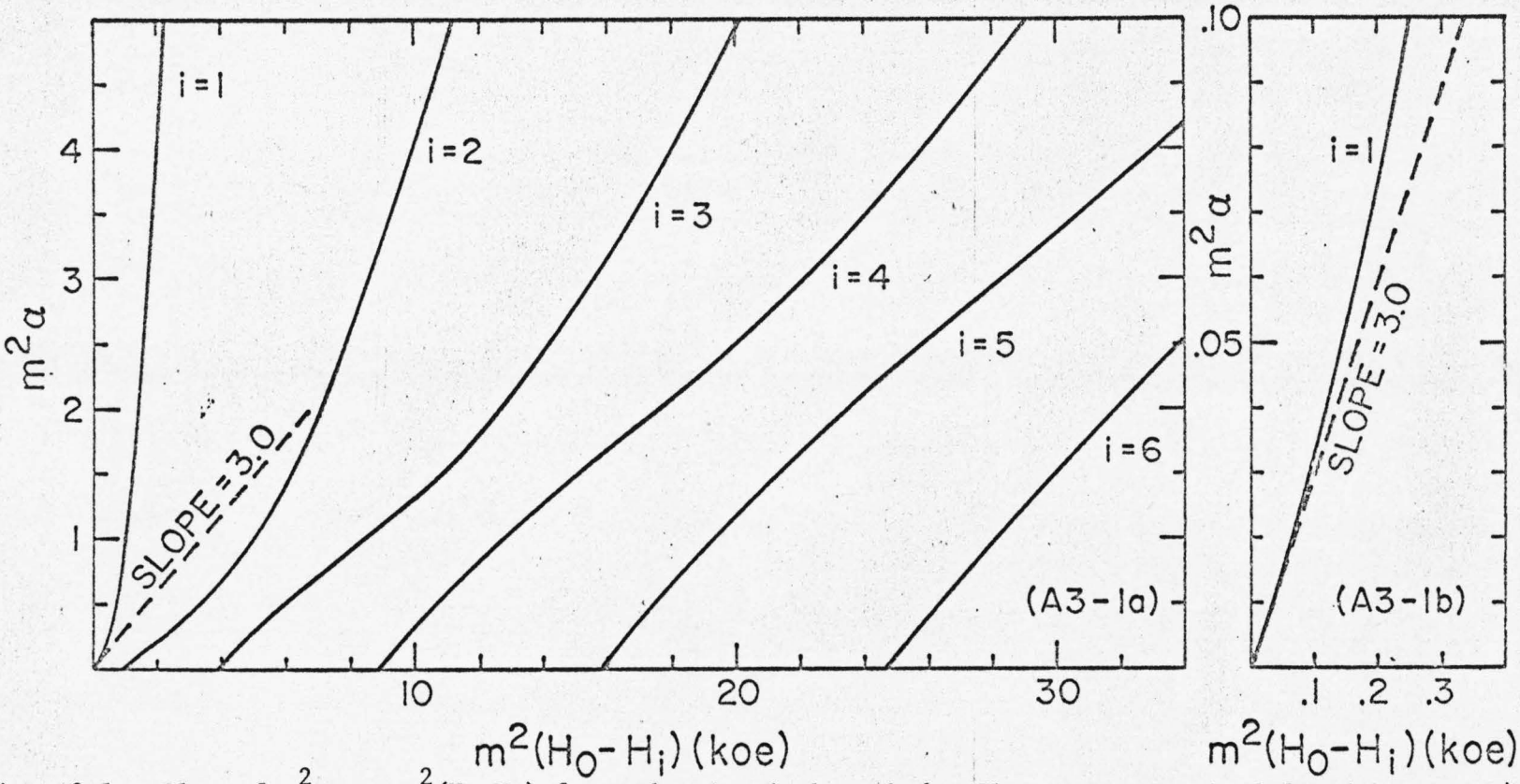

Fig. A3-1a Plot of $m^2\alpha$ vs. $m^2(H_o-H_i)$ for modes i = 1 through 6. The constant m is defined by the relation. $L = m10^3$Å. These results are specialized to 81% Ni-19% Fe permalloy films with $A = 10^{-6}$ erg/cm, $4\pi M = 10^4$Oe and $\gamma = 2.94$ MHz/Oe.

Fig. A3-1b Data for $m^2\alpha$ vs. $m^2(H_o-H_i)$ of Fig. A3-1a plotted on an expanded scale. This figure is useful for deducing the resonance field deviations of very thin films. The straight line asymptote has a slope of 3.0. It shows that for small $m^2\alpha$, the first mode resonance field deviation from H_o (the uniform mode resonance field of an ideal film) corresponds closely to the difference between the respective average demagnetizing fields, i.e. $H_o-H_i = \alpha/3$, or equivalently $\langle 4\pi NM\rangle = 4\pi M(1 - \alpha/3)$.

where $h_o' = \frac{H_1}{2A/M}$, $\omega_o' = \frac{\omega/\gamma}{2A/M}$, $m_o' = \frac{4\pi M}{2A/M}$

and

$$\delta^2 = \frac{8\pi M^2 \alpha}{AL^2} \quad . \tag{A3.23}$$

These equations can be conveniently rewritten as

$$\left.\begin{aligned} \frac{\partial^2 m_x}{\partial \zeta^2} &= h_o m_x - \omega_o m_y \\ \frac{\partial^2 m_y}{\partial \zeta^2} &= (h_o + m_o)\, m_y - \omega_o m_x - \zeta^2 m_y \end{aligned}\right\} \tag{A3.24}$$

Be setting $\zeta = \sqrt{\delta}\, y$ and $h_o, \omega_o, m_o = \frac{h_o'}{\delta}, \frac{\omega_o'}{\delta}, \frac{m_o'}{\delta}$.

In this, as in the case of perpendicular resonance, these equations have a series of solutions, but for simplicity, since typically in parallel resonance only one mode is detected experimentally, the following considerations are restricted to the main solution which satisfies the boundary condition of Eq. (A3.9), and which corresponds to the applied field H_1.

The resonance field of the main mode of an ideal film ($\alpha = 0$) is related to ω by the following equation. It can be readily derived from Eq. (3.1) of Chapter 3 by setting $H_k = 0$ and $N = 1.0$.

$$\frac{\omega^2}{\gamma^2} = (H_o + 4\pi M) H_o \quad . \tag{A3.25}$$

Careful analysis of the numerical results obtained from solving Eq. (A3.24) shows that H_1, the resonance field of the main mode of a film with a reasonable parabolic inhomogeneity in demagnetizing field, is related to ω by the following equation:

$$\frac{\omega^2}{\gamma^2} = [H_1 + 4\pi M(1 - \frac{\alpha}{3})]H_1 \qquad \text{(A3.26)}$$

where as stated in Section A3.2, $4\pi M(1 - \frac{\alpha}{3})$ is the average demagnetizing field across the film thickness. It is this result, when compared with the prediction of Eq. (A3.25) above that, as in the perpendicular resonance case, led to the conclusion of Chapter 2, that the interpretation of the main mode of a film with an inhomogeneous demagnetizing field as the uniform mode, would allow a very good measure of its average demagnetizing field.

The procedure followed in the numerical computation of H_1 is as follows:

a) choose γ, $4\pi M$ and A.

b) choice of H_1, ω, and δ defines h_o, ω_o, and m_o.

c) assume a value of $m_y(0)$.

d) integrate equations (A3.23) until either $\frac{\partial m_x}{\partial \zeta}$ or $\frac{\partial m_y}{\partial \zeta}$ change sign.

e) if $\frac{\partial m_x}{\partial \zeta}$ changes sign first choose a lower value of $m_y(0)$. If $\frac{\partial m_y}{\partial \zeta}$ changes sign first choose a lower value of $m_y(0)$.

f) repeat steps d and e until both $\frac{\partial m_x}{\partial \zeta} = \frac{\partial m_y}{\partial \zeta} = 0$ simultaneously, or equivalently when both m_x and m_y satisfy the boundary

condition of Eq. (A3.9). The value of ζ at which this condition is satisfied is defined as $\zeta_{max} = \sqrt{\delta}\,\frac{L}{2}$ and determines L. The value of ζ_{max} can be easily determined to an accuracy of .1%.

g) calculate corresponding α from Eq. (A3.23).

h) by repeating steps b through g for several discrete values of H_1, ω, and δ, the plot of α vs. L can then be used to estimate the relation between H_1 and ω for other combinations of α and L.

The graphical representation of α vs. L, with two frequencies (9.8 and 4.9 Ghz) and three fields for each frequency as parameters, is presented in Fig. A3-2. These results are specialized to 81%Ni-19% Fe permalloy films. Interpolation between the two sets of curves can be used to determine H_1 for other combinations of α and L at these two frequencies. The results of this figure were used to establish the validity of Eq. (A3.26) at 9.8 and 4.9 Ghz. The extent of the validity of this equation can be readily appreciated from a comparison of the results tabulated in columns 2 and 4 of Table 2-2 in Chapter 2. Column 2 represents $4\pi M\,\frac{\alpha}{3}$ where $4\pi M = 10^4$ Oe and $\alpha = 3.3 \times 10^{-7}/L$, and column 4 represents the difference between the demagnetizing field of an ideal film, $4\pi M$, and the effective demagnetizing field calculated from Eq. (A3.25) by using H_1 instead of H_o. The value of H_1 was deduced from Fig. A3-2.

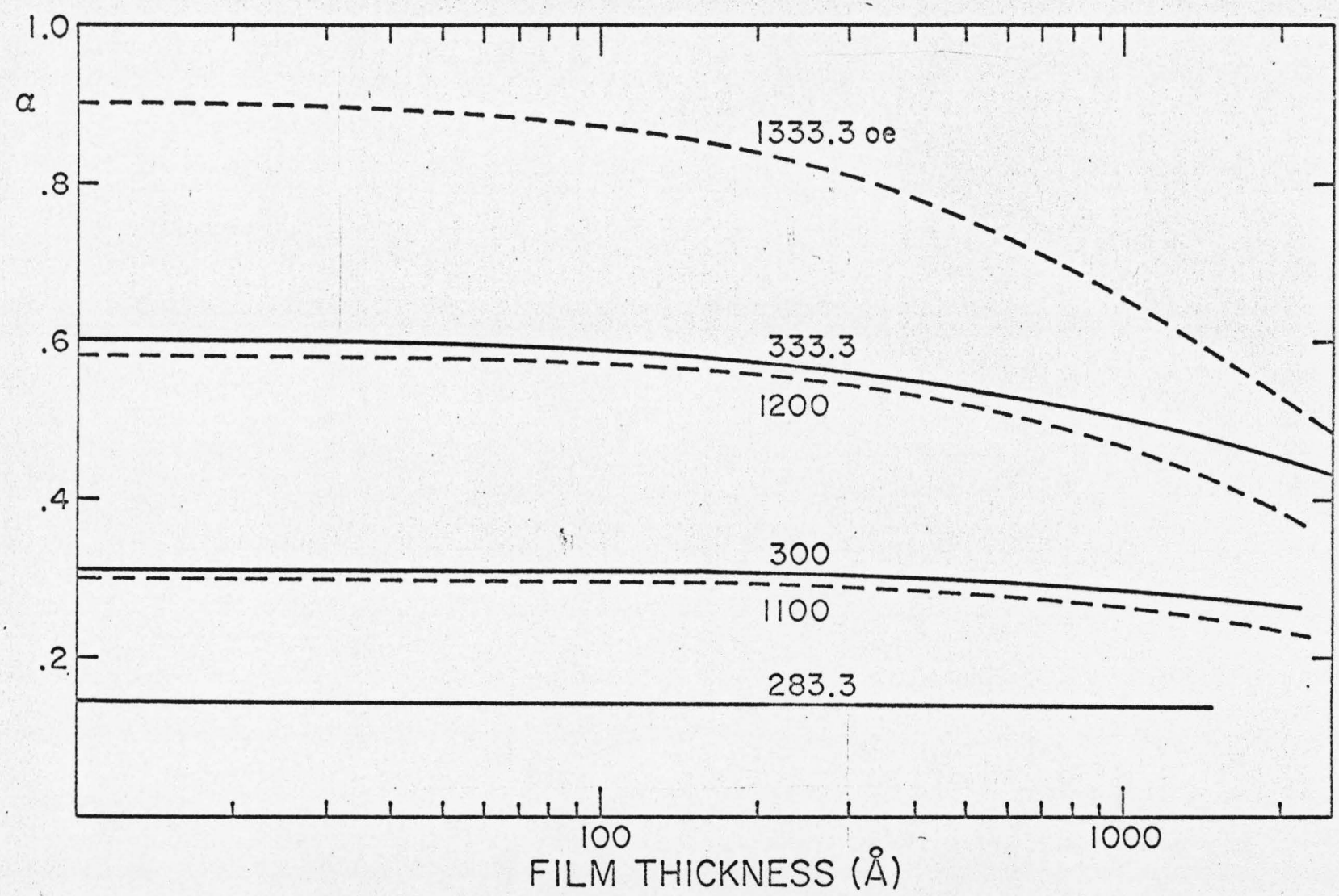

Fig. A3-2 Plot of α vs. L with two frequencies and three fields for each frequency as parameters. The solid curves and dashed curves correspond to f = 4.9 and 9.8 GHz respectively. The three fields for each frequency are labeled on the respective curves. These curves are specialized to 81% Ni-19% Fe permalloy films with A = 1.0×10^{-6} erg/cm, $4\pi M$ = 10 kOe. and γ = 2.94 MHz/Oe.

A3.4 Implications of an Inhomogeneity of Magnetization in the Parabolic Model Calculations

In this case, as opposed to the previous two, N is taken to be homogeneous and 1.0 across the film thickness, while M itself is a function of the variable perpendicular to the film plane. Specifically, for the perpendicular resonance geometry, M is defined as

$$M = M_o(1 - \frac{4\alpha z^2}{L^2}) \tag{A3.27}$$

where α is the per unit decrease of the magnetization at the film surfaces.

The implications of this definition can be most readily appreciated from Eqs. (A3.5) and (A3.10). First, the $\nabla^2\overline{M}$ factor of Eq. (A3.5) will give rise to z dependent exchange terms in Eq. (A3.1) in addition to the demagnetizing terms of Eq. (A3.7). Second, depending on what is assumed for the exchange constant, the $2A/M^2$ factor of Eq. (A3.5) will also give rise to even more complicated z dependent exchange contributions to the basic differential equation. The detailed nature of these terms will depend on what is assumed for the ratio of A/M^2. Three obvious choices for this ratio are: A constant, A/M constant or A/M^2 constant. Third, independent of the latter complication, the inclusion of these z dependent exchange terms in Eq. (A3.1), does not lead to an exact differential equation in the sense of Eq. (A3.12). It contributes terms of order higher than z^2, which are only negligible for the combination of small α and large L. For example for the case where $2A/M^2$ is assumed to be constant, $\alpha << 1$

and $L \gtrsim 200$ Å, the differential equation for $m_i^+ = m_{xi} + m_{yi}$ is

$$\frac{\partial^2 m_i^+}{\partial x^2} = (\lambda_i + \delta_i^2 z^2 - \beta_i^2 z^4 + \text{h.o.t.}) m_i^+ \tag{A3.28}$$

where

$$\lambda_i = \frac{M_o}{2A}\left(\frac{\omega}{\gamma} + 4\pi M_o - H_i + \frac{16\,\alpha\,A}{M_o\,L^2}\right) \tag{A3.29}$$

$$\delta_i^2 = \frac{8\pi M_o^2 \alpha}{AL^2} - \frac{4\lambda_i \alpha}{L^2} \tag{A3.30}$$

and

$$\beta_i^2 = \frac{16\alpha^2}{L^4}\,\lambda_i \quad . \tag{A3.31}$$

Comparison of Eqs. (A3.28) through (A3.31) with Eqs. (A3.12) through (A3.14) reveals the added complexity of this problem. The conditions which would make the inhomogeneity of magnetization problem equivalent to the inhomogeneous demagnetizing case of Section A3.2 are:

$$\beta_i^2 z^2 \ll \delta_i^2, \quad \text{for} \quad 0 \le z^2 \le \frac{L^2}{4}\ , \tag{A3.32}$$

$$\frac{2\ A/M_o}{4\pi M_o}\ \lambda_i \ll 1, \tag{A3.33}$$

and

$$\frac{16\ \alpha\ A}{M_o L^2} \ll H_i \quad . \tag{A3.34}$$

Estimates of the above inequalities, for $0 \leq \alpha \leq .10$, show that although Eq. (A3.32) is well satisfied, Eqs. (A3.33) and (A3.34) become marginal below 500 Å. In view of the above limits it is tempting to conclude that, to first order, the numerical results of Section A3.2 also adequately apply to the inhomogeneous magnetization case. However, this is only approximately correct, since as pointed out above, the solutions of Section A3.2 satisfy the boundary condition of Eq. (A3.9), whereas in the case under consideration they must satisfy Eq. (A3.10).

Equation (A3.10) when specifically applied to the parabolic model takes the form:

$$\frac{1}{m_{x,y}} \frac{\partial m_{x,y}}{\partial z} = \mp \frac{4}{L} \frac{\alpha}{1 - \alpha} \quad \text{at } z = \pm \frac{L}{2} \quad . \tag{A3.35}$$

This condition is different from Eq. (A3.9). Its use with the results of Section A3.2 is only valid for very small α.

The consequences of these considerations for the parallel resonance geometry are considerably more complicated since they appear in a coupled pair of differential equations. However, a similar analysis to the one used for the perpendicular resonance results shows that the results of Section A3.3 are also applicable for the inhomo-

geneous magnetization case for the above limited combinations of α and L.

It is in view of the above difficulties that it was decided to avoid a detailed extension of the parabolic model to study the implications of an inhomogeneous magnetization. As discussed in Section 2.3.3 of Chapter 2, this possibility, for the perpendicular resonance case, was considered with the more tractable abrupt surface layer of reduced magnetization model.

APPENDIX 4

RECOMMENDATIONS FOR MEASUREMENT OF A IN FILMS OF COMPOSITION OTHER THAN 81% Ni-19% Fe

It is hoped that the suggestions of this Appendix will aid in an extension of S.W.R. to measure the exchange constant and several other properties of materials other than the 81% Ni-19% Fe alloy used in this investigation. As explained in Section 3.2 of Chapter 3 this alloy is nearly ideally suited for S.W.R. measurements. The use of any other material will require special attention to the following characteristics: saturation magnetization, perpendicular anisotropy, film thickness, and resonance linewidths.

First, knowledge of the saturation magnetization is essential to determine A since it always appears in conjunction with M in the relevant mode separation terms of Eq. (2.8) in Chapter 2. As can be seen from this equation the presence of a significant perpendicular anisotropy, as can arise through a magnetoelastic interaction in magnetostrictive materials, would not allow a measurement of M from resonance alone, because M is intrinsically associated with $H_{k_\perp}$ in the relevant terms. Therefore, the use of S.W.R. to determine A in films with a significant perpendicular anisotropy will require an independent measurement of M. This could be conveniently determined from knowledge of the magnetic moment, as measured with a hysteresis loop tracer, torque magnetometer or vibrating sample magnetometer, and the volume of a film. Furthermore, knowledge of M would then allow a direct (though generally less accurate) measurement of $H_{k_\perp}$.

Second, the value of $4\pi NM - H_{k_\perp}$ has to be compatible with available ranges of magnetic fields and R.F. frequencies. This constraint particularly applies to the perpendicular resonance case described by the following equation:

$$\frac{2A_k}{M}^2 = \frac{2A}{M}\left(\frac{p\pi}{L}\right)^2 = \frac{\omega}{\gamma} + 4\pi NM - H_{k_\perp} - H. \qquad \text{(A4.1)}$$

As can be readily seen from this equation the ability to excite the uniform mode and an adequate number of higher order spin wave modes depends directly on the value of $4\pi NM - H_{k_\perp}$, and the available ranges of ω/γ and H. The experimental facility used for this investigation provides a frequency range of 1 to 9 GHz and a field range of 2 to 3 kOe. This means that allowing for a typical exchange field range of 2 to 3 kOe this facility is limited to investigate S.W.R. characteristics in materials whose effective demagnetizing field, $(4\pi NM - H_{k_\perp})$, is less than 13 to 14 kOe. Specifically, it can only be readily used for Ni-Fe alloys with Ni content in excess of 60% (Bozorth, p. 109) and Ni-Co alloys, with Ni content in excess of 35% (Bozorth, p. 279). Its use for material with effective demagnetizing fields higher than 14 kOe will require new magnet pole faces or a new magnet with a higher field range.

The importance of the film thickness can also be readily appreciated from the left hand side of Eq. A4.1. The number of spin wave modes that can be excited within the above frequency and field limitations is to a large extent a function of film thickness. The thickness of a film should be chosen on the basis of an estimate of 2A/M for a material and the nominal number of modes (5 to 6 modes) which would establish

a reliable slope of the graphical representation of H vs p^2. Furthermore, the use of at least two substantially different film thicknesses is recommended since it would allow a check for consistency similar to the one carried out in Chap. 3.

The choice of film thickness must also be reconciled with the resonance linewidths so that the minimum mode separation of the low order modes is of the order of the linewidths. Smaller mode separations would make it difficult to unambiguously determine the spectroscopic location and identification of the resonance modes. This is not a severe constraint in 81% Ni-19% Fe films since their linewidths rarely exceed 30 Oe, but it can become important for other materials. For example the linewidths of pure Ni films can be as large as 300 Oe. Furthermore such an increase in linewidths makes it more difficult to detect the resonance excitations of the relatively weaker higher order modes. In such cases the use of a resonant cavity with better sensitivity than a strip line system is recommended. The necessary X-band microwave hardware and associated electronics are available within the electrical engineering group at Caltech.

Finally Table A4-1 summarizes the slope (L^2) products obtained for a set of films whose actual composition is 68% Ni-32% Fe. These films were prepared from a 75% Ni-25% Fe melt. As in the case of 81% Ni-19% Fe films discussed in Table 3-1 of Chap. 3 the products corresponding to perfect pinning assignment show a 55% spread. On the other hand this spread reduces to only 7% for the unpinned assignment. Using the value of $4\pi M$ = 13,000 Oe, as determined with a torque magnetometer, the average value of A deduced from these measurements is $(1.09 \pm .04) \times 10^{-6}$ erg/cm.

This value of A is 6% higher than that of 81% Ni-19% Fe films. This difference is consistent with the relative values of the Curie temperatures of these materials (Bozorth, p. 446).

Table A4-1

Product of $(L)^2$ and the corresponding slope deduced from the graphical representation of H vs p^2 at f = 7.5 GHz. For four coevaporated 68% Ni-32% Fe films.

	Pinned Case		Unpinned Case	
Film Thickness Å	Slope L^2 x 10^{-8} G cm^2		Slope L^2 x 10^{-8} G cm^2	
898	1.18	55% Spread	2.05	7% Spread
1755	1.55		2.02	
2690	1.73		2.03	
3760	1.89		2.16	

REFERENCES

B. E. Argyle and S. H. Charap, J. Appl. Phys. 35, 802 (1964).

G. C. Bailey, J. Appl. Phys. 41, 1012 (1970).

R. M. Bozorth, Ferromagnetism (D. Van Nostrand, 1951).

M. H. Davies et al., J. of Metals 3, 889 (1951).

R. T. Foley et al., J. Electrochem. Sol. 102, 440 (1955).

H. Gradmann and J. Müller, Phys. Stat. Sol. 27, 313 (1968).

M. Hatherly et al., Proc. Phys. Soc. 84, 55 (1964).

K. Hauffe, Oxidation of Metals (Plenum Press, 1965), p. 267 and p. 310.

C. Herring, Magnetism, edited by Rado and Suhl, IV, (Academic Press, 1966).

F. B. Humphrey and A. R. Johnston, Rev. Sci. Instr. 34, 348 (1963).

N. Inamura and S. Chikazumi, J. Phys. Soc. Japan 25, 125 (1968).

I. S. Jacobs and C. P. Bean, Magnetism, edited by Rado and Suhl III, (Academic Press, 1963), p. 271.

G. O. Johnson and C. H. Wilts, J. Appl. Phys. 42, 335 (1971).

C. Kittel, Phys. Rev. 110, 1295 (1958).

R. B. Leighton, Principles of Modern Physics, (McGraw Hill, 1959), Chap. 14.

R. D. Lowde, J. Appl. Phys. 36, 884 (1965).

G. I. Lykken and D. R. Schmitz, J. Appl. Phys. 41, 1024 (1970).

J. W. Mayer, L. Eriksson, and J. A. Davies, Ion Implantation in Semiconductors, (Academic Press, 1970), Chap. 4.

S. Methfessel et al., J. Phys. Soc. Japan 17 Suppl. B-I, 607 (1962).

C. A. Neugebauer, Phys. Review 116, 1441 (1959).

C. A. Neugebauer, Z. Angevandte Physik XIV, 182 (1961).

M. Nisenoff and R. W. Terhune, J. Appl. Phys. 36, 732 (1965).

P. Pincus, Phys. Review 118, 658 (1960).

A. M. Portis, Appl. Phys. Letters 2, 69 (1963).

E. Schlömann and R. I. Joseph, J. Appl. Phys. 41, 1024 (1970).

M. H. Seavey, Jr. and P. E. Tannenwald, Phys. Rev. Letters 1, 168 (1958).

M. H. Seavey, Jr., "Electromagnetic Theory of Spin Wave Resonance", Lincoln Laboratory M.I.T. Technical Report No. 239, (1961).

R. F. Soohoo, Phys. Rev. 131, 594 (1963).

M. Sparks, Ferromagnetic Relaxation Theory, (McGraw Hill, 1964), Chap. 3.

M. Sparks, Phys. Rev. Letters 22, 1111 (1969).

S. Tolansky, Multiple Beam Interferometry of Surface Films, (Oxford University Press, London, 1948).

R. Weber, IEEE Trans. on Mag. Mag-4, 28 (1968).

R. Weber, P. E. Tannenwald, and C. H. Bajorek, Appl. Phys. Letters 16 35 (1970).

P. E. Wigen et al., J. Appl. Phys. 35, 3302 (1964).

P. Wolf, "Spin Wave Resonance in Films Magnetized Parallel to the Surface", Abstract published in J. Appl. Phys. 34, 1139 (1963). Details of this paper were published in an IBM Zurich Research Laboratory Note in 1963.